

Department of Biomedical Sciences  
University of Veterinary Medicine Vienna  
Institute of Pharmacology and Toxicology  
Head: Univ.-Prof. Dr.med.univ. Veronika Sexl

# **Unravelling the role of CDK6 and STAT5 in NPM-ALK-driven malignant transformation**

**Master's thesis**

**Master's Programme Comparative Biomedicine (MSc)**

**University of Veterinary Medicine Vienna**



submitted by

**Klavdija Bastl, BSc**

Vienna, May 2021

**Supervision**

Barbara Maurer, PhD

Institute of Pharmacology and Toxicology

Department of Biomedical Sciences

University of Veterinary Medicine Vienna

**Reviewer**

Univ.-Prof. Dr. DI. Richard Moriggl

Institute of Animal Breeding and Genetics

Unit for Functional Cancer Genomics

University of Veterinary Medicine Vienna

## Declaration of Honour

*"I declare on my word of honour that I have written this paper on my own and that I have not used any sources or resources other than stated and that I have marked those passages and ideas that were either verbally or textually extracted from sources. This also applies to drawings, sketches, graphic representations as well as to sources from the internet.*

*The paper has not been submitted in this or similar form for assessment at any other domestic or foreign post-secondary educational institution and has not been published elsewhere. The present paper complies with the version submitted electronically."*

Date: 25.06.2021

Signature

A handwritten signature in blue ink, appearing to read 'Dast', written over a horizontal line.

## Acknowledgements

First and foremost, I am ever so grateful to Prof. Dr. Veronika Sexl for her support and for giving me the opportunity to join her laboratory and become a member of the JAK-STAT group.

I want to express my sincere gratitude to my supervisor Dr. Barbara Maurer, whose expertise was invaluable in formulating the research questions and methodology. Thank you for introducing me to the Sexl laboratory and allowing me to work on exciting projects. I want to express my most profound appreciation for her trust, motivation and scientific discussions. Her insightful feedback pushed me to sharpen my thinking and brought my work to a higher level. I could not have imagined having a better supervisor and mentor for my Master thesis. Thank you for guiding me to become a better scientist.

I want to thank Sebastian Kollmann and Tania Brandstötter for their patience, excellent support and all the knowledge they shared with me. Furthermore, I would like to thank all members of the Sexl lab for making my time at the VetMed especially memorable.

Thank you to my reviewer Prof. Dr. Richard Moriggl for providing critical scientific comments and recommendations for the thesis, as well as Prof. Dr. Dieter Klein and all other professors of the Comparative Biomedicine program at the VetMed for their excellent lectures and for turning us into well-rounded scientists.

Also, I would like to say a sincere thank you to my parents and brother for their life-long support and encouragement. Last but not least, I want to thank Tobias for taking care of all my ups and downs. Thank you for always welcoming me with an open embrace and unconditional love.

## Abstract

The oncogenic fusion protein nucleophosmin-anaplastic lymphoma kinase (NPM-ALK) is predominantly found in anaplastic large cell lymphoma (ALCL), a non-Hodgkin T cell malignancy. Approximately 65% of systemic ALCL patients develop recurrent disease after first-line chemotherapy or targeted ALK inhibition. Obtaining additional insight into the mechanism of malignant transformation mediated by NPM-ALK will improve therapeutic strategies to avoid the development of resistances and patient relapse.

Signal transducer and activator of transcription 5 (STAT5) is considered a proto-oncogene in leukaemia/lymphoma, but its role in NPM-ALK-driven tumours has not been extensively studied. Besides its role in cell cycle progression, Cyclin-dependent kinase 6 (CDK6) has been shown to regulate transcription in multi-protein complexes. According to recent work in our lab, NPM-ALK tumours express high levels of CDK6, and its deletion is associated with a delayed onset of NPM-ALK-mediated thymic lymphomas in mice.

Using *Cdk6*- and *Stat5a*- or *Stat5b*-deficient *NPM-ALK<sup>+T</sup>* mouse models, we show that the combined absence of CDK6 and STAT5A or STAT5B entirely prevents the formation of thymic lymphomas. Our observation of direct interaction between CDK6 and STAT5 implies the existence of a transcriptional regulatory complex essential for NPM-ALK-mediated malignant transformation. We found indications that NPM-ALK directly and indirectly – via JAK2 – phosphorylates STAT5A and STAT5B, which function as direct effectors of malignant transformation by promoting cell growth and survival. Due to cell-intrinsic and pharmacologic limitations, we failed to observe synergistic effects when targeting kinase-independent and kinase-dependent functions of CDK6 and STAT5 activation. Performing RNA- and ChIP-sequencing in *NPM-ALK<sup>+T</sup> wt*, *Cdk6<sup>-/-</sup>*, *Stat5b<sup>-/-</sup>* and *Cdk6<sup>-/-</sup> Stat5b<sup>-/-</sup>* murine thymi – during early transformation – will allow us to pinpoint essential direct downstream effectors of CDK6 and STAT5. We infer that specific combined targeting of STAT5 and CDK6, or their common downstream effector, could provide novel treatment opportunities, leading to a beneficial and possibly curative outcome in refractory and relapsed ALK<sup>+</sup> ALCL patients.

# Table of Contents

Declaration of Honour.....	III
Acknowledgements.....	IV
Abstract.....	V
Table of Contents.....	VI
Table of Figures and Illustrations .....	IX
Table of Tables.....	XI
List of Abbreviations .....	XII
Erythroid-associated factor .....	XV
<b>1 Introduction.....</b>	<b>1</b>
1.1 <i>Blood cancers – leukaemia and lymphomas</i> .....	1
1.2 <i>Anaplastic large cell lymphoma</i> .....	1
1.2.1 Classification.....	2
1.2.2 Primary Cutaneous and Systemic ALCL.....	2
1.2.3 ALK <sup>+</sup> and ALK <sup>-</sup> systemic ALCL .....	2
1.3 <i>NPM-ALK-driven ALCL</i> .....	3
1.3.1 NPM-ALK transgenic murine model.....	4
1.3.2 ALK deregulation through the NPM-ALK fusion protein.....	4
1.3.3 Oncogenic NPM-ALK signalling .....	5
1.4 <i>Treatment of ALK<sup>+</sup> ALCL</i> .....	8
1.5 <i>Thymus and T cell development</i> .....	9
1.5.1 Normal T cell development.....	9
1.5.2 NPM-ALK in T cell development.....	10
1.6 <i>JAK-STAT signalling</i> .....	11
1.6.1 STAT5A and STAT5B .....	14
1.6.2 STAT5A/B regulation of T cell development .....	15
1.6.3 The role of JAK-STAT5 in leukaemia and lymphoma .....	16
1.6.4 Inhibitors of JAK-STAT signalling .....	17
1.6.5 STAT5A/B as potential opponents in NPM-ALK <sup>+</sup> lymphoma .....	19
1.7 <i>CDKs and the cell cycle</i> .....	19
1.7.1 Kinase-dependent functions of CDK6 .....	20
1.7.2 Kinase-independent functions of CDK6 .....	22
1.7.3 The role of CDK6 in T cell development.....	23
1.7.4 The role of CDK6 in leukaemia and lymphoma.....	24
1.7.5 CDK6 in NPM-ALK <sup>+</sup> lymphoma.....	24
1.7.6 CDK6 inhibitors and degraders .....	24
1.8 <i>The connection between CDK6 and STAT5</i> .....	25
1.9 <i>Thesis aim</i> .....	25
<b>2 Materials and Methods .....</b>	<b>26</b>
2.1 <i>Materials</i> .....	26
2.1.1 Reagents.....	26

## VII

2.1.2	Buffers .....	28
2.1.3	Consumables .....	29
2.1.4	Devices .....	30
2.1.5	Cell lines .....	31
2.1.6	Animals.....	32
2.1.7	Primers .....	33
2.1.8	Antibodies .....	33
2.2	<i>Methods</i> .....	36
2.2.1	Generation of <i>in vivo</i> <i>NPM-ALK<sup>+T</sup></i> mouse models .....	36
2.2.2	Ageing of <i>NPM-ALK<sup>+T</sup></i> mouse models .....	36
2.2.3	Tissue collection and processing.....	36
2.2.4	Genotyping .....	37
2.2.5	Tissue histology .....	38
2.2.6	Cell culture .....	39
2.2.7	Growth curve.....	40
2.2.8	Limiting cell dilution assay .....	41
2.2.9	Pharmacological perturbations.....	41
2.2.10	shRNA-mediated knockdown of <i>NPM-ALK<sup>+T</sup></i> cell lines .....	42
2.2.11	Generation of Ba/F3 <i>NPM-ALK</i> -expressing cell line .....	43
2.2.12	<i>Ex vivo</i> <i>NPM-ALK</i> -mediated transformation of BM cells .....	44
2.2.13	Colony formation assay (CFA) .....	44
2.2.14	Flow cytometry .....	45
2.2.15	Western blotting .....	46
2.2.16	Co-immunoprecipitation (co-IP) .....	49
2.2.17	mRNA expression analysis.....	50
2.2.18	Statistical analysis and reproducibility.....	51
<b>3</b>	<b>Results</b> .....	<b>53</b>
3.1	<i>Combined absence of CDK6 and STAT5A or STAT5B inhibits NPM-ALK-driven thymic lymphoma development</i> .....	53
3.2	<i>NPM-ALK is present in NPM-ALK<sup>+</sup> Cdk6<sup>-/-</sup> Stat5a<sup>-/-</sup> and NPM-ALK<sup>+</sup> Cdk6<sup>-/-</sup> Stat5b<sup>-/-</sup> thymi</i> .....	57
3.3	<i>NPM-ALK<sup>+</sup> Cdk6<sup>-/-</sup> Stat5a<sup>-/-</sup> and NPM-ALK<sup>+</sup> Cdk6<sup>-/-</sup> Stat5b<sup>-/-</sup> thymi have an unaltered cell-type composition</i> .....	57
3.4	<i>Cdk6<sup>-/-</sup> Stat5a<sup>-/-</sup> and Cdk6<sup>-/-</sup> Stat5b<sup>-/-</sup> BM cells fail to undergo NPM-ALK-mediated transformation..</i>	59
3.5	<i>Generation of primary murine NPM-ALK<sup>+</sup> cell lines</i> .....	62
3.6	<i>NPM-ALK<sup>+</sup> Stat5a<sup>-/-</sup> and Stat5b<sup>-/-</sup> cells regain the expression of transcriptionally silenced Cdk6</i> .....	62
3.7	<i>NPM-ALK<sup>+</sup> cell line characterisation</i> .....	65
3.7.1	The absence of STAT5A or STAT5B results in a proliferation defect .....	65
3.7.2	Cell cycle shift and increased apoptosis in <i>Stat5b<sup>-/-</sup></i> cells.....	66
3.7.3	Conditioned medium rescues the growth defect of <i>Stat5a<sup>-/-</sup></i> or <i>Stat5b<sup>-/-</sup></i> cell lines .....	68
3.7.4	Increased pY-STAT3/5 levels in the absence of CDK6.....	69
3.8	<i>Pharmacological inhibition of NPM-ALK<sup>+</sup> cell lines</i> .....	71
3.8.1	<i>Stat5a</i> , <i>Stat5b</i> or <i>Cdk6</i> deficiency does not sensitise <i>NPM-ALK<sup>+</sup></i> cells to ALK inhibition .....	71
3.8.2	<i>Stat5a</i> or <i>Stat5b</i> deficiency fails to sensitise <i>NPM-ALK<sup>+</sup></i> cells to kinase inhibition or degradation of CDK6 .....	72
3.8.3	<i>Cdk6</i> deficiency fails to sensitise <i>NPM-ALK<sup>+</sup></i> cells to (pan-)JAK inhibition .....	74
3.8.4	PDGFR inhibition .....	75
3.9	<i>Pharmacological perturbations of CDK6 and STAT5 activation do not result in synergistic effects..</i>	76
3.9.1	Combined inhibition of JAK1/2 and CDK6.....	77
3.9.2	Targeting ALK alongside CDK6 .....	78
3.10	<i>ALK- or pan-JAK-inhibition diminishes pY-STAT5 levels</i> .....	80

## VIII

3.11	<i>NPM-ALK – directly and indirectly – phosphorylates STAT5 proteins.....</i>	81
3.12	<i>STAT5A and STAT5B physically interact with CDK6.....</i>	85
<b>4</b>	<b>Discussion.....</b>	<b>86</b>
4.1	<i>STAT5A and STAT5B display oncogenic properties in NPM-ALK<sup>+</sup> lymphoma.....</i>	86
4.2	<i>CDK6 and STAT5A or STAT5B deficiencies are incompatible in NPM-ALK-driven transformation and disease.....</i>	87
4.3	<i>The absence of CDK6 triggers compensatory mechanisms in NPM-ALK<sup>+</sup> cells.....</i>	88
4.4	<i>Cytokines facilitate growth and survival of transformed NPM-ALK<sup>+</sup> Stat5a<sup>-/-</sup> and Stat5b<sup>-/-</sup> cells in overcoming their proliferation disadvantage.....</i>	88
4.5	<i>Targeting of CDK6 and STAT5 in transformed NPM-ALK<sup>+</sup> cells.....</i>	90
4.5.1	<i>NPM-ALK directly phosphorylates STAT5A/B, thereby contributing to JAK-inhibitor insensitivity.....</i>	90
4.5.2	<i>CDK6 kinase-independent functions seem to be important in NPM-ALK<sup>+</sup> lymphoma progression.....</i>	91
4.5.3	<i>Combinatorial treatments resulted in additive but not synergistic effects.....</i>	92
4.6	<i>STAT5A and STAT5B directly interact with CDK6, driving NPM-ALK-mediated transformation and disease maintenance.....</i>	93
4.7	<i>The interplay between STAT5A/B, CDK6 and NPM-ALK.....</i>	94
<b>5</b>	<b>Outlook.....</b>	<b>96</b>
<b>6</b>	<b>Conclusion.....</b>	<b>100</b>
<b>7</b>	<b>References.....</b>	<b>101</b>

## Table of Figures and Illustrations

<b>Figure 1: Classification of ALCL subtypes and drivers of the disease</b> .....	3
<b>Figure 2: Structure scheme of wild type ALK and NPM-ALK fusion protein</b> .....	4
<b>Figure 3: The oncogenic effects of constitutive NPM-ALK signalling in ALCL are mediated by a complex network of redundant and interacting pathways</b> .....	8
<b>Figure 4: Schematic overview on canonical JAK-STAT signalling</b> .....	13
<b>Figure 5: STAT proteins induce transcription through four distinct mechanisms</b> .....	13
<b>Figure 6: Cytokines and their respective JAKs signalling over STAT5</b> .....	15
<b>Figure 7: Adverse effects of JAK-inhibition</b> .....	18
<b>Figure 8: Cell cycle phases and their essential CDK-Cyclin complexes</b> .....	20
<b>Figure 9: Cyclin fluctuation in the cell cycle</b> .....	21
<b>Figure 10: Regulation of the G1/S transition</b> .....	21
<b>Figure 11: The kinase-dependent and kinase-independent functions of CDK6 in cancer</b> .....	23
<b>Figure 12: Schematic map of pLENC vector</b> .....	42
<b>Figure 13: <i>Cdk6</i><sup>-/-</sup> NPM-ALK<sup>+T</sup> <i>Stat5a</i><sup>-/-</sup> and <i>Cdk6</i><sup>-/-</sup> NPM-ALK<sup>+T</sup> <i>Stat5b</i><sup>-/-</sup> are born at a submendelian ratio</b> .....	54
<b>Figure 14: The concomitant absence of CDK6 and STAT5A or STAT5B prevents NPM-ALK-driven transformation</b> .....	55
<b>Figure 15: H&amp;E staining of experiment endpoint samples</b> .....	56
<b>Figure 16: NPM-ALK protein is present in the thymi of NPM-ALK<sup>+</sup> <i>Cdk6</i><sup>-/-</sup> <i>Stat5a</i><sup>-/-</sup> and <i>Cdk6</i><sup>-/-</sup> <i>Stat5b</i><sup>-/-</sup> mice</b> .....	57
<b>Figure 17: No significant changes in thymic cell populations in the absence of CDK6 and/or STAT5B in the NPM-ALK transgenic model</b> .....	58
<b>Figure 18: <i>Cdk6</i><sup>-/-</sup> <i>Stat5a</i><sup>-/-</sup> and <i>Cdk6</i><sup>-/-</sup> <i>Stat5b</i><sup>-/-</sup> BM cells fail to transform during ex vivo NPM-ALK-infection</b> .....	60
<b>Figure 19: Colony formation is positively correlated with Sca-1 expression on GFP<sup>+</sup> cells</b> .....	61
<b>Figure 20: Numbers of established primary murine cell lines</b> .....	62
<b>Figure 21: sh<i>Cdk6</i> infected NPM-ALK<sup>+</sup> cells display a growth disadvantage compared to sh<i>Renilla</i> controls</b> .....	63
<b>Figure 22: shRNA-mediated knockdown of <i>Cdk6</i> is incompatible with <i>Stat5a</i><sup>-/-</sup> and <i>Stat5b</i><sup>-/-</sup></b> .....	64
<b>Figure 23: NPM-ALK<sup>+</sup> <i>Stat5a</i><sup>-/-</sup> and <i>Stat5b</i><sup>-/-</sup> cell lines display a growth disadvantage compared to NPM-ALK<sup>+</sup> wt</b> .....	66
<b>Figure 24: NPM-ALK<sup>+</sup> <i>Stat5a</i><sup>-/-</sup> and <i>Stat5b</i><sup>-/-</sup> cells display a growth disadvantage and undergo increased apoptosis</b> .....	68
<b>Figure 25: The growth disadvantage of NPM-ALK<sup>+</sup> <i>Stat5a</i><sup>-/-</sup> and <i>Stat5b</i><sup>-/-</sup> is partially rescued by conditioned medium</b> .....	69
<b>Figure 26: Transformed <i>Cdk6</i><sup>-/-</sup> cell lines harbour increased levels of pY-STAT5 and pY-STAT3</b> .....	70
<b>Figure 27: Healthy NPM-ALK<sup>+</sup> <i>Cdk6</i><sup>-/-</sup> thymic tissue express high levels of pY-STAT5</b> .....	71
<b>Figure 28: All NPM-ALK<sup>+</sup> genotypes react similarly to ALK inhibition</b> .....	72
<b>Figure 29: No genotype difference in response to CDK6 inhibitor or degrader</b> .....	74
<b>Figure 30: NPM-ALK<sup>+</sup> cells lines are not sensitive to JAK-inhibition</b> .....	75
<b>Figure 31: NPM-ALK<sup>+</sup> cells lines do not respond to PDGFR inhibition</b> .....	76
<b>Figure 32: Kinase inhibition or degradation of CDK6 combined with JAK1/2 kinase inhibition results in an additive but not a synergistic effect</b> .....	78
<b>Figure 33: Kinase inhibition or degradation of CDK6 combined with ALK inhibition results in an additive but not a synergistic effect</b> .....	79
<b>Figure 34: ALK inhibitor Crizotinib and the CDK6 degrader BSJ-03-123 show the highest Bliss synergy score</b> .....	80
<b>Figure 35: NPM-ALK inhibitors diminish pY-STAT5 levels</b> .....	81

<b>Figure 36: NPM-ALK-infected parental Ba/F3 cell line exhibits increased protein levels of the transgene.....</b>	<b>83</b>
<b>Figure 37: IC<sub>50</sub> concentration of Ba/F3 cells is highly dependent on the addition of IL-3.....</b>	<b>83</b>
<b>Figure 38: NPM-ALK directly and indirectly via JAK2 phosphorylates STAT5.....</b>	<b>84</b>
<b>Figure 39: CDK6 physically associates with STAT5A and STAT5B.....</b>	<b>85</b>
<b>Figure 40: NPM-ALK uncouples canonical JAK2-STAT5 signalling.....</b>	<b>91</b>
<b>Figure 41: Proposed regulation mechanism of NPM-ALK-mediated malignant transformation via CDK6 and STAT5 proteins.....</b>	<b>94</b>
<b>Figure 42: The NPM-ALK transgene is expressed in DN and DP thymocytes.....</b>	<b>98</b>

## Table of Tables

<b>Table 1: Reagents</b> .....	26
<b>Table 2: Buffers</b> .....	28
<b>Table 3: Consumables</b> .....	29
<b>Table 4: Devices</b> .....	30
<b>Table 5: Cell lines</b> .....	32
<b>Table 6: Mouse strains</b> .....	32
<b>Table 7: Primers for qPCR</b> .....	33
<b>Table 8: Primers for genotyping</b> .....	33
<b>Table 9: Primary antibodies used for protein analysis by Western blot</b> .....	33
<b>Table 10: Secondary antibodies used for protein analysis by Western blot</b> .....	34
<b>Table 11: Immunoprecipitation Antibodies</b> .....	34
<b>Table 12: Flow Cytometry Antibodies and dyes</b> .....	34
<b>Table 13: Immunohistochemistry Antibodies</b> .....	35
<b>Table 14: Plasmids</b> .....	35
<b>Table 15: PCR reaction mix</b> .....	38
<b>Table 16: Recipe for stacking and separation gels</b> .....	47
<b>Table 17: iScript cDNA synthesis reaction mix</b> .....	50
<b>Table 18: qPCR reaction mix</b> .....	51

## List of Abbreviations

AKT, PKB	Protein kinase B
ALCL	Anaplastic large cell lymphoma
ALK	Anaplastic lymphoma kinase
AP1	Activator protein 1
APS	Ammonium persulfate
AXL	AXL receptor tyrosine kinase
BCL-2	B cell lymphoma 2
BCL2A1	BCL-2-related protein A1
BCL-x <sub>L</sub>	BCL-like 1
BCL2L11, BIM	BCL-2-like protein 11
BCR-ABL	Abelson-breakpoint cluster region
BM	Bone marrow
BSA	Bovine serum albumin
C/EBP $\beta$	CCAAT/enhancer-binding protein, beta
CD	Cluster of differentiation
CDC42	Cell division cycle 42
CDK	Cyclin-dependent kinase
CDKN	Cyclin-dependent kinase inhibitors
CFA	Colony forming assays
ChIP-seq	Chromatin immunoprecipitation sequencing
CIP/KIP	CDK interacting protein/Kinase inhibitory protein
KIT, CD117	c-Kit proto-oncogene
CLTCL	Clathrin heavy chain-like 1
IP	Immunoprecipitation
DMEM	Dulbecco's modified eagle medium
DMSO	Dimethyl sulfoxide
DN	Double-negative
DNAJC6	DnaJ Hsp40 homolog, Subfamily C, Member 6
DNRG1	N-myc downstream regulated 1
DNMT1	DNA methyltransferase 1
DOCS8	Dedicator of cytokinesis 8
DP	Double-positive

### XIII

DUSP22	Dual specificity phosphatase 22
EGFR	Epidermal growth factor receptor
EPO	Erythropoietin
ERBB4	ERB-B2 receptor tyrosine kinase 4
ERK	Extracellular signal-regulated kinases
FACS	Fluorescence-activated cell sorting
FCS	Fetal calf serum
FELASA	Federation for Laboratory Animal Science Association
FGFR	Fibroblast growth factor receptor
FFPE	Formalin-fixed paraffin-embedded
FLT3-ITD	FMS-like tyrosine kinase 3 - internal tandem duplication
FOS	Fos proto-oncogene
FOXO3A	Forkhead box O3A
FOXP3	Forkhead box P3
G0, G1, G2	Gap phase 0, 1, 2
GAB2	GRB2-associated-binding protein 2
GAS	Gamma interferon activation sites
GATA3	GATA-binding protein 3
GFP	Green fluorescent protein
GH	Growth hormone
GM	Granulocyte-macrophage
GRB2	Growth factor receptor-bound protein 2
H&E	Hematoxylin and Eosin
HER2	ERB-B2 receptor tyrosine kinase 2
HSC	Hematopoietic stem cell
HSC-70	Heat shock protein 70
IC50	Inhibitory concentration
IFN	Interferon
IHC	Immunohistochemistry
IL	Interleukin
IL2RA	Interleukin 2 receptor, alpha
IR	Insulin receptor
IRES	Internal ribosome entry site
JAK	Janus kinase

JAKinib	JAK inhibitor
JNK	JUN N-terminal kinase
JUN	V-jun avian sarcoma virus 17 oncogene homolog
JUNB	JunB proto-oncogene
KD	Kinase domain
Ki67	Kiel antibody hybridoma 67
LCK	lymphocyte-specific protein tyrosine kinase
LEF1	Lymphoid enhancer binding factor 1
LIF	Leukemia inhibitory factor
LSC	Leukemia stem cell
MAPK	Mitogen-activated protein kinase
MAP3K5	Mitogen-activated protein kinase kinase kinase 5
MCL1	Myeloid cell leukaemia sequence 1
MET	Mesenchymal-epithelial transition factor
MFI	Median fluorescence intensity
MFI	Median fluorescence intensity
MPN	Myeloproliferative neoplasm
mTOR	Mechanistic target of Rapamycin
MYC	Myc proto-oncogene
NANOG	Nanog homeobox
NDRG1	N-myc downstream regulated 1
NF- $\kappa$ B	Nuclear factor kappa-B
NHL	Non-hodgkin lymphoma
NK	Natural killer
NOTCH2	Notch receptor 1
NPM1, NPM	Nucleophosmin
NTC	Non-template control
OCT4	Octamer-binding transcription factor 4
OSM	Oncostatin M
PDGFR	Platelet-derived growth factor receptor
PI	Propidium iodide
PI3K	Phosphoinositide 3-kinase
PIM	Pim-1 proto-oncogene
Plat-E	Platinum-E

PLC- $\gamma$	Phospholipase C gamma
PTCL-NOS	Peripheral T cell lymphoma, not otherwise specified
PTPN	Protein tyrosine phosphatase, non-receptor type
PVDF	Polyvinylidene fluoride
pXX	Protein XX
pY-XXX	Tyrosine phosphorylated protein
RAC1	Ras-related C3 botulinum toxin substrate 1
RANBP2	Ran-binding protein 2
RAS	Rat sarcoma virus
RB	Retinoblastoma
RIPA	Radioimmunoprecipitation assay
RNA-seq	RNA sequencing
ROS1	Ros proto-oncogene 1
RTK	Receptor tyrosine kinases
RUNX3	Runt-related transcription factor 3
S	S phase
SCA-1	Spinocerebellar ataxia type 1
SCF	Stem cell factor
GM-CSF	Granulocyte-macrophage colony-stimulating factor
G-CSF	Granulocyte colony-stimulating factor
SEM	Standard error of the mean
SGK1	Serum/glucocorticoid regulated kinase 1
SH2	Src Homology 2
SHPX	Protein-tyrosine phosphatase XC
shRNA	Short hairpin RNA
SNX9	Sorting nexin 9
SOCS	Suppressor of cytokine signalling
SOS1	Son of sevenless
SOX2	SRY-box 2
SSH2	Slingshot protein phosphatase 2
STAT	Signal transducer and activator of transcription
TCR	T cell receptor
TEMED	Tetramethylethylenediamine
TER-119	Erythroid-associated factor

TFG	TRK-fused gene
THY1.2	Thymocyte antigen 1.2
TNF	Tumour necrosis factor
Tp53, p53	Tumour protein 53
TPO	Thrombopoietin
TYK2	Tyrosine kinase 2
VAV	Vav proto-oncogene
VEGF-A	Vascular endothelial growth factor A
WT	Wild type
X <sup>-</sup>	X-negative
X <sup>+</sup>	X-positive
XXX	Homo sapiens or Mus musculus protein
XXX	Homo sapiens gene
Xxx	Mus musculus gene
ZAP	Zeta-chain-associated protein kinase 70

# 1 Introduction

## 1.1 Blood cancers – leukaemia and lymphomas

In 2020, 19.3 million new cancer cases were diagnosed worldwide, accompanied by 10.0 million cancer-caused deaths (Sung et al., 2021). Compared to the most common cancer types – lung (11.7% incidence) and breast (11.4% incidence) – blood cancers are considered rare. Blood cancers are subdivided into four major categories: Leukaemia (2.5%), multiple myeloma (0.9%), Hodgkin (0.4%) and non-Hodgkin lymphomas (2.8%). Nevertheless, they make up a significant 6.6% of all cancer incidence worldwide (Sung et al., 2021). Due to the heterogeneous nature of blood cancers, it has been impossible to develop targeted therapies for all of them. Thus, despite significant advances in diagnosis and treatment for some blood cancers, many lymphomas, leukaemias, and multiple myelomas remain a significant public health concern.

## 1.2 Anaplastic large cell lymphoma

Non-Hodgkin lymphoma (NHL) is a lymphoid tissue neoplasm originating from precursor or mature B, T or natural killer (NK) cells. T cell NHLs represent a heterogeneous spectrum of lymphoid malignancies, with different immunophenotypic, genetic and clinical features, as well as various aetiologies and responses to therapy. The most prevalent subtypes of T cell NHLs are: peripheral T cell lymphoma, not otherwise specified (PTCL-NOS; 26%), angioimmunoblastic T cell lymphoma (19%), anaplastic large cell lymphoma (ALCL, 12%), adult T cell leukaemia/lymphoma (10%) and extra-nodal NK/T cell lymphoma (10%) (Vose et al., 2008).

ALCL is a very aggressive form of lymphoma, causing chemotherapy resistance and recurrent disease in 40–65% of patients (Huang et al., 2018), most frequently in children. The requirement for further treatment options leads us to focus on a specific subtype of ALCL driven by aberrant anaplastic lymphoma kinase (ALK) rearrangements, in short, ALK-positive (ALK<sup>+</sup>) ALCL.

### 1.2.1 Classification

ALCL is a biologically and clinically heterogeneous subtype of T cell lymphoma, affecting children and adults. It is distinguished by its aberrant anaplastic cytology and constant high membrane expression of the cluster of differentiation (CD)30 molecule, a member of the tumour necrosis factor (TNF) receptor superfamily (Stein et al., 1985). ALCL characteristically forms cohesive clusters of large pleomorphic cells with a high mitosis rate (ten Berge et al., 2003). Large kidney-shaped cells are “hallmark cells” for this type of tumour, although 10–20% ALK<sup>+</sup> ALCL tumours have also been shown to contain small cells and lymphohistiocytic variants (Klapper et al., 2008).

### 1.2.2 Primary Cutaneous and Systemic ALCL

ALCL presents as two distinct entities – a localised (primary) cutaneous disease or widespread systemic disease (**Figure 1**) – each with different clinical and biologic features (Stein et al., 2000). Primary cutaneous ALCL is a lymphoproliferative disease of the skin with 5-year disease-free survival rates of > 90% (Querfeld et al., 2010). The systemic ALCL type is an aggressive lymphoma that generally affects primary and secondary lymphatic organs (e.g., thymus and lymph nodes) but may secondarily involve the skin and other extra-nodal sites (Savage et al., 2008).

### 1.2.3 ALK<sup>+</sup> and ALK<sup>-</sup> systemic ALCL

Systemic ALCL is further subdivided based on the expression of the ALK protein – into ALK-positive (ALK<sup>+</sup>) and ALK-negative (ALK<sup>-</sup>) ALCL (**Figure 1**). ALK<sup>+</sup> ALCL exhibits a chromosomal translocation involving the ALK gene, leading to its aberrant expression (S. W. Morris et al., 1994). ALK<sup>+</sup> ALCLs shows a broad morphogenic spectrum, always manifesting in cells with eosinophilic regions near their horseshoe- or kidney-shaped nuclei (Benharroch et al., 1998).

Alongside the common uniform CD30 expression, ALK<sup>-</sup> ALCL also morphologically resembles ALK<sup>+</sup> ALCL but lacks the characteristic ALK protein expression (Medeiros & Elenitoba-Johnson, 2007). Nevertheless, ALK<sup>-</sup> ALCL differs from ALK<sup>+</sup> ALCL in a clinically worse survival and higher expression of the immunophenotypical markers CD2 and CD3 (Savage et al., 2008). The development of next-generation sequencing technologies has identified an increasing number of mutations or enhanced expression of oncogenes, as well as lost tumour suppressors in ALK<sup>-</sup> ALCL. Loss of function alterations have been identified in the tumour suppressors: Dual specificity phosphatase 22 (*DUSP22*) and Tumour protein p63 (*TP63*)

(Parrilla Castellar et al., 2014; Vasmatazis et al., 2012). Furthermore, gain of function alterations of proto-oncogenes, more specifically activating rearrangements involving Ros proto-oncogene 1 (*ROS1*) and Tyrosine kinase 2 (*TYK2*), as well as overexpression of ERBB2 receptor tyrosine kinase 4 (*ERBB4*) (Scarfo et al., 2016) and hyperactivating mutations in Janus kinase (*JAK*)1/Signal transducer and activator of transcription (*STAT*)3 genes (Crescenzo et al., 2015; Luchtel et al., 2019) have also been recently identified.

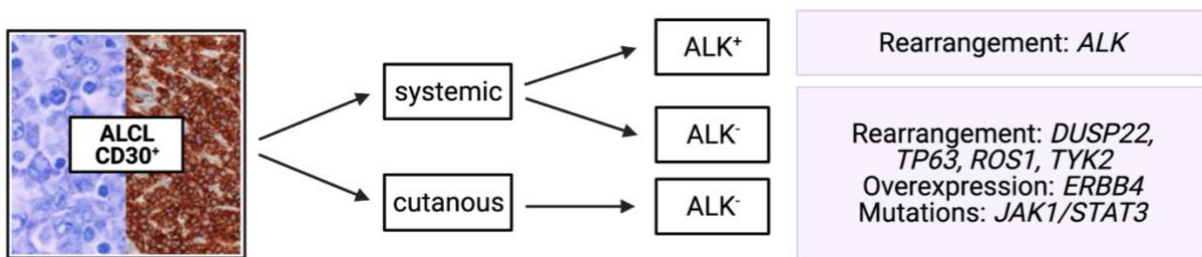


**Figure 1: Classification of ALCL subtypes and drivers of the disease** (adapted from (Gaulard & de Leval, 2016))

CD30<sup>+</sup> ALCL is subdivided into systemic and cutaneous ALCL, which are further differentiated based on ALK expression. Systemic ALCL presents as ALK<sup>+</sup> or ALK<sup>-</sup>, while cutaneous ALCL mainly presents as ALK<sup>-</sup>. ALK<sup>+</sup> ALCL is driven by rearrangements of the *ALK* kinase, mainly the NPM-*ALK* translocation. ALK<sup>-</sup> ALCL may carry *DUSP22*, *TP63*, *ROS1*, *TYK2* rearrangements, *ERBB4* overexpression or even mutations of the *JAK1/STAT3* axis (Gaulard & de Leval, 2016).

### 1.3 NPM-ALK-driven ALCL

The *ALK* gene has been shown to fuse with multiple targets in ALK<sup>+</sup> ALCL, including the TRK-fused gene (*TFG*), Clathrin heavy chain-like 1 (*CLTCL*) and Ran-binding protein 2 (*RANBP2*) (Duyster et al., 2001). However, ALK is most frequently activated through the non-random t(2;5) chromosome translocation, which causes the fusion of the ubiquitously expressed Nucleophosmin 1 (NPM1, also NPM) to the receptor tyrosine kinase *ALK* gene (S. W. Morris et al., 1994; Shiota et al., 1994). The oncogenic NPM-*ALK* fusion protein is considered to drive more than 70% of all CD30-positive (CD30<sup>+</sup>) ALCL cases, leading to enhanced proliferation and survival of tumour cells (Andraos et al., 2021). However, the mechanism of malignant transformation mediated by the constitutively active NPM-*ALK* tyrosine kinase is not yet fully understood. Its better understanding will improve therapeutic strategies to avoid the development of resistances and relapses (Andraos et al., 2021; Sharma et al., 2018).

### 1.3.1 NPM-ALK transgenic murine model

A vital model for dissecting the molecular mechanisms of ALK-mediated transformation was developed in 2003 by Roberto Chiarle et al., in which the transcription of the human NPM-ALK is driven by the CD4 promoter, thereby restricting its expression to T cells. These mice were born with the anticipated Mendelian distribution and healthy lymphoid organs, including an expected quantity and proportion of helper and suppressor T cells. However, all NPM-ALK transgenic mice developed malignant lymphoproliferative diseases – primarily thymic lymphomas – after a brief latency period. Interestingly, the thymic lymphomas displayed an immature T cell phenotype and frequently expressed the CD30 surface marker (Chiarle et al., 2003).

### 1.3.2 ALK deregulation through the NPM-ALK fusion protein

ALK is a transmembrane receptor tyrosine kinase (RTK) and belongs to the Insulin receptor (IR) superfamily. It is transiently expressed in specific central and peripheral nervous systems regions and reaches a maximum expression level around birth (reviewed by Chiarle et al., 2008). The human *ALK* gene encodes a protein of 1,620 amino acids giving rise to a protein of approximately 180 kDa (**Figure 2a**), which – through post-translational modifications (such as N-linked glycosylation) – appears as 220 kDa on SDS-PAGE gels (Iwahara et al., 1997). As an RTK, ALK dimerises upon ligand binding, thereby bringing the intracellular kinase domains into proximity. Similar to other IR family protein, the ALK kinase is activated by tyrosine trans-autophosphorylation of YxxxYY motifs within the activation loop of the kinase domain (Tartari et al., 2008).

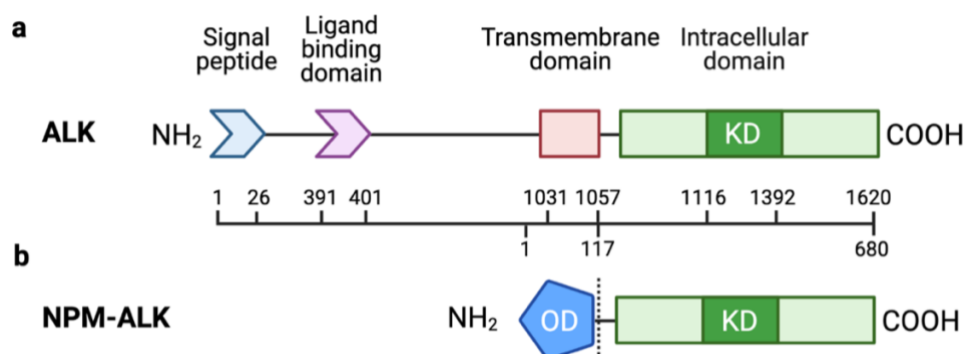


**Figure 2: Structure scheme of wild type ALK and NPM-ALK fusion protein**

**a)** Wild type ALK protein consists of the N-terminal signal peptide, ligand-binding domain, transmembrane domain and C-terminal intracellular domain. The intracellular domain also includes a kinase domain, which becomes catalytically active upon ligand binding. **b)** The NPM-ALK fusion protein consists of the ALK C-terminal intracellular domain – including the kinase domain (KD) – fused to the NPM oligomerisation domain (OD) (Kourentzi et al., 2020).

The ALK kinase acquires oncogenic transforming capabilities through the t(2;5) chromosomal rearrangement with NPM. The ALK fusion partner NPM is ubiquitously expressed in the nucleus and has been implicated in several essential cellular processes, including cell division, transcription, chromatin remodelling, genome stability and DNA repair (Lindstrom, 2011).

The fusion of the *ALK* intracellular domain to the *NPM* oligomerisation domain (OD) allows NPM-ALK to become ligand-independent (**Figure 2b**). The OD-mediated dimerisation of NPM-ALK leads to cross-autophosphorylation of the kinase domain activation loop motif, thereby constitutively activating the NPM-ALK protein (Bischof et al., 1997).

### 1.3.3 Oncogenic NPM-ALK signalling

The introduction of aberrant constitutive active tyrosine kinase activity displays clear oncogenic potential, as it leads to changes in numerous cellular processes (Duyster et al., 2001). NPM-ALK has been shown to promote cell proliferation, survival, angiogenesis and cytoskeletal rearrangements (Chiarle et al., 2003; Kuefer et al., 1997; Wellmann et al., 1997). Similar to most normal and oncogenic tyrosine kinases, oncogenic ALK transformation is mediated by altering numerous interconnected intracellular signalling pathways, including the Rat sarcoma virus (RAS)-Extracellular signal-regulated kinase 1 (ERK1, also ERK), the JAK-STAT (STAT3 being mainly studied) and the Phosphatidylinositol 3-kinase (PI3K)-Akt serine/threonine kinase (AKT) pathway (summarised in **Figure 3**) (R. Y. Bai et al., 1998; R. Y. Bai et al., 2000; Chiarle et al., 2005; Zamo et al., 2002).

#### 1.3.3.1 Proliferation

NPM-ALK has been shown to accelerate the cell cycle entry into the S phase (Wellmann et al., 1997), accompanied by significant upregulation of Cyclin A and Cyclin D1 and enhanced expression of proliferation genes – Fos proto-oncogene (*FOS*), V-jun avian sarcoma virus 17 oncogene homolog (*JUN*) and Myc proto-oncogene (*MYC*) (Chiarle et al., 2008).

Furthermore, NPM-ALK acts as a docking molecule for numerous adaptors and scaffolding molecules, which aid to activate downstream signalling pathways, including the RAS-ERK pathway (Fujimoto et al., 1996; Pulford et al., 2004). Involvement of the Protein-tyrosine phosphatase 2C (SHP2, also known as PTPN11) in NPM-ALK-mediated cell proliferation has recently been described. NPM-ALK-activated SHP2 stimulates ALCL growth through ERK1/2 phosphorylation, probably as the result of its binding to Growth factor receptor-bound protein

2 (GRB2)–Son of sevenless 1 (SOS1) complex (Sattler et al., 2002; Voena et al., 2007). In contrast to the increased activity of SHP2, a loss of the Protein-tyrosine phosphatase 1C (SHP1, also known as PTPN6), caused by hypermethylation of its promoter, occurs in approximately 50% of ALCL cases (Honorat et al., 2006). SHP1 acts as a tumour-suppressor gene, and its absence is usually correlated with uncontrolled cell growth, predominantly through activation of the JAK3-STAT3 pathway (Han et al., 2006).

It has been shown that NPM-ALK phosphorylates JUN N-terminal kinase (JNK) and leads to the upregulation of the Activator protein 1 (AP1) transcription factor family members. For example, the upregulation of JUN leads to the downregulation of the Cyclin-dependent kinase inhibitor (CDKN) 1A (p21) and simultaneous upregulation of Cyclins D3 and A, causing uncontrolled cell-cycle progression (Leventaki et al., 2007; Wellmann et al., 1997).

Phospholipase C-gamma (PLC $\gamma$ ) also binds to phosphorylated tyrosine residues of NPM-ALK via its Src homology 2 (SH2) domain and contributes to NPM-ALK-mediated transformation (R. Y. Bai et al., 2000).

### **1.3.3.2 Survival**

Enhanced survival in ALCL is derived from ALK-mediated activation of numerous signalling cascades, mainly JAK-STAT and PI3K-AKT, that promote the expression of several anti-apoptotic gene products, including BCL-2-like 1 (BCL-x<sub>L</sub>) and Forkhead box O3A (FOXO3A) (R. Y. Bai et al., 2000; Chiarle et al., 2008; Gu et al., 2004; Zamo et al., 2002; Zhang et al., 2002).

In addition, STAT3 has a central role in numerous haematopoietic malignancies, including NPM-ALK mediated tumorigenesis (Chiarle et al., 2005; Zamo et al., 2002). NPM-ALK can directly phosphorylate STAT3 or JAK3, which can further contribute to STAT3 activation (Amin et al., 2003; Zamo et al., 2002). Activated STAT3 promotes the expression of anti-apoptotic factors and cell-cycle regulators, such as BCL-x<sub>L</sub>, Survivin, Cyclin D3, CCAAT/Enhancer-binding protein beta (C/EBP $\beta$ ) and Myeloid cell leukaemia sequence 1 (MCL1) among many other gene products (Coluccia et al., 2004; Piva et al., 2006; Zamo et al., 2002).

STAT5A and STAT5B have been shown to regulate the expression of anti-apoptotic factors – such as B cell lymphoma 2 (BCL-2), BCL-x<sub>L</sub>, and MCL1 in various haematopoietic malignancies (summarised by (Maurer et al., 2019)). Inhibition of STAT5B significantly impairs

NPM-ALK-induced transformation *in vitro* and *in vivo* by triggering apoptosis (Ruchatz et al., 2003). STAT5B, but not STAT5A, has also been proposed as a mediator of the transforming properties of NPM-ALK (Zhang et al., 2007), although studies suggest that JAK2 is required for the mechanism of activation (Nieborowska-Skorska et al., 2001).

In ALCL cells, NPM-ALK binds to and activates PI3K via the regulatory p85 subunit, triggering activation of its downstream effectors AKT1/2 (R. Y. Bai et al., 2000). Stimulation of PI3K-AKT pathway results in the control of the cell cycle through the phosphorylation of the CDK inhibitor p27, increasing its proteasomal degradation (Slupianek & Skorski, 2004). Moreover, NPM-ALK-mediated AKT-activation leads to FOXO3A phosphorylation, its exclusion from the nucleus, thereby preventing its transcriptional activity (Gu et al., 2004). This results in the upregulation of Cyclin D2, downregulation of BCL-2-Like 11 (BCL2L11, also known as BIM) and CDKN1B (p27) that together results in cancer cell survival and cell-cycle progression (Gu et al., 2004). In ALCL, the activation of the mammalian target of rapamycin (mTOR) and its target proteins are mainly transduced by the RAS-ERK cascade (Marzec et al., 2007). The mTOR inhibitor rapamycin strongly affects cell growth and induces apoptosis in ALCL cells (Marzec et al., 2007).

#### **1.3.3.3 Cell migration and cytoskeletal rearrangements**

ALCL is associated with peculiar anaplastic histomorphological features (including changes in cell shape), which are associated with an increased cell migration rate of lymphoid cells *in vitro* (Ambrogio et al., 2005; Armstrong et al., 2004; Chiarle et al., 2008; Stein et al., 2000; Voena et al., 2007). These effects are the consequence of aberrant ALK tyrosine kinase activity on key regulators of cytoskeletal rearrangements. Transformation by oncogenic ALK induces actin filament depolymerisation and loss of cell-matrix adhesion (Ambrogio et al., 2005), thereby influencing the morphology, migration and transformation of ALK-expressing tumour cells (Ambrogio et al., 2005; Voena et al., 2007). A prime example is ALK-mediated modulation of the Rhodopsin family GTPase activity, which results in RAS-related c3 botulinum toxin substrate 1 (RAC1) activation, increasing cell migration and invasion (Chiarle et al., 2008; Colomba et al., 2008).

#### **1.3.3.4 Immunophenotype**

ALCL is immunophenotypically characterised by the sustained expression of CD30, modulated by ALK-mediated STAT3 phosphorylation, and ERK1/2 signalling, which induces the

expression of the JunB proto-oncogene (JUNB) (Hsu et al., 2006). The engagement of CD30 by its natural ligand CD30L activates both the canonical and the alternative NF $\kappa$ B pathways, resulting in pleiotropic effects, including proliferation, differentiation, cell-cycle inhibition and apoptosis (Wright et al., 2007). Nevertheless, the full contribution of CD30 expression to ALCL pathogenesis is still unclear.

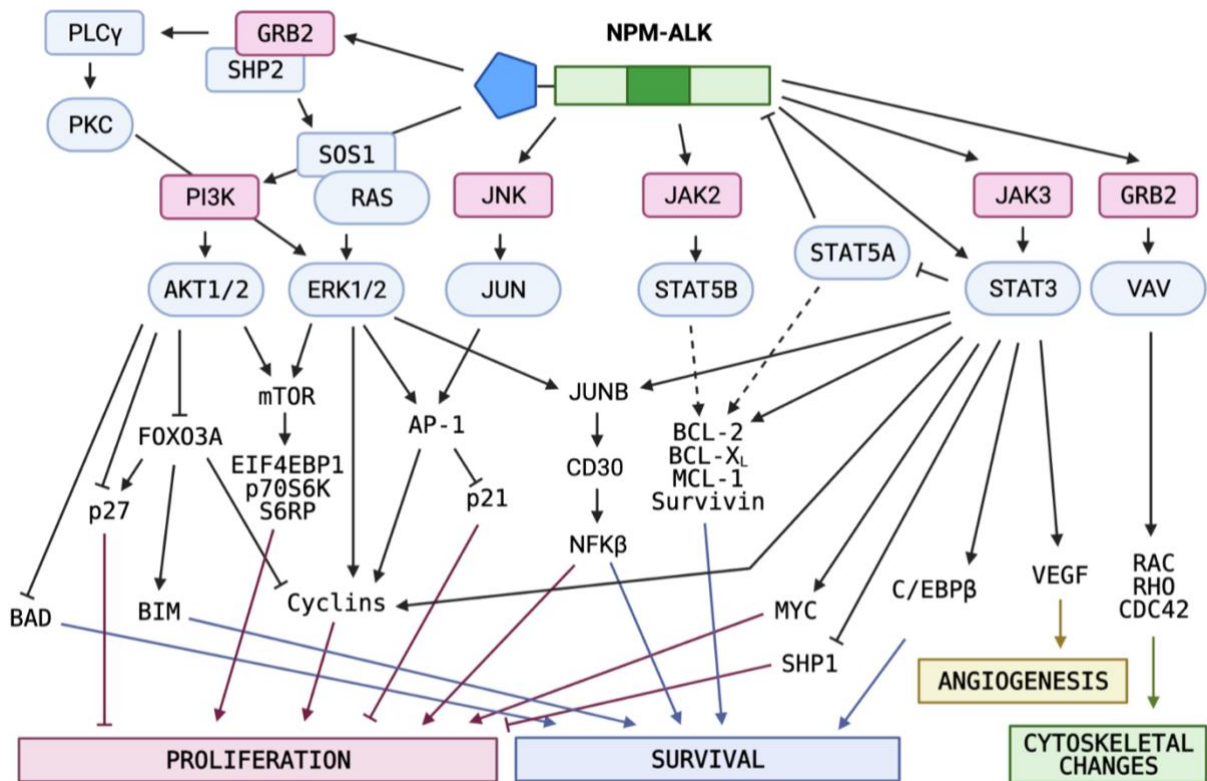


**Figure 3: The oncogenic effects of constitutive NPM-ALK signalling in ALCL are mediated by a complex network of redundant and interacting pathways**

So far, only a few of the fusion protein's potential phosphorylation sites have been characterised for ligand binding. NPM-ALK is linked to various signalling pathways, including the PI3K, Mitogen-activated protein kinase (MAPK), and JAK-STAT pathways, through the signalosome formation, attracted to the fusion protein. Their downstream effectors control major cellular functions – proliferation, survival, angiogenesis and cytoskeletal rearrangements. Full lines represent confirmed signalling mechanism in NPM-ALK-driven ALCL, while dotted lines represent signalling mechanisms confirmed in other haematological malignancies. Protein Kinase C (PKC), Vav proto-oncogene (VAV), Cell division cycle 42 (CDC42).

#### 1.4 Treatment of ALK<sup>+</sup> ALCL

Anthracycline-based combination therapy leads to long-term event-free survival in about 60% of cases. Besides haematopoietic stem cell transplantation, vinblastine monotherapy, brentuximab vedotin (targeting CD30<sup>+</sup> cells), and ALK inhibitors have been reported in the

treatment of refractory ALK<sup>+</sup> ALCL (Prokoph et al., 2018). ALK is an ideal drug target, as its endogenous expression is limited to neonatal neuron development (S. W. Morris et al., 1997). Small molecular weight tyrosine kinase inhibitors of ALK, e.g. the 2011 FDA-approved agent Crizotinib (Camidge et al., 2012), have been mainly used in ALK<sup>+</sup> non-small cell lung cancer and are now approved and more frequently used in ALCL (Fukano et al., 2020; Pfizer, 2021). ALK inhibitors bind to the ATP pocket of the abnormal ALK protein, thereby blocking its access to energy and prevent trans-autophosphorylation of the ALK dimer and the downstream effectors. However, ALK inhibitor therapy can lead to on-target (secondary mutations in ALK) and off-target (e.g., the upregulation of epidermal growth factor receptor (EGFR), c-Kit proto-oncogene (KIT) and MEK-ERK signalling) resistances (Pinto et al., 2020), increasing the requirement for alternative combinatorial treatment strategies. For example, the combination of ALK inhibition with blockade of the Interleukin (IL)-10/STAT3 (Prokoph et al., 2020) or the mTOR pathways (Kim et al., 2020) were suggested.

## **1.5 Thymus and T cell development**

The term T cells stem from the location of their development and maturation – the thymus. The thymus is a specialised primary lymphoid organ of the immune system, consisting of a left and a right lobe. It is subdivided into numerous smaller sections called lobules, each consisting of a thymic cortex and the inner medulla (Murphy & Weaver, 2016).

### **1.5.1 Normal T cell development**

Lymphoid progenitor cells (thymocytes) develop from haematopoietic stem cells in the bone marrow (BM) and migrate through the blood to finally reach the thymus. When the progenitor cells enter the thymus, they lack the most characteristic T cell surface markers. The interaction with the thymic stroma starts the differentiation and first T cell-specific surface molecules like CD2 and Thymocyte Antigen 1.2 (THY1.2) are expressed in human and murine T cells respectively. Here, the developing cells are still negative for the CD3-receptor complex (CD3 and T cell receptor (TCR)  $\alpha$ - and  $\beta$ -chains) as well as the co-receptors CD4 and CD8 – hence called double-negative (DN) thymocytes. At this stage, the precursors can give rise to the  $\alpha$ : $\beta$  and  $\gamma$ : $\delta$  T cells as well as NKT cells (Murphy & Weaver, 2016).

In the DN stage, further differentiation stages can be attributed by CD25 (IL-2R  $\alpha$ -chain) and CD44 expression, an adhesion molecule involved in lymphocyte activation, by designating

them to DN1 (CD44<sup>+</sup>CD25<sup>-</sup>), DN2 (CD44<sup>+</sup>CD25<sup>+</sup>), DN3 (CD44<sup>low</sup>CD25<sup>-</sup>), and DN4 (CD44<sup>-</sup>CD25<sup>-</sup>) stage. During these development steps, DN2 cells start to rearrange the  $\beta$ -chain locus (D $\beta$  to J $\beta$  rearrangements) and stay DN3 until V $\beta$  to DJ $\beta$  rearrangement is finished and pairs with the surrogate  $\alpha$ -chain to form the pre-TCR, which is transported to the cell surface. Pre-T cells begin to cycle and become DN4 cells, which eventually further proliferate and express CD4 and CD8 – becoming double-positive (DP) thymocytes. Cells failing to complete  $\beta$ -chain rearrangement die. Next, DP thymocytes rearrange the  $\alpha$ -chain locus, allowing every cell with a functional  $\beta$ -chain can associate with various  $\alpha$ -chains to increase the variety (Murphy & Weaver, 2016).

Only 2% of DP  $\alpha$ : $\beta$  CD3<sup>+</sup> expressing thymocytes survive positive and negative selection, maturing into CD4<sup>+</sup> or CD8<sup>+</sup> single-positive cells. Despite arising from a common precursor during thymic development, CD4<sup>+</sup> or CD8<sup>+</sup> single-positive cells develop distinct functions and make up the core of most adaptive immune responses (Vacchio & Bosselut, 2016). The T cells that have undergone negative and positive selection are released into circulation of the periphery and lymphoid organs. There, they have to find and fight their foreign antigen or cancer cells that display neoantigens. It is only through antigen recognition through their TCR, the T cells become activated, clonally expand and differentiate into effector and memory T cells (Murphy & Weaver, 2016).

### 1.5.2 NPM-ALK in T cell development

It is now accepted that most ALCLs are derived from the expansion of transformed T lymphocytes, which have undergone a clonal neoplastic transformation, as confirmed by genomic studies of their TCR loci. Even in tumour cells that do not express any evident T cell-associated surface markers, a clonally altered TCR  $\beta$  chain gene can be detected in 50–60% of cases. Furthermore, many molecules defining the T cell lineage and those involved in the transmission of TCR signals (e.g., TCR, CD3 and the zeta-chain-associated protein kinase 70 (ZAP70)) are downregulated or even absent in ALCL (Bonzheim et al., 2004).

Surprisingly, CD4 expression is frequently seen in > 50% of cases, whereas CD8 expression is uncommon (Lamant et al., 2011; Malcolm et al., 2016). According to recent research, stem cell-like features are enriched in a subpopulation of NPM-ALK-positive (NPM-ALK<sup>+</sup>) ALCL cell lines and primary tumours. Gene set enrichment analysis of NPM-ALK<sup>+</sup> ALCL cell lines revealed a gene expression profile associated with early thymic progenitors and expression of

pluripotency-associated transcription factors like the Octamer-binding transcription factor 4 (OCT4), SRY-box 2 (SOX2), and Nanog homeobox (NANOG) (Martinengo et al., 2014; Moti et al., 2015).

Epigenetic alterations (e.g., DNA methylation) are critical in stem cell differentiation (Berdasco & Esteller, 2011). NPM-ALK-activated STAT3 promotes the expression of DNA methyltransferase 1 (DNMT1), which contributes to the significant loss of T cell lineage identity seen in NPM-ALK<sup>+</sup> ALCL by epigenetically silencing several critical genes from the TCR complex and its signalling pathway (Ambrogio et al., 2009; Hoareau-Aveilla & Meggetto, 2017). The expression of T cell differentiation transcription factors – Lymphocyte-specific protein-tyrosine kinase (LCK), GATA binding protein 3 (GATA3) and Lymphoid enhancer-binding factor 1 (LEF1) – is tightly regulated, as they are critical for the development and function of T cells. These genes are repressed and hypermethylated in T cell progenitors and are demethylated upon differentiation (Kitagawa et al., 2015; Luo & Li, 2013). Interestingly, these critical transcription factors remain hypermethylated in NPM-ALK<sup>+</sup> ALCL (Hassler et al., 2016). A high throughput DNA methylation analysis was performed on patient samples with systemic NPM-ALK<sup>+</sup> ALCL and normal human T lymphocytes. The obtained DNA methylation patterns of NPM-ALK<sup>+</sup> ALCL were linked to particular thymic phases in T cell development, implying that the disease originated from early thymic progenitor CD34<sup>+</sup> CD1a<sup>-</sup> cells (Hassler et al., 2016; Moti et al., 2015).

Recent studies have revealed that the NPM-ALK transgene can transform mature human peripheral CD4<sup>+</sup> T cells into ALCL by restoring a thymic progenitor-like pattern (Congras et al., 2020; Zhang et al., 2013). Furthermore, the NPM-ALK-mediated induction of an undifferentiated immunophenotype in thymic cells is accompanied by induction of the MYC-Notch receptor 1 (NOTCH1) axis and dysregulation of critical epigenetic enzymes, such as DNMT1 (Redl et al., 2021).

## **1.6 JAK-STAT signalling**

The Janus kinase (JAK)-signal transducer and activator of transcription (STAT) signalling pathway controls many biological processes like proliferation, differentiation and is of particular importance in immune cells (Liongue et al., 2016; Myllymäki & Rämetsä, 2014). It consists of four principal components – cytokine, receptor, JAK and STAT – which allows for rapid integration of signals from the cell surface to target gene transcription in the nucleus (Liongue et al., 2016;

Myllymäki & Rämets, 2014). In most vertebrates, the family consists of four JAK (JAK1, JAK2, JAK3, TYK2) and seven STAT (STAT1, STAT2, STAT3, STAT4, STAT5A, STAT5B, STAT6) genes, which integrate the signals of more than 50 cytokines, growth factors, chemokines and their corresponding receptor chains (Liongue et al., 2016; Myllymäki & Rämets, 2014).

Signal transduction of the canonical JAK-STAT pathway is initiated upon the binding of cytokines or growth factors to their respective cell-surface receptors (**Figure 4**). JAKs are associated with the intracellular receptor chains and are activated upon binding cytokine or growth factor. The binding leads to a conformational change of the receptors, bringing the associated JAKs in close proximity, facilitating JAK activation via trans-autophosphorylation to increase their catalytic activity. The activated JAK kinase domain phosphorylates the receptor chains, thereby creating high-affinity SH2 docking sites for the STAT proteins (Hammarén et al., 2018; R. Morris et al., 2018; Rani & Murphy, 2015; Waters & Brooks, 2015). The negative feedback switching off the signal is provided mainly by Suppressors of cytokine signalling (SOCS) proteins (Endo et al., 1997), Protein inhibitors of activated STAT (PIAS), and protein tyrosine phosphatases (PTPs) (Wormald & Hilton, 2004). PTPs can mediate JAK phosphorylation in the cytoplasm and STAT dephosphorylation in the nucleus.

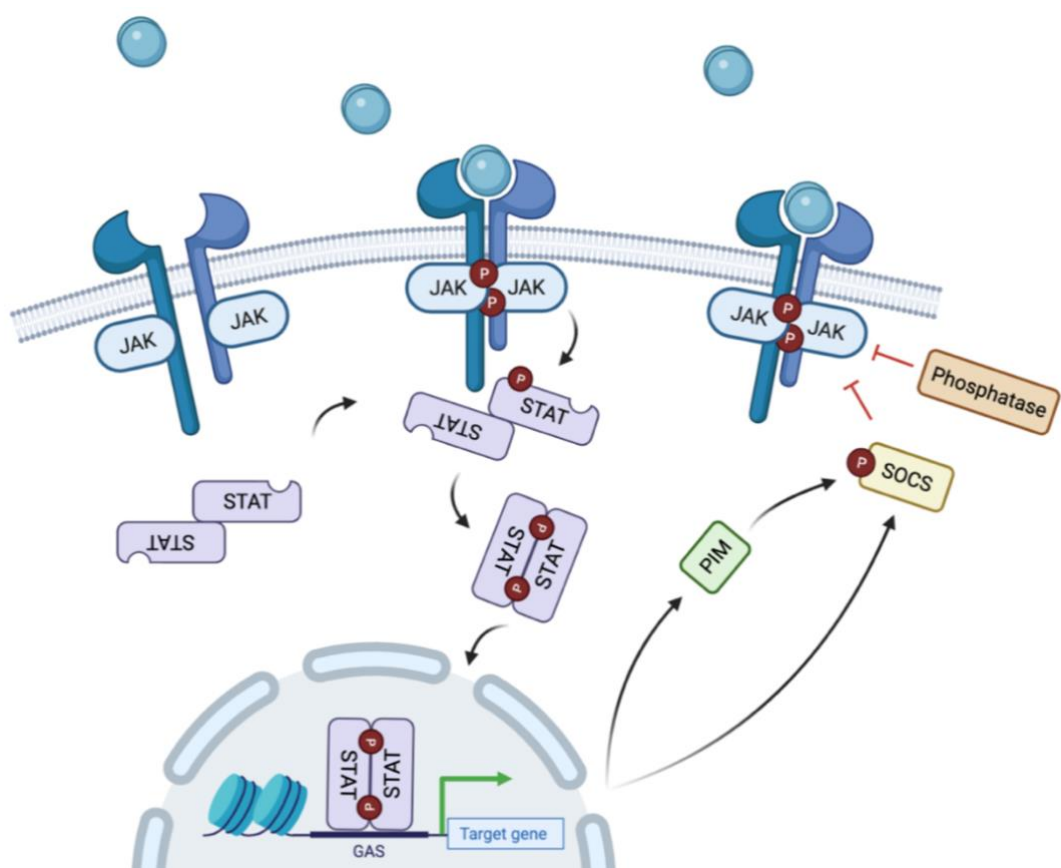


**Figure 4: Schematic overview on canonical JAK-STAT signalling**

Upon dimerisation of receptors through cytokine or growth factor stimulation, JAKs are trans-autophosphorylated and associated with unphosphorylated STAT dimers. STATs are tyrosine phosphorylated (pY-STAT), which results in their parallel dimerisation and translocation to the nucleus to activate gene transcription. JAK-STAT signalling is negatively regulated through many different mechanisms. Shown are phosphatases and SOCS proteins, which block further STAT activation in the cell cytoplasm. The Pim-1 proto-oncogene (PIM1, also PIM) and SOCS protein are direct STAT target genes, where PIM phosphorylates SOCS, thereby regulating its stability and function (adapted from B. Maurer and (D. E. Levy & Darnell Jr, 2002)).

Pre-dimerised STATs reside in the cytoplasm or at the cytokine receptor in an inactive anti-parallel confirmation. Upon JAK-mediated tyrosine phosphorylation, STATs change their confirmation to parallel homo- or heterodimers (Bernadó et al., 2009; Neculai et al., 2005; Zhong et al., 2005). Phosphorylated STAT-dimers detach from the receptors, potentially undergo additional post-translational modifications, and translocate to the nucleus, where they initiate transcription of respective target genes (**Figure 5**). STATs can bind as dimers, tetramers or in interaction with other proteins in multifactorial complexes (D. Levy & Marié, 2012; A. V. Villarino et al., 2017).

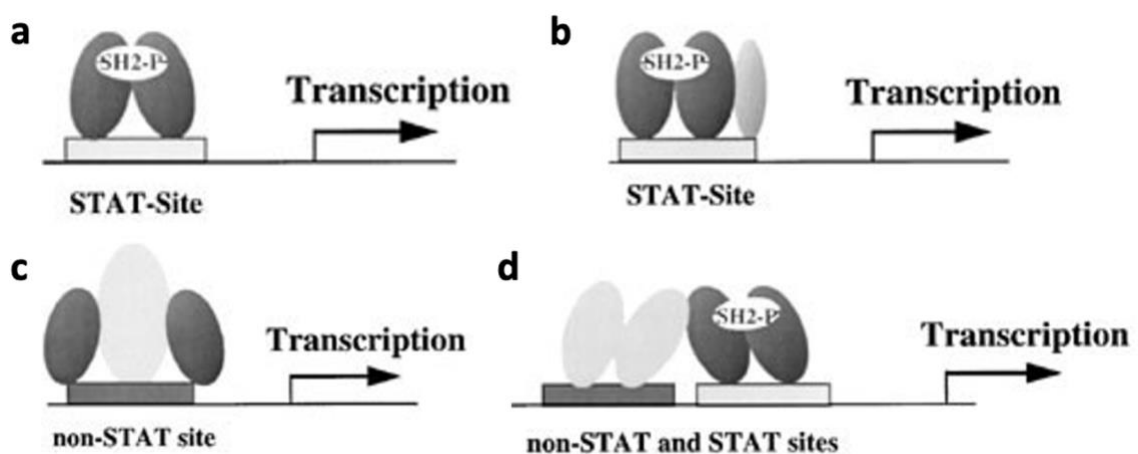


**Figure 5: STAT proteins induce transcription through four distinct mechanisms (Shuai, 2000)**

Stat5 dimers are able to bind DNA and **a**) independently or **b**) as part of protein complexes directly drive transcription at  $\gamma$ -activation sites (GAS). The induction of transcription is also possible via protein interactions at non-STAT DNA binding sites or through **d**) cooperational binding of STAT and non-STAT transcription factors to clustered independent DNA regions (Shuai, 2000).

However, the JAK-STAT signalling cascade cannot solely be viewed as a linear model, as interconnections to other signalling pathways are possible (e.g., STAT5 has been shown to interact with PI3K via the scaffolding adaptor GRB2-associated-binding protein 2 (GAB2), thereby influencing PI3K-AKT-mTOR pathway activation) (Yamada & Kawauchi, 2013).

### 1.6.1 STAT5A and STAT5B

The STAT5 locus comprises two highly homologous genes, *STAT5A* and *STAT5B*. The complete genetic abrogation of *STAT5A* and *STAT5B* results in perinatal lethality on C57BL/6 or Balb/c backgrounds; but 1–2% mice devoid of *STAT5* from heterozygous breedings on mixed Sr129 x C57BL/6 backgrounds are suffering from dwarfism, severe microcytic anaemia, and reduced numbers of CD8<sup>+</sup> T cells (Cui et al., 2004; Hoelbl et al., 2006). Mouse models either lacking *STAT5A* or *STAT5B* display different phenotypes, indicating non-redundant roles in non-haematopoietic compartments. *STAT5A*, but not *STAT5B*, is required for mammary gland development and prolactin signalling, whereas *STAT5B* is predominantly involved in hepatic growth hormone signalling (Liu et al., 1995; Liu et al., 1997; Udy et al., 1997; Yamaji et al., 2009).

However, their functions are considered largely redundant in haematopoietic cells (A. V. Villarino et al., 2017). *STAT5B* is expressed at higher levels in differentiated haematopoietic cell types than *STAT5A* (Maurer et al., 2019). In normal haematopoiesis, *STAT5A* and *STAT5B* are critical effectors of numerous cytokines, which signal through JAK1, -2 or -3-bound surface receptors, as depicted in **Figure 6**. *STAT5A* and *STAT5B* are fundamental for myelopoiesis, lymphoid development, megakaryopoiesis, macrophage, basophil, eosinophil, and mast cell functions (Rani & Murphy, 2015; A. V. Villarino et al., 2017).

Furthermore, *STAT5A* and *STAT5B* also have important roles in apoptosis. They upregulate the expression of pro-survival genes like *Bcl-2*, *Bcl-x<sub>L</sub>* and Bcl-2-related protein A1 (*Bcl2A1*) and downregulate the expression of Caspases 3 and 9. They also exhibit essential functions in proliferation, such as the upregulation of D type Cyclins (de Groot et al., 2000; Debierre-Grockiego, 2004).

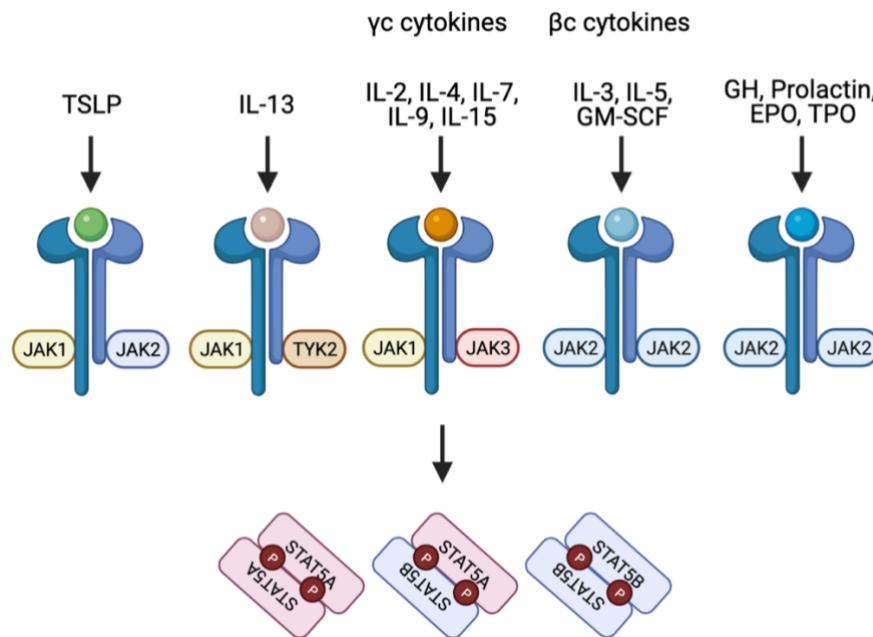


**Figure 6: Cytokines and their respective JAKs signalling over STAT5**

STAT5A/B operate as essential signalling molecules downstream of numerous cytokine and growth factor receptors, e.g., IL-2, -3, -4, -5, -7, -9, -13, -15, Thymic stromal lymphopoietin (TSLP), Erythropoietin (EPO), Thrombopoietin (TPO), Growth hormone (GH), Prolactin and Granulocyte-macrophage (GM) Colony-stimulating factor (CSF) (Maurer et al., 2019; Vainchenker & Constantinescu, 2013).

### 1.6.2 STAT5A/B regulation of T cell development

STAT5A and STAT5B proteins are critical downstream mediators of IL-2R and IL-7R signalling, and hence play a vital role in T cell development, function, and survival (reviewed by (Heltemes-Harris & Farrar, 2012; Kelly et al., 2003; Owen & Farrar, 2017)). *Stat5a/b*<sup>-/-</sup> mice display a severely decreased number of CD4<sup>+</sup> and CD8<sup>+</sup> T cells and a higher fraction of CD4<sup>-</sup>CD8<sup>-</sup> thymocytes (Hoelbl et al., 2006; Yao et al., 2006). Recent studies investigating STAT5A and STAT5B target genes in T cells have revealed common STAT5A and STAT5B binding sites at numerous proliferation and survival genes, including serum/glucocorticoid regulated kinase 1 (*SGK1*), *BCL-2* and *MCL1*, implicating STAT5 redundant functions in these cell processes. Furthermore, both STAT5A and STAT5B directly induce the expression of the CD8 master regulator Runt-related transcription factor 3 (*RUNX3*) (Kanai et al., 2014). The differentiation of CD8<sup>+</sup> and CD4<sup>+</sup> T cells is regulated by STAT5A/B in a dose-dependent manner, where the loss of *Stat5b* led to a more pronounced reduction of mature T cells compared to *Stat5a* (Maurer, Nivarthi, et al., 2020; Nivarthi et al., 2015; Owen & Farrar, 2017; Pham et al., 2018; A. Villarino et al., 2016).

In addition to redundant functions in cell proliferation and apoptosis, STAT5A or STAT5B specific roles have been described (Kanai et al., 2014). STAT5A binds to genes involved in neural development and function, such as N-myc downstream regulated 1 (*NDRG1*), DnaJ Hsp40 homolog, Subfamily C, Member 6 (*DNAJC6*), and Slingshot protein phosphatase 2 (*SSH2*), as well as other cell survival and proliferation-associated genes like Mitogen-activated protein kinase kinase kinase 5 (*MAP3K5*) and *BCL-xL*. Meanwhile, STAT5B appears to play a distinct role in T cell development and function by promoting the transcription of Dedicator of cytokinesis 8 (*DOCK8*), Sorting nexin 9 (*SNX9*), *FOXP3* and Interleukin 2 receptor, alpha (*IL2RA*). Their findings imply that one or more STAT5A and/or STAT5B co-activators may play a key role in determining distinct binding capacities and gene regulatory behaviours (Kanai et al., 2014).

### **1.6.3 The role of JAK-STAT5 in leukaemia and lymphoma**

As mentioned, the JAK-STAT proteins are important pro-proliferative signalling molecules, which can lead to cancer development upon deregulation (Bousoik & Montazeri Aliabadi, 2018). STAT5A and STAT5B may have distinct functions in leukaemia, as constitutive activation of either protein can cause a disease with a unique phenotype — STAT5A has been linked to aggressive multi-lineage leukaemia, whilst STAT5B has been linked to NK and T cell leukaemia/lymphoma (Burchill et al., 2003; Moriggl et al., 2005; Onishi et al., 1998). More recently, activating mutations were almost exclusively found in *STAT5B* and not in *STAT5A*, mainly resulting in various forms of PTCL ((Pham et al., 2018) and summarised by (Maurer et al., 2019)). Transgenic mouse models expressing gain-of-function mutants of STAT5A or STAT5B in the haematopoietic system develop lethal CD8<sup>+</sup> T cell neoplasia (Maurer, Nivarthi, et al., 2020; Pham et al., 2018). The gene expression profiles of these hyperactive STAT5A and STAT5B model RNA-sequencing profiles share an overlap of 373 (28.8%) commonly deregulated genes and are highly correlated to human peripheral T cell lymphoma (Maurer, Nivarthi, et al., 2020). Furthermore, oncogenes such as the Abelson-breakpoint cluster region (BCR-ABL), FMS-like tyrosine kinase 3-internal tandem duplication (FLT3-ITD) and NPM-ALK can directly phosphorylate STAT proteins to induce proliferative or anti-apoptotic gene expression (Brachet-Botineau et al., 2020). In the context of BCR-ABL-driven leukaemia, STAT5B has been attributed a more important role compared to STAT5A (S. Kollmann et al., 2019).

#### 1.6.4 Inhibitors of JAK-STAT signalling

The inhibition of JAK-STAT signalling can be achieved by targeting JAKs or STATs. All of the JAK inhibitors (JAKinibs) reported thus far are ATP competitive and bind to the active kinase conformation (type I inhibitors) (Virtanen et al., 2019). JAKs are no longer capable of phosphorylating substrates such as STATs, preventing cytokine-dependent gene regulation (Furumoto & Gadina, 2013). There are currently eight approved JAK inhibitors (JAKinibs) successfully used to treat myeloproliferative neoplasms (MPNs), rheumatoid arthritis and psoriasis (Harrington et al., 2020). Ruxolitinib (JAK1- and JAK2-selective inhibitor) and Fedratinib (selective JAK2 inhibitor) are mainly used for the treatment of MPNs, while Tofacitinib (JAK1/3), Baricitinib (JAK1/2) and Upadacitinib (JAK1) are approved for the treatment of rheumatoid arthritis and psoriasis. Due to the success of combination treatments for MPNs, the use of Ruxolitinib has also been expanded to leukaemias, lymphomas and other immune cell disorders (Dao et al., 2020).

Because of the expanding use of JAKinibs, it has become increasingly vital to address the wide range of factors that may be influenced by JAK inhibition. As previously mentioned, multiple immune-regulatory cytokines signal through JAK-STAT, making JAK signalling indispensable for normal haematopoiesis and function of the immune system. Therefore, JAKinibs often cause severe adverse effects (**Figure 7**), such as the development of anaemia, thrombocytopenia, an increased incidence of infections and even the occurrence of malignancies (Bottos et al., 2016; Gadina et al., 2018; Porpaczy et al., 2018; Schwartz et al., 2017). Therefore, the development of more specific inhibitors targeting downstream components of these pathways is desirable to prevent or minimise the occurrence of serious adverse effects.

Cancer cells are more dependent on STAT activity than healthy cells, suggesting STAT proteins as suitable targets for anti-cancer therapy. Numerous attempts of developing direct STAT3 or STAT5 inhibitors have been previously described (reviewed by (Orlova et al., 2019)). However, only very few compounds have been shown to target STATs directly. Wingelhofer et al. (2018) have reported a novel selective and specific STAT5 SH2-domain-targeting compound (AC-4-130), which directly binds to STAT5, disrupts its activation, dimerisation and nuclear translocation, thereby preventing STAT5-dependent gene transcription. Preclinical evaluations have revealed that AC-4-130 efficiently blocks pathological levels of STAT5 activity and synergistically increases the cytotoxicity of the JAK1/2 inhibitor Ruxolitinib

(Wingelhofer et al., 2018). The AC-4-130 STAT5 inhibitor represents a lead compound, which is being further improved for clinical trials. As STAT5 plays a crucial role in regulating haematopoietic stem cell self-renewal, the clinical approval of STAT5 inhibitors would provide novel treatment opportunities to possibly eradicate the cancer stem cell pool (Tolomeo et al., 2019).

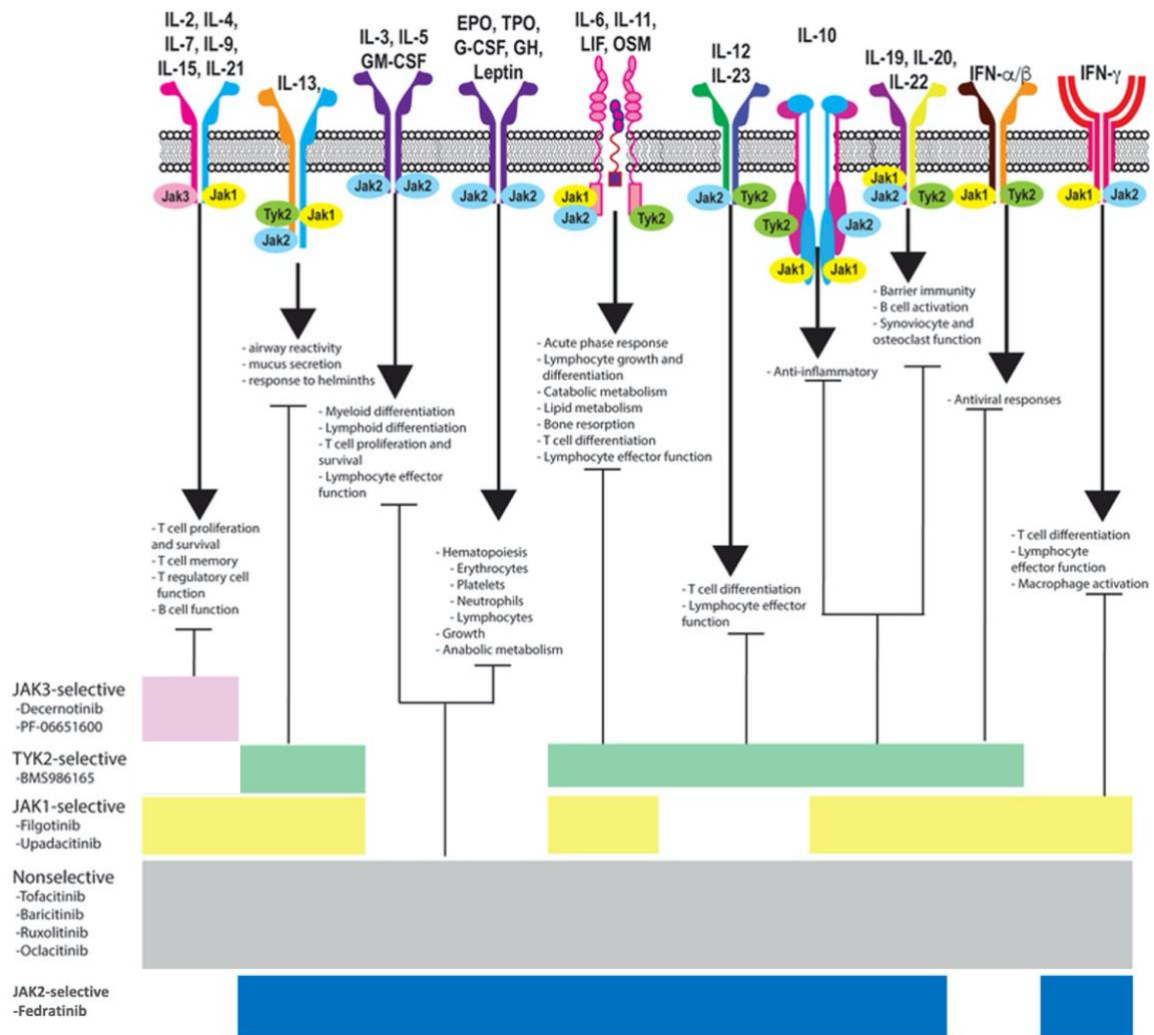


**Figure 7: Adverse effects of JAK-inhibition** (modified from (Schwartz et al., 2017))

Type I and II cytokine receptors physically associate with JAKs, thereby allowing the transduction of downstream intracellular signals. Because numerous cytokine signals converge on the level of JAK signalling, inhibiting a single JAK interferes with multiple biological functions. Therefore, JAKinibs may be used for numerous disease indications but combined use could cause a wide array of side effects. For example, first-generation nonselective JAKinibs broadly impact many JAKs and thus have adverse effects on haematopoiesis or neurotoxicity. Meanwhile, a JAK3 selective inhibitor, for example, has a more restricted action and will only affect T cell proliferation and memory (Gadina et al., 2018; Schwartz et al., 2017). Leukemia inhibitory factor (LIF), oncostatin M (OSM), interferon (IFN)- $\alpha/\beta$ , IFN- $\gamma$ .

### 1.6.5 STAT5A/B as potential opponents in NPM-ALK<sup>+</sup> lymphoma

The roles of STAT5A and STAT5B in NPM-ALK-driven lymphomagenesis have only been addressed in a minimal number of studies. It was reported that NPM-ALK<sup>+</sup> cells express predominately STAT5B, which controls proliferation and apoptosis (Ruchatz et al., 2003). The NPM-ALK/STAT3 signalling axis has been shown to methylate the promoter of STAT5A, resulting in epigenetic silencing. Forced expression of STAT5A resulted in NPM-ALK downregulation via direct transcriptional inhibition (Zhang et al., 2007). Taken together, these observations point to opposing functions – tumour-suppressive STAT5A and oncogenic STAT5B – in NPM-ALK<sup>+</sup> ALCL. NPM-ALK remains the only oncogene displaying antagonistic roles for STAT5A and STAT5B (Nieborowska-Skorska et al., 2001; Zhang et al., 2007). Despite having 94% structural similarity, it remains unclear how STAT5A and STAT5B carry out their separate tasks. Further studies to elucidate the roles of STAT5A/B in ALK<sup>+</sup> ALCL are needed to elucidate its potential as a drug target.

### 1.7 CDKs and the cell cycle

The cell cycle consists of two distinct phases: mitosis (cell division) and the interphase (**Figure 8**). The interphase is further subdivided into the gap 1 (G1), DNA synthesis (S) and gap 2 (G2) phase. Following mitosis (M), the cell returns to the quiescent G0 phase. These cells can enter G1 upon activation by mitogenic stimuli (Norbury & Nurse, 1992).

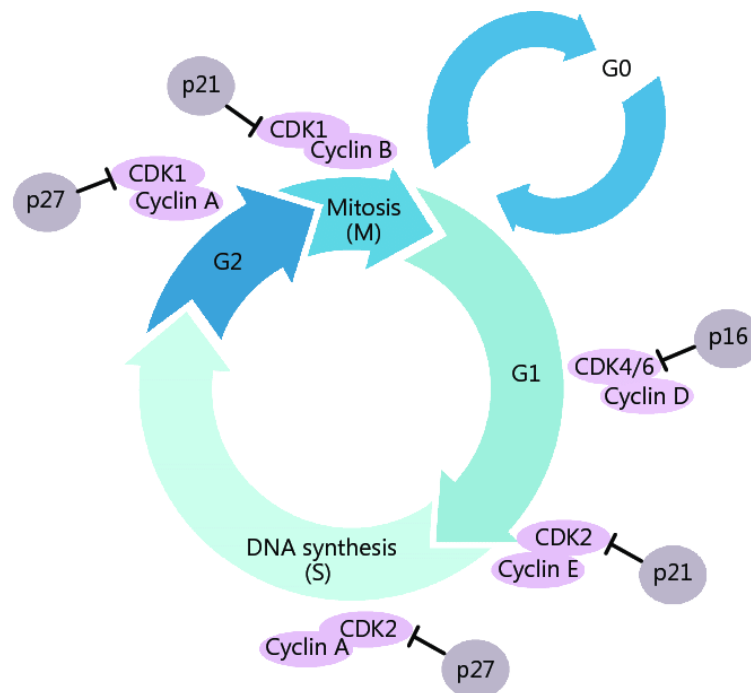


**Figure 8: Cell cycle phases and their essential CDK-Cyclin complexes** (J. Bai et al., 2017)

Each phase in the cell cycle is regulated by multiple CDK-Cyclin complexes and their respective CDK-inhibitors. These complexes are composed of three interphase CDKs (CDK2, CDK4, and CDK6), a mitotic CDK1 and ten Cyclins belonging to four distinct classes (A-, B-, D-, and E-type Cyclins). G1 entry is mediated by D-type Cyclins associating with CDK4/6, while CDK2-Cyclin E complexes regulate the late G1 phase and the G1/S phase transition. In later stages, Cyclin A replaces Cyclin E as the partner of CDK2, thereby controlling DNA synthesis and replication in the S phase. In G2, Cyclin A subsequently associates with CDK1, later replaced by Cyclin B, thereby triggering mitosis (J. Bai et al., 2017).

Cell cycle progression is modulated by a family of serine/threonine kinases, called Cyclin-dependent kinases (CDKs) (Sherr & Roberts, 1999). As the name suggests, CDKs require the presence of regulatory subunits, the Cyclins, to become catalytically active (Sherr & Roberts, 2004). CDKs, in complex with their respective Cyclins, are essential for regulating cell-cycle progression and have an important role in transcription (reviewed by (Malumbres & Barbacid, 2009)).

### 1.7.1 Kinase-dependent functions of CDK6

As mentioned, CDK4 and CDK6 associate with D-type Cyclins (D1, D2, D3), thereby enabling the cell to pass from the G1 to the S phase (K. Kollmann & Sexl, 2013; Matsushime et al., 1994; Morgan, 1997). While the levels of most Cyclins fluctuate throughout the cell cycle (**Figure 9**), the levels of D-type Cyclins reflect the presence of growth factors and mitogens (Sherr & Roberts, 1999). In the G1 phase, cells with the opportunity to decide whether to initiate DNA replication or not. Crosstalk between signalling pathways at the G1 phase enables cells to take external and internal cues into account in coordinating higher-level functions such as differentiation, growth, stress reactions and inflammation.

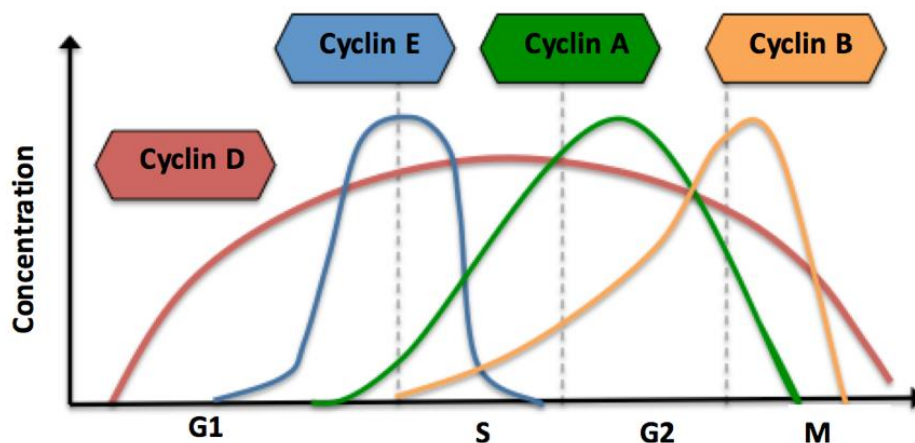


**Figure 9: Cyclin fluctuation in the cell cycle** (UBC, 2021)

The Cyclin oscillations brought on by changes in Cyclin gene expression and degradation by the ubiquitin-mediated proteasome system, cause oscillations in CDK activity, which drive the cell cycle. D-type Cyclins do not behave like other Cyclins in that their concentrations rise gradually (without oscillation) throughout the cell cycle in response to mitogenic cues (UBC, 2021).

CDK4/6-Cyclin D complexes mediate the phosphorylation of the Retinoblastoma (RB) protein family members, resulting in the dissociation of E2F transcription factors from RB-mediated repression (**Figure 10**). The activation of E2F-dependent genes allows for G1 to S phase progression and DNA synthesis (Classon & Harlow, 2002; Matsushime et al., 1994; Tigan et al., 2016). The CDK interacting protein/Kinase inhibitory protein (CIP/KIP) family, which includes Cyclin-dependent kinase inhibitors (CDKN) p21, p27, and p57, and the INK4 family, which includes p15, p16, p18, and p19, control the activation and inhibition of CDK4/6-Cyclin D complexes. CIP/KIP family members can inhibit a broader range of CDK-Cyclin complexes, including CDKs 1, 2, 4, and 6, whereas INK4 proteins only inactivate CDK4/6-Cyclin D complexes (Blain et al., 1997; James et al., 2008; LaBaer et al., 1997; Russo et al., 1998). However, depending on their phosphorylation status – mediated by nonreceptor tyrosine kinases – CIP/KIP family members can act as positive and negative cell cycle regulators (James et al., 2008). The versatility of CIP/KIP proteins as regulatory subunits is highlighted by their contribution to the assembly, stabilization, and nuclear translocation of CDK4/6-Cyclin D complexes (Choi & Anders, 2014; LaBaer et al., 1997).

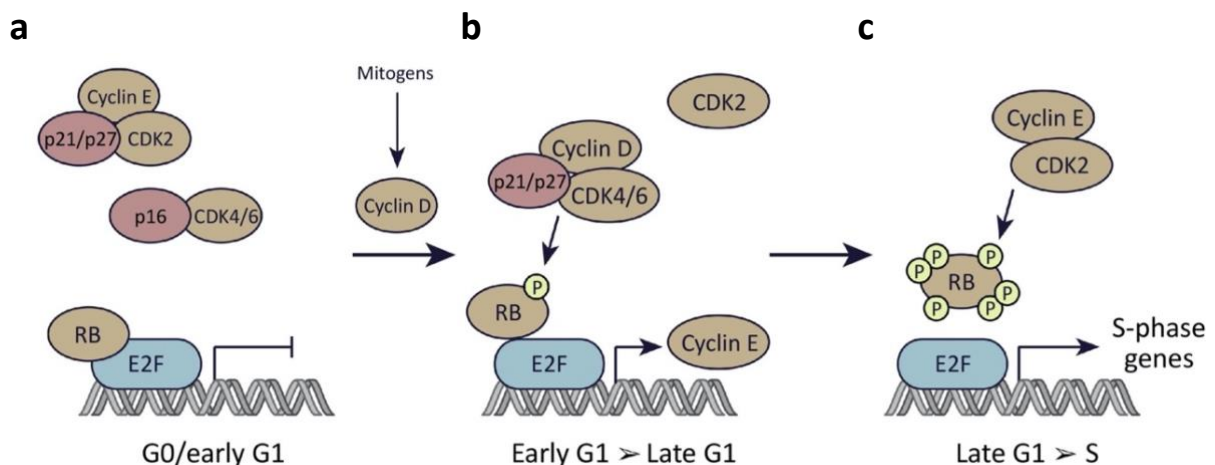


**Figure 10: Regulation of the G1/S transition** (Goel et al., 2018)

**a)** Prior to phosphorylation, RB is associated with promoters via E2F, allowing it to recruit chromatin-modifying enzymes that keep the chromatin compact and transcriptionally repressed (Gordon & Du, 2011; Talluri & Dick, 2012). CIP/KIP family proteins inhibit CDK2-Cyclin E complexes from RB phosphorylation, and CDK4/6 CDKs are inhibited by P16. **b)** Upon satisfying external conditions – the presence of mitogens – p16 is replaced by Cyclin D

in the CDK4/6 complex. This drives the hypo-phosphorylation of RB, resulting in partial dissociation of the repressor complex, allowing for E2F-mediated transcription (Burke et al., 2014; Choi & Anders, 2014; Harbour et al., 1999; Rubin et al., 2005). During the late G1 phase, E2F activates numerous genes, including Cyclin E, which binds to CDK2 and leads to RB hyper-phosphorylation and the E2F transcription factor release (Burke et al., 2014). Meanwhile, CIP/KIP proteins – p21 and p27 – bind to the CDK4/6 complex, isolating themselves from other CDKs, such as CDK2, to prevent further inhibition. **c)** This feedback loop allows the activation of CDK-Cyclin complexes that act later during cell cycle progression (Choi & Anders, 2014; Sherr & Roberts, 1999; Tigan et al., 2016), thereby ensuring the irreversible progression of the cell cycle through the S phase (Dyson, 1998).

### 1.7.2 Kinase-independent functions of CDK6

CDK6 but not CDK4 has an additional function as a transcriptional regulator – where, amongst others, the group of Veronika Sexl largely contributed to the advances of the field (Bellutti et al., 2018; Buss et al., 2012; Handschick et al., 2014; K. Kollmann et al., 2013; Scheicher et al., 2015; Uras et al., 2019). CDK6 has been demonstrated to form multiprotein complexes and function as a chromatin-bound cofactor that induces transcription of genes controlling angiogenesis, cell cycle inhibition, stem cell activation, and immunological response. CDK6-containing transcriptional complexes induce the expression of the tumour suppressor p16<sup>INK4a</sup> and the pro-angiogenic Vascular endothelial growth factor A (VEGF-A). In haematopoietic and leukemic stem cells (HSC and LSC), CDK6 regulates stem cell activation by interfering with the transcription of a key stem cell regulator – Early growth response 1 (*Egr1*). The absence of CDK6 prevents the repopulation of the stem cell niche upon competitive transplantation (Scheicher et al., 2015). Studies have shown that in the nucleus, CDK6 physically interacts with the Nuclear factor kappa-B (NF-κB) subunit p65 and drives the transcription of several NF-κB target genes. Its recruitment to certain chromatin regions of inflammatory genes is critical in determining cytokine and chemokine repertoires in chronic inflammation and cancer (Handschick et al., 2014; Uras et al., 2019). In summary, the kinase-dependent and -independent roles of CDK6 have important roles in numerous vital cellular processes, as described in **Figure 11**.

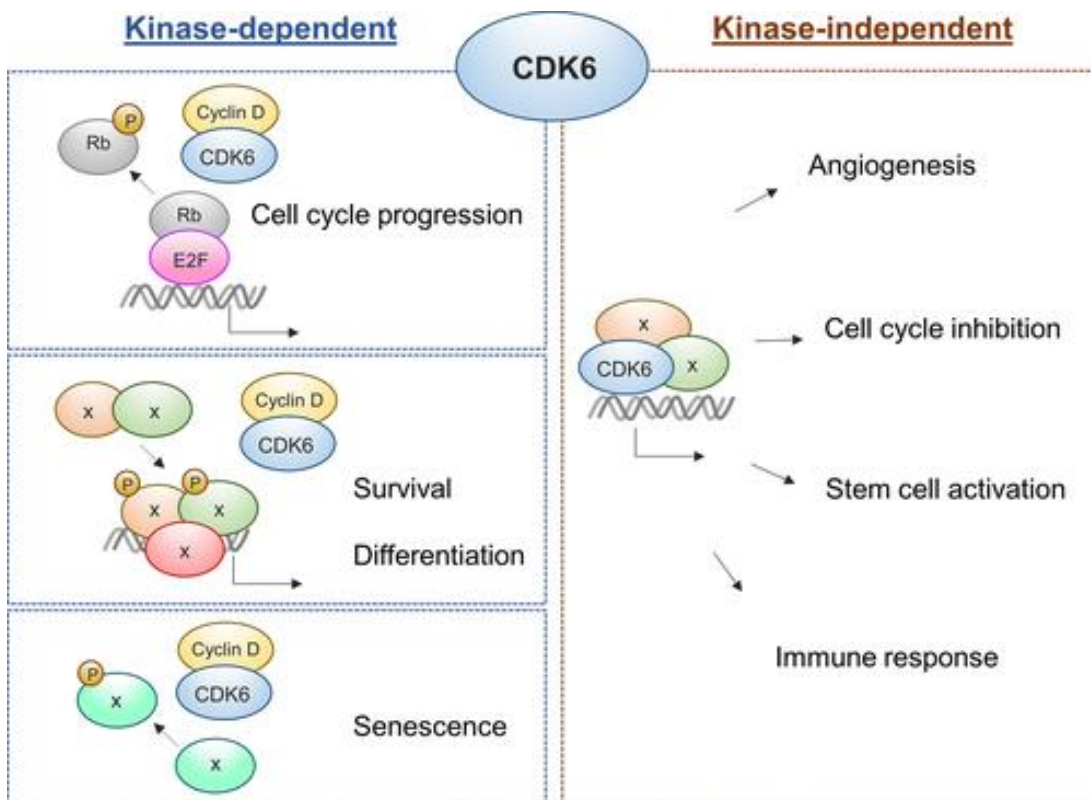


**Figure 11: The kinase-dependent and kinase-independent functions of CDK6 in cancer** (Nebenfuehr et al., 2020)

CDK6 functions as a chromatin-bound cofactor that stimulates transcription of genes affecting angiogenesis, cell cycle inhibition, stem cell activation, and immunological response in a kinase-independent way. By binding to D-type Cyclins, the kinase-dependent phosphorylation functions of CDK6 are able to regulate cell cycle progression, survival, differentiation and senescence (reviewed by (Nebenfuehr et al., 2020)).

### 1.7.3 The role of CDK6 in T cell development

Thymocyte development is negatively affected in *Cdk6*-deficient mice (Malumbres et al., 2004). Reduced proliferation and increased apoptosis during NOTCH1-dependent T-cell development prevent immature thymocytes from undergoing normal expansion (Hu et al., 2009). The differentiation capacity of HSCs into mature T cells is also impaired. Similar observations of reduced proliferation were made in a mouse model expressing a CDK6 kinase-dead allele, indicating that CDK6 kinase activity is required for thymocyte development. In mature thymocyte subsets, there was a striking contrast between the complete loss of CDK6 and the inactivation of its kinase function, where the presence of the kinase-dead allele dramatically increased the frequency of DN T cells (Hu et al., 2011).

#### **1.7.4 The role of CDK6 in leukaemia and lymphoma**

Components of the CDK6-Cyclin D complexes are frequently dysregulated (e.g., CDK6 overexpression) in haematological malignancies – including T-cell lymphoblastic lymphoma and leukaemia (Chilosi et al., 1998). CDK6 is not only crucial in the development of leukaemia, but it also modulates the response to oncogene-induced stress by antagonizing oncogene-induced activation of the Tumour protein 53 (TP53, p53). In the absence of CDK6, lymphoid cells are driven to alter or delete p53 in order to cope with the stress caused by the oncogene (Bellutti et al., 2018). Studies have shown that *Cdk6*-deficient mice are resistant to AKT-driven lymphomagenesis, implying that CDK6 involvement in NOTCH-AKT-dependent T cell development and cancer is not compensated by CDK4 (Hu et al., 2009).

#### **1.7.5 CDK6 in NPM-ALK<sup>+</sup> lymphoma**

We and others have shown that human and murine NPM-ALK tumours express high levels of CDK6 (K. Kollmann et al., 2013; Redl et al., 2021). Deletion of CDK6 is associated with a delayed onset of NPM-ALK-mediated thymic lymphomas in mice (K. Kollmann et al., 2013), and human NPM-ALK cell lines are sensitive to CDK4/6 kinase inhibitors (Hoareau-Aveilla et al., 2019). This positions CDK6 as a potential drug target in ALK<sup>+</sup> ALCL.

#### **1.7.6 CDK6 inhibitors and degraders**

Cell cycle deregulation is one of the most common features of human cancer, caused by aberrant CDK activation (Cordon-Cardo, 1995). CDKs have been a popular target for pharmacological suppression due to their involvement in cancer initiation and progression (reviewed by (Malumbres & Barbacid, 2009)). Since then, numerous CDK4 and CDK6 dual kinase inhibitors, interfering with the ATP binding pocket, have successfully entered the clinics (Nebenfuehr et al., 2020; Sherr et al., 2016).

Palbociclib, Ribociclib and Abemaciclib have been approved for the treatment of ERB-B2 receptor tyrosine kinase 2 (HER2)-negative breast cancer and are currently undergoing clinical trials to test their efficacy in solid tumours and leukaemia (Sobhani et al., 2019). Palbociclib not only interferes with the cell cycle but also targets other kinase-dependent functions of CDK6, thereby inducing a senescence-like phenotype and enhancing cancer cell immunogenicity (Goel et al., 2018). Many side effects of CDK4/6 inhibitors, including neutropenia, lymphopenia, anaemia and thrombocytopenia, are explained by the role of CDK6 in haematopoiesis (Maurer, Brandstoetter, et al., 2020).

In addition to CDK4/6 inhibitors, specialized protein degraders called PROTACs that hijack the cell's proteasomal degradation machinery have recently been developed (Rana et al., 2019). By selectively targeting CDK6, these drugs not only target the kinase-independent regulatory roles of CDK6, but they also avoid the probable elevation of CDK6 expression reported in patients treated with CDK4/6 kinase inhibitors, which generally leads to therapy resistance (Yang et al., 2017).

## **1.8 The connection between CDK6 and STAT5**

It has been shown that CDK6 directly interacts with STAT3 to regulate gene expression (e.g., p16 (K. Kollmann et al., 2013)). Our lab has generated various lines of evidence also pinpointing to an interplay of CDK6 and STAT5: In the absence of CDK6, the progression of STAT5-dependent JAK2<sup>V617F</sup>- and BCR-ABL-driven haematopoietic diseases decelerates and disease symptoms are ameliorated (Scheicher et al., 2015; Uras et al., 2019). This thesis will present further evidence pointing towards the interaction of CDK6 and STAT5A/5B and highlight the therapeutic potential of their combinatorial inhibition as alternative treatment strategies for resistant or refractive NPM-ALK-driven ALCL.

## **1.9 Thesis aim**

We have previously shown that in the absence of CDK6, a transgenic murine model of ALK<sup>+</sup> ALCL exerts a later disease onset. STAT5 is considered a proto-oncogene in leukaemia/lymphoma, but its role in NPM-ALK-driven tumours, and more precisely – the roles of STAT5A and STAT5B – have not been extensively studied. Resistance mechanisms towards ALK inhibitors have to be anticipated, and alternative treatment strategies are highly needed to allow for a full molecular response. Understanding the mechanism of the disease would allow us to pursue novel therapeutic strategies, leading to a beneficial or curative outcome in NPM-ALK tumours.

In this thesis, we will address the necessity of CDK6 and STAT5A or STAT5B in NPM- mediated-malignant transformation. We also aim to discover whether NPM-ALK directly phosphorylates STAT5A or STAT5B, as has been shown for STAT3 (Zamo et al., 2002). Finally, we aim to unravel the so-far unknown interplay of CDK6 and STAT5A/B in NPM-ALK-driven tumours, which shall be directly applicable for pharmacologic intervention in ALK<sup>+</sup> ALCL patients.

## 2 Materials and Methods

### 2.1 Materials

#### 2.1.1 Reagents

**Table 1: Reagents**

Reagents	Company
Roti Histofix (4% Formaldehyde)	Roth
Proteinase K	Sigma Aldrich
Propan-2-ol	Roth
100% Ethanol	Scharlau
Methanol	Sigma Aldrich
Distilled water (ddH <sub>2</sub> O)	MiliQ
dNTP Mix	Fermentas
Dream Tag DNA Polymerase	Fermentas
Agarose	peqLAB
Ethidium Bromide	Roth
Gene Ruler™ 100 bp DNA ladder	Fermentas
Gene Ruler™ 1 bk DNA ladder	Fermentas
DNA Gel Loading Dye (6X)	Fermentas
Histo-Clear	Samova
Haematoxylin solution	Merck
Eukitt® mounting medium	Sigma Aldrich
Aquatex	Merck
Dako Target Retrieval Solution, Citrate buffer pH 6	Agilent
Avidin/Biotin	Abcam
Superblock	Thermo Scientific
Hydrogen peroxide (H <sub>2</sub> O <sub>2</sub> )	Roth
RPMI-1640 Medium	Sigma Aldrich
Dulbecco's Modified Eagles Medium (DMEM)	Sigma Aldrich
Fetal Calf Serum (FCS)	Capricorn

Penicillin	Sigma Aldrich
Streptomycin	Sigma Aldrich
$\beta$ -mercaptoethanol	Sigma Aldrich
Recombinant murine IL-3, IL-10	R&D Systems (Biomedica)
Recombinant murine IL-7	StemCell Technologies
Recombinant murine IL-6	IMP
Stem Cell Factor (SCF)	Preprotech
Dimethyl sulfoxide (DMSO)	Sigma Aldrich
Etoposide	Selleckchem
BSJ-03-123 (CDK6 degrader)	Selleckchem
Ruxolitinib	Cayman Chemical Company
Tofacitinib	Selleckchem
Crizotinib	Selleckchem
Alecetinib	Selleckchem
Palbociclib	Selleckchem
Imatinib	Selleckchem
Crenolanib	Selleckchem
Liquid nitrogen	MVE
Methylcellulose	StemCell
RNeasy Mini Kit	Qiagen
iScript cDNA Synthesis Kit	BioRad
RNAse-free H <sub>2</sub> O	Qiagen
Formaldehyde	Sigma Aldrich
30% Acrylamide (Bis-acrylamide)	Roth
N,N,N',N'-Tetramethylethylenediamine (TEMED)	Sigma Aldrich
10% Ammonium Persulfate (APS)	Thermo Scientific
Protease inhibitor cocktail (Complete Tablete)	Roche
Sodium Orthovanadate	Sigma Aldrich
BCA Protein Assay Kit	Pierce-Thermo Scientific
Bovine Serum Albumin (BSA)	Roth
Clarity™ Western ECL substrate	BioRad

Page Ruler Protein ladder (10–180 kDa)	Thermo Scientific
Pierce™ Western Blot Signal Enhancer	Thermo Scientific
Cell-TiterGlo® Luminescent cell Viability Assay	Promega
Polybrene	Thermo Scientific
PowerUp SYBR Green PCR Master Mix	BioRad

### 2.1.2 Buffers

Unless stated otherwise, the buffer solutions were created in house and the standard chemicals were purchased from Sigma Aldrich, Carl Roth or Merck.

**Table 2: Buffers**

Buffer	Final Concentration/Amounts	Component
1x PBS	137 nM 2.7 mM 4.3 mM 1.4 mM	NaCl KCl Na <sub>2</sub> HPO <sub>4</sub> * 2H <sub>2</sub> O KH <sub>2</sub> PO <sub>4</sub>
RIPA buffer	150 mM 1.0% 0.5% 0.1% 50 mM	NaCl Triton X-100 Sodium Deoxycholate SDS TRIS (pH 8.0)
1x Laemmli buffer	100 mM 2.5% 10%	Tris/HCl (pH 6.8) SDS Glycerol
4x Laemmli loading buffer, 20 ml	2 g 4 ml 1 ml 8 ml 800 µl	DTT 20% SDS 1 M Tris-HCl (pH 6.8) 99.9% Glycerol Bromphenol blue Add H <sub>2</sub> O to 20 ml
10x SDS-PAGE running buffer	250 mM 1920 mM 10 mM 17.5 mM	TRIS Glycine EDTA-Na <sub>2</sub> SDS Pellets
10x Transfer buffer	250 mM 1.92 M	TRIS Glycine Add H <sub>2</sub> O to 1 L

1x Transfer buffer	300 ml 600 ml 2100 ml	10x Transfer buffer 100% EtOH H <sub>2</sub> O
10x pY-TBST	100 ml 43.8 g 20 ml 10 ml	1 M Tris/HCl (pH 8.0) NaCl 500 nM EDTA TWEEN-20
Blocking solution	5%	Milk powder Add 1x pY-TBST
20x TAE	96.8 g 21.8 g 5.85 g	Tris-Base Acetic acid EDTA (pH 8.0) Add H <sub>2</sub> O to 1 L
DNA lysis buffer	50 mM 100 mM 100 mM 1%	Tris/HCl EDTA-Na <sub>2</sub> NaCl SDS
Eosin Y	0.1% 80% 0.25%	Eosin 100% EtOH Acetic acid
(Propidium iodide) PI buffer	113.9 mg 100 mg 100 ml	0.1% Na-Citrat dyhidrat 0.1% Triton-X-100 1xPBS
Acidic alcohol	1% 70%	HCl EtOH
Wash/Stain buffer	2% 0.2%	FCS (Capricorn) TWEEN-20 In 50 ml PBS
10x PCR buffer II	200 mM 450 mM	Tris/HCl KCl

### 2.1.3 Consumables

**Table 3: Consumables**

Material	Company
Fisherbrand™ Cell Strainer (70 µm)	Fisher Scientific
Syringes (50 ml, 10 ml, 3 ml)	Henry Schein Medical

Polyvinylidene fluoride (PVDF) Membrane	Merck
Whatman Paper	Hartenstein A.
Sterile filter (45 nm, 70 nm)	Starstedt
Falcon tubes (15 ml, 50 ml)	Starstedt
Flat bottom sterile cell culture plates (96-well, 48-well, 24-well, 12-well, 6-well)	Corning
Round Bottom Sterile Cell Culture Plates (96-well)	Corning
Sterile Cell Culture Dish (3.5 cm, 10 cm)	Corning
PCR Strips with Caps	4titude
PCR Plate (96 well)	4titude
qPCR Plate (96 well)	4titude
(q)PCR Plate Seal	4titude
Histology Cassettes	VWR
Graduate Filter Tips (10 µl, 20 µl, 100 µl, 200 µl, 1000 µl)	Starlab
Seriological Pipettes (5 ml, 10 ml, 25 ml, 50 ml)	Starlab
Superfrost Plus microscope slides	Menzel-Gläser
Eppendorf Tubes	Eppendorf
Falcon Tubes (15 ml, 50 ml)	Fisher Scientific
Magnetic Beads	BioRad
Cryogenic vials (Cryotubes)	Greiner Bio-One
Nitrile Gloves	Hartmann
Round Bottom Polystyrene Tube (with Cell Strainer Snap Cap)	Corning
Round Bottom Polypropylene Tube	Corning

#### 2.1.4 Devices

**Table 4: Devices**

Devices/Apparatus	Company
Rotina420 Centrifuge	Hettich Zentrifugen
Magnetic rack	MACS Miltenyi Biotec
PCR Detection System CFX96™ Real Time System	BioRad

Thermocycler	BioRad
Nanodrop One	Thermo Scientific
BD FACS Aria	BD Bioscience
CytoFLEX S	Beckman Coulter
Heating block (Thermoheater Compact)	Eppendorf
ChemiDoc™ Touch Imageing System	BioRad
Enspire Microplate reader	Perkin Elmer
CytoFLEX	Beckman Coulter
Sonicator	Bandelin
Pipette (0.2–2 µl, 1–10 µl, 2–20 µl, 20–200 µl, 100–1000 µl)	Gilson
Pippete boy	Integra
Zeiss Axioimager Z1 with PixelINK camera	Zeiss & Pixelink
Mr. Frosty	Sigma Aldrich
Flourescent microscope	Olympus
Fresco™ Microcentrifuges	Thermo Fisher Scientific
Gel Doc™ EZ Imager	BioRad
Agarose Gel Caster	BioRad
Mini-Sub GT Electrophoresis Cell	BioRad
PowerPac Universal Power Supply	BioRad
Microtome	Leica
EnSpire plate reader	Perkin Elmer
Vortex	IKA
BLACK and WHITE cel plates	Crescent Scientific
Mini-PROTEAN System	BioRad
Criterion System	BioRad
Rotating shaker	Stuart
Shaker	Labnet International

### 2.1.5 Cell lines

The murine Ba/F3 cell line was kindly provided by Dr. Deininger (Huntsman Cancer Institute, University of Utah, Salt Lake City, UT, USA) in 2013. ALK<sup>-</sup> ALCL cell line Mac2A were obtained from Dr. Merkel (Medical University of Vienna) and have previously been derived from

advanced cutaneous tumour nodules with anaplastic morphology (Davis et al., 1992; Ehrentraut et al., 2013). The virus packaging cell line Platinum-E (Plat-E) was obtained from Cell Biolabs, Inc.

**Table 5: Cell lines**

Name of the cell line	Type of the cell line
Ba/F3	IL-3-dependent murine pro B cell line
Mac2A	ALK <sup>+</sup> ALCL cell line
Platinum-E (Plat-E)	Retroviral Packaging cell line

### 2.1.6 Animals

The mice were bred on C57BL/6N background and housed in a specific-pathogen free facility under standardized conditions at the University of Veterinary Medicine Vienna according to Federation for Laboratory Animal Science Association (FELASA) guidelines. All animal experiments were carried out according to the animal license protocol approved by the institutional Ethics Committee, Animal Welfare Committee of the University of Veterinary Medicine Vienna and the Austrian Ministry of Education, Science and Research authorities. Mice used for ageing experiments were monitored daily for signs of disease. For *ex vivo* experiments the mice were age- (8–12 weeks) and gender-matched.

**Table 6: Mouse strains**

Mouse strain	Mouse background
<i>NPM-ALK<sup>+T</sup></i>	<i>C57BL/6N</i>
<i>NPM-ALK<sup>+T</sup> Cdk6<sup>-/-</sup></i>	<i>C57BL/6N</i>
<i>NPM-ALK<sup>+T</sup> Stat5a<sup>-/-</sup></i>	<i>C57BL/6N</i>
<i>NPM-ALK<sup>+T</sup> Stat5b<sup>-/-</sup></i>	<i>C57BL/6N</i>
<i>NPM-ALK<sup>+T</sup> Cdk6<sup>-/-</sup> Stat5a<sup>-/-</sup></i>	<i>C57BL/6N</i>
<i>NPM-ALK<sup>+T</sup> Cdk6<sup>-/-</sup> Stat5b<sup>-/-</sup></i>	<i>C57BL/6N</i>
<i>wt</i>	<i>C57BL/6N</i>
<i>Cdk6<sup>-/-</sup></i>	<i>C57BL/6N</i>
<i>Cdk6<sup>-/-</sup> Stat5a<sup>-/-</sup></i>	<i>C57BL/6N</i>
<i>Cdk6<sup>-/-</sup> Stat5b<sup>-/-</sup></i>	<i>C57BL/6N</i>

### 2.1.7 Primers

All primers were obtained from Eurofins MWG/Operon. All sequences are written in 5' to 3' direction.

**Table 7: Primers for qPCR**

Gene	Primer Sequence
<i>Rplp0</i>	Fw GCTTTCTGGAGGGTGTCC Rv GCTTCAGCTTTGGCAGGG
<i>NPM-Alk</i>	Fw GTTCAGGGCCAGTGCATATT Rv TTGGGGTTGTAGTCGGTCAT

**Table 8: Primers for genotyping**

Gene	Primer	Primer sequence
<i>NPM-Alk</i>	cre fr cre rev myo fw myo rev	TCCCTTGGGGGCTTTGAAATAACACC CGAGGTGCGGAGCTTGCTCAGC TTACGTCCATCGTGGACAGC TGGGCTGGGTGTTAGCCTTA
<i>Stat5a</i>	Stat5a fw Stat5a m rev Stat5a wt rev	GAGACCTTAGAAGTAGGCTTGGCT TGACGAGTTCTTCTGAGGGGAT GGAATGAGGGAGGAGCGTC
<i>Stat5b</i>	Stat5a fw Stat5a m rev Stat5a wt rev	CCAAGAGTACTTCATCATCCAGTACCAG TGACTAGGGGAGGAGTAGAAGGTG GAACCAGGATCTCTTCTGCTTCCTC
<i>Cdk6</i>	Cdk6 m fw Cdk6 wt rev Cdk6 wt fw Cdk6 m rev	CTAAAGCGCATGCTCCAGAC AGAGATCTCCACAGGGTTCCAC TCAGCTAGCGCTGCGCTCAT GCTCCACCCTTAAAGTTTCC

### 2.1.8 Antibodies

**Table 9: Primary antibodies used for protein analysis by Western blot**

Antibody	Company	Mouse/Rabbit	Catalogue No.	Dilution
pALK (Y1278/1282/1283)	Cell Signaling	Rabbit	3983S	1:500
ALK (D5F3)	Cell Signaling	Rabbit	3633P	1:500

pSTAT5 (Y694/699)	Becton Dickinson	Mouse	611965	1:1,000
STAT5A/B	R&D Systems	Rabbit	AF2168	1:1,000
pSTAT3 (Y705)	Cell Signaling	Rabbit	9131S	1:1,000
STAT3 (D3Z2G)	Cell Signaling	Rabbit	12460	1:1,000
CDK6 (H-96)	Santa Cruz	Rabbit	sc-7180	1:1,000
CDK6 (DSC-90)	Santa Cruz	Mouse	sc-56282	1:1,000
HSC-70	Santa Cruz	Monoclonal mouse	sc-7298	1:1,000
$\beta$ -ACTIN	Sigma Aldrich	Monoclonal mouse	A5136	1:1,000
A-TUBULIN	Cell Signaling	Rabbit	2144	1:1,000

**Table 10: Secondary antibodies used for protein analysis by Western blot**

Antibody	Company	Catalogue No.	Dilution
Anti-mouse IgG HRP-linked antibody	Cell Signaling	7076	1:10,000
Anti-rabbit IgG HRP-linked antibody	Cell Signaling	7074	1:10,000

**Table 11: Immunoprecipitation Antibodies**

Antibody	Company	Catalogue No.
STAT5A	R&D	MAB2174
STAT5B	Abcam	Ab178941

All flow cytometry antibodies and dyes were obtained from eBioscience unless indicated otherwise (**Table 12**).

**Table 12: Flow Cytometry Antibodies and dyes**

Antigen	Fluorochrome	Catalogue No.
CD117 (KIT)	PE-Cy5, APC	15-1171-83, 17-1171-82
CD11b	FITC, eFluor <sup>®</sup> 450	11-0112-82, 48-0112-82
CD25	APC	17-0251-81
CD3	eFluor <sup>®</sup> 450	48-0032-82
CD3e	PerCP Cy5.5	45-0031-82

CD4	FITC, PE	11-0041-82, 12-0041-82
CD44	PE	12-0441-82
CD8a	FITC, PE, PerCP Cy5.5, APC	11-0081-82, 12-0081-82, 45-0081-82, 17-0081-82
TER-119	eFluor 450	48-5921-82
TCR $\gamma\delta$	FITC	11-5711-81
SYTOX™ Green Nucleic Acid Stain	SYTOX™ Green	S7020 (Invitrogen™)
DAPI	PB	D9542 (Sigma)
Annexin-V	PE	A35111 (Invitrogen)
Propidium Iodide (PI)	PE	P1304MP (Invitrogen)
pY-STAT5 (Tyr694)	PE	12-9010-42
pY-STAT3 (Tyr705)	FITC	11-9033-42

**Table 13: Immunohistochemistry Antibodies**

Antibody	Company	Catalogue No.	Dilution	Unmasking buffer
Ki67 (D3B5)	Cell Signaling Technology	12202	1:400	Citrate

### 2.1.8.1 Plasmids

The *pMSCV-NPM-ALK* vector was a gift from Lukas Kenner (Staber et al., 2007). The *pLENC* vector backbone was a gift from Johannes Zuber (Addgene plasmid # 111163 ; <http://n2t.net/addgene:111163> ; RRID:Addgene\_111163). Furthermore, the *shStat5a*, *shStat5b*, *shCdk6* and *shRenilla* plasmid derivatives were synthesized in the lab as previously described.

**Table 14: Plasmids**

Plasmid	Backbone	Components
NPM-ALK	<i>pMSCV</i>	<i>pMSCV-NPM-ALK</i> -Internal ribosome entry site ( <i>IRES</i> )- <i>GFP</i>
<i>shStat5a</i>	<i>pLENC</i>	<i>pMSCV-shStat5a-PGK-NeoR-IRES-mCherry</i>
<i>shStat5b</i>	<i>pLENC</i>	<i>pMSCV-shStat5b-PGK-NeoR-IRES-mCherry</i>
<i>shCdk6</i>	<i>pLENC</i>	<i>pMSCV-shCdk6-PGK-NeoR-IRES-mCherry</i>
<i>shRen</i>	<i>pLENC</i>	<i>pMSCV-shRenilla(713)-PGK-NeoR-IRES-mCherry</i>

## 2.2 Methods

### 2.2.1 Generation of *in vivo* NPM-ALK<sup>+T</sup> mouse models

The transgenic NPM-ALK mouse model (Chiarle et al., 2003) develops ALCL. The NPM-ALK transgene is expressed under the CD4 promoter. Therefore, the fusion protein is only present in thymocytes after CD4 promoter activation in the DP stage of thymocyte maturation. NPM-ALK transgenic mice were crossed with *Cdk6*<sup>-/-</sup> (Malumbres et al., 2004), *Stat5a*<sup>-/-</sup> (Liu et al., 1997), and *Stat5b*<sup>-/-</sup> (Udy et al., 1997) mice. All NPM-ALK transgenic mice were hemizygous, and non-transgenic littermates served as controls. The *Stat5a* and *Stat5b* loci were bred heterozygous to produce full-body homozygote knockouts. The *Cdk6* locus was bred to be homozygous. At weaning, ear punches served for labelling of mice and were used for genotyping (described in chapter 2.2.4).

### 2.2.2 Ageing of NPM-ALK<sup>+T</sup> mouse models

*NPM-ALK*<sup>+T</sup> wt, *Cdk6*<sup>-/-</sup>, *Stat5a*<sup>-/-</sup>, *Stat5b*<sup>-/-</sup>, *Cdk6*<sup>-/-</sup> *Stat5a*<sup>-/-</sup> and *Cdk6*<sup>-/-</sup> *Stat5b*<sup>-/-</sup> mice were utilised for ageing experiments and were monitored daily for signs of disease. The ageing experiment endpoint was defined as the development of thymic lymphoma, which manifested in breathing difficulties for the mice. At first signs of disease – breathing difficulties or any disease indications according to FELASA guidelines – mice were sacrificed by cervical dislocation, and the tissues of interest were collected.

### 2.2.3 Tissue collection and processing

The sacrificed mouse's ear tissue was collected for re-genotyping in Eppendorf tubes and stored at -20°C. Tissues of interest were excised, weighed, collected in ice-cold PBS or RPMI-1640 medium (Sigma Aldrich) (e.g., for immediate flow cytometry and *in vitro* analysis) or formalin-fixed and paraffin-embedded for histological and immunohistochemical examinations. Formalin-fixation was done in Roti Histofix (4% Formaldehyde, Carl Roth) at 4°C for 24 h. Afterwards, tissues were dehydrated by automated ethanol gradients (Scharlau) and placed in disposable plastic histology cassettes (VWR) to hold tissue specimens during the paraffin embedding process.

### 2.2.3.1 Single-cell suspensions

Single-cell suspensions of thymocytes were obtained by mincing the excised thymi and thymic lymphomas through 70 µm cell strainers (Fischer Scientific) and washed twice with PBS to remove any fat residue.

Murine BM cells were recovered by crushing of femora and tibiae in PBS using a mortar and pestle. The single-cell suspension was filtered through a 70 µm cell strainer (Fisher Scientific) and washed once with PBS.

### 2.2.3.2 Downstream processing

The single-cell suspensions were either cultured *in vitro* (described in 2.2.6.1), directly used for immediate downstream analysis, such as RNA (described in 2.2.17) or protein extraction (described in 2.2.15) and flow cytometry (described in 2.2.14), cryo-preserved (described in 2.2.6.4) or pelleted and snap-frozen in liquid nitrogen, then stored at -80°C for RNA or protein extraction at a later time.

### 2.2.4 Genotyping

Each mouse was genotyped by PCR and re-genotyped when sacrificed. Ear tissue of sacrificed mice was digested with 500 µl DNA lysis buffer supplemented with 12.5 µl Proteinase K (Sigma Aldrich). The digestion was performed for 2–3 h at 55°C on a constantly shaking block heater (Eppendorf) at 800 rounds per minute (rpm) or o/n not shaking. Next, 200 µl of 5 M NaCl was added to the digestion and centrifuged for 10 min at 14,000 g. 450 µl of the supernatant was transferred into a new Eppendorf tube (Eppendorf) with 300 µl of Propan-2-ol (Roth) and incubated at -20°C for at least 5 min. After 15 min centrifugation at 14,000 G, the supernatant was discarded, and the pellet was washed with 1 ml 70% Ethanol (EtOH, Scharlau) and centrifuged for 10 min at 14,000 g. After removing the supernatant, the pellet was airdried for at least 30 min and then resuspended in 100–150 µl distilled water (ddH<sub>2</sub>O, MiliQ).

The PCR reactions were prepared on ice as described in **Table 15**. Each reaction was mixed well in PCR 96-well-plates (4titude) and was run on the thermal cycler (BioRad) using the following protocol: single step of 95°C (5 min); followed by 35 cycles of 95°C (30 sec), 60°C (Cdk6, NPM-Alk) or 55°C (Stat5a, Stat5b) (40 sec), 72°C (40 sec); a single step of 72°C (5 min) and 20°C (hold).

**Table 15: PCR reaction mix**

Reagent	Volume per reaction
10 $\mu$ M Primer mix	variable
10x PCR buffer II	2.00 $\mu$ l
15 mM MgCl <sub>2</sub>	2.00 $\mu$ l
2 mM dNTPs	2.00 $\mu$ l
DNA TAQ Polymerase	0.10 $\mu$ l
ddH <sub>2</sub> O	Fill up to 18 $\mu$ l

Each PCR product was mixed with 4  $\mu$ l 6x DNA loading dye (Thermo Scientific). 15  $\mu$ l were loaded on a 1.5% (w/v) agarose gel immersed in 1x Tris Acetate (TAE) buffer until appropriate separation occurred. DNA was visualized with ethidium bromide (Roth) in TAE Gel (1:20,000) exposed to ultraviolet (UV) light in the ChemiDoc™ Touch Imaging System (BioRad). As a reference marker, the Gene Ruler™ 100 bp DNA ladder (Thermo Scientific) was used.

### 2.2.5 Tissue histology

For histological or immunohistochemical analyses, 3  $\mu$ m thick consecutive Formalin-Fixed Paraffin-Embedded (FFPE) sections were cut using a standard microtome (Leica) and transferred to “Superfrost Plus” microscope slides (Menzel-Gläser). Following H&E staining or immunohistochemistry, light microscopic images were captured with a PixeLINK camera (Pixelink) and the corresponding acquisition software on a Zeiss Aixolmager Z.1 (Zeiss, magnification:  $\times$ 100,  $\times$ 200 and  $\times$ 400).

#### 2.2.5.1 Haematoxylin and Eosin staining

Sections were stained with Haematoxylin and Eosin (H&E) using standard procedures. Therefore, sections were deparaffinised in Histo-Clear (Samova) followed by rehydration in a descending EtOH (Scharlau) gradient to ddH<sub>2</sub>O (MiliQ). Sections were incubated in Haematoxylin solution (Merck) for 10 min and subsequently rinsed in tap water. The slides were shortly exposed to acidic alcohol (1% HCl in 70% EtOH) and again rinsed in tap water. Counter staining of nuclei was achieved by incubation in Eosin Y buffer for 2 min. Sections were dehydrated in an ascending EtOH (Scharlau) gradient and mounted using Eukitt mounting medium (Sigma Aldrich).

### 2.2.5.2 Immunohistochemistry (IHC)

Tissue sections were deparaffinized with Aquatex (Merck) and rehydrated in Histo-Clear and a descending EtOH (Samova) gradient to ddH<sub>2</sub>O (MiliQ). Heat-induced antigen retrieval was performed in citrate buffer. Slides were processed and counterstained as previously described (Hassler et al., 2012). In brief, the endogenous Peroxidase was blocked with 3% H<sub>2</sub>O<sub>2</sub> (Roth) for 10 min, before sequentially treated with Avidin/Biotin block (Abcam) and Superblock (Thermo Scientific) for 10 min each. Slides were incubated with primary antibody against the marker of proliferation Ki67 (**Table 12**) diluted in 1% PBS/BSA over night at 4°C, incubated with the corresponding HRP-bound secondary antibody and developed. Stainings were performed in three biological replicates for each genotype.

### 2.2.6 Cell culture

All cells were grown at 37°C and 5% CO<sub>2</sub> in a humidified atmosphere. The cells were split/expanded 3–4 times a week. The centrifugation steps were carried out with the Hettich centrifuge (Rotina 420) at 1000–1200 rounds per minute (rpm) for 5 min at room temperature (RT). For dead-live centrifugation, the centrifugation speed was set to 500 rpm.

#### 2.2.6.1 Generation of primary murine *NPM-ALK<sup>+T</sup>* cell lines

The NPM-ALK cell lines were established from primary thymic lymphomas. Single-cell suspensions were resuspended in 2.5 ml of complete RPMI medium (RPMI-1640 medium (Sigma-Aldrich); supplemented with 10% heat-inactivated FCS (Capricorn), 10 U/ml Penicillin/Streptomycin (Sigma Aldrich), 50 nM β-mercaptoethanol (Sigma Aldrich)) and monitored in culture for two weeks.

#### 2.2.6.2 Cultivation of murine cell lines

The primary murine NPM-ALK cell lines, as well as the Ba/F3 cells (Palacios & Steinmetz, 1985) and its derivatives expressing the NPM-ALK transgene (Staber et al., 2007), were cultured in complete RPMI medium. The parental Ba/F3 cells were additionally cultured with recombinant murine IL-3 (1 or 2 ng/ml, R&D systems).

### **2.2.6.3 Cultivation of human cell lines**

The ALK<sup>-</sup> ALCL cell line Mac2A was grown in complete RPMI medium. Platinum-E (Plat-E) retroviral packaging cell line was cultured and maintained in complete DMEM medium (Sigma Aldrich; 10% FCS (Capricorn), 10 U/ml Penicillin/Streptomycin (Sigma Aldrich)).

### **2.2.6.4 Freezing of single-cell suspensions**

Single-cell suspensions of cell lines or primary murine tissue were pelleted and resuspended in 2x Resuspension medium (DMEM medium, 40% FCS), followed by 1:1 addition of 2x Freezing medium (DMEM medium, 40% FCS, 30% DMSO). The cryogenic vials (Greiner Bio-One) were filled with 1 ml of dissociated cells, labelled and stored at  $-80^{\circ}\text{C}$  in a Mr. Frosty (Sigma-Aldrich) to allow for a slow cooldown. The following day, the cryogenic vials were transferred to a long term  $-80^{\circ}\text{C}$  storage.

### **2.2.6.5 Thawing of single-cell suspensions**

In brief, cryogenic vials (Greiner Bio-One) were placed into a  $37^{\circ}\text{C}$  degree water bath until thawed. The freshly thawed cells were then dispersed into 10 ml of the respective culture media and centrifuged at 200 g or 5 min at RT. After the centrifugation, the cells were cultured and maintained as described previously in 2 and 3 or immediately used for downstream processing.

### **2.2.6.6 Preparation of conditioned media**

Primary murine cell lines of all four genotypes were grown in 6-well dishes (Corning) with complete RPMI medium until the cells reached confluency (2–3 days). The cells were washed with PBS and resuspended in 3 ml of fresh complete RPMI medium, and placed in one well of a 6-well-plate (Corning). After an incubation period of 24 h at  $37^{\circ}\text{C}$ , the conditioned media was filtered using a  $0.45\ \mu\text{m}$  filter (Starstedt) and then diluted 1:1 by addition of respective primary culture media. The final conditioned medium was aliquoted into 15 ml tubes (F and stored at  $-80^{\circ}\text{C}$  or immediately used for experiments.

### **2.2.7 Growth curve**

Cells were washed and resuspended in complete RPMI medium.  $5 \times 10^3$  or  $1 \times 10^4$  cells were seeded per cell line in one well of a 48-well plate (Corning). Cells were counted via flow-

cytometry (CytoFLEX, Beckman Coulter) over a period of 7–14 days and expanded if necessary.

### **2.2.8 Limiting cell dilution assay**

Cells were washed and resuspended in complete RPMI or conditioned medium. They were seeded in technical triplicates in 96-well-plates in 200  $\mu$ l medium, in the following numbers: 50, 100, 500,  $1 \times 10^3$ ,  $5 \times 10^3$ . The cell number was monitored via flow cytometry (CytoFLEX, Beckman Coulter) over a period of 7–14 days and expanded if necessary.

### **2.2.9 Pharmacological perturbations**

#### **2.2.9.1 Single drug treatments**

$3 \times 10^3$ ,  $5 \times 10^3$  or  $1 \times 10^4$  murine cells were seeded in complete RPMI medium in transparent U-well 96-well-plates (Corning). Serial dilutions of Ruxolitinib (Cayman Chemical Company), Tofacitinib, Crizotinib, Alecetininib, Palbociclib and Crenolanib (all Selleckchem) were added to the cells in technical triplicates, mixed well by pipetting and incubated for 72 h. Additionally, each cell line had a DMSO (Sigma Aldrich) only control and a positive Etoposide control (10  $\mu$ M, Selleckchem). The CDK6 degrader concentrations (BSJ-03-123, Selleckchem) were renewed every 24 h.

#### **2.2.9.2 CellTiter-Glo viability assay**

CellTiter-Glo<sup>®</sup> (Promega) reagent was used to determine cell viability. For CellTiter-Glo<sup>®</sup> measurement, 100  $\mu$ l of the cells were transferred into white 96-well-plates (Crescent technologies), mixed 1:1 with the 1:5 in PBS pre-diluted CellTiter-Glo<sup>®</sup> reagent and incubated on thermoblock (Eppendorf) shaking on 37°C, protected from light, for 15 min. The chemiluminescence was measured on an EnSpire plate reader (PerkinElmer). The chemiluminescence measurements were normalised to the DMSO only control and the positive control was set to 100% inhibition. The inhibitory concentrations (IC<sub>50</sub>) were determined using GraphPad Prism<sup>®</sup> 8 by non-linear regression.

#### **2.2.9.3 Combinatorial treatments**

$5 \times 10^3$  murine cells were seeded in complete RPMI medium in transparent U-well 96-well-plates (Corning). Combinatorial treatments were performed by simultaneously

applying two drug treatments on the separate axis of the 96-well-plate. Serial dilutions of inhibitors (Ruxolitinib (Cayman Chemical Company), Crizotinib, Palbociclib, both Selleckchem) or CDK6 degrader (BSJ-03-123, Selleckchem) were added to the cells and incubated for 72 h. Each cell line had one DMSO (Sigma Aldrich) only control and single-drug treatments for each drug and concentration. As previously mentioned, the CDK6 degrader concentrations (BSJ-03-123, Selleckchem) were renewed every 24 h.

Cell viability following combinatorial treatments was performed as previously described (2.2.9.2). The Combinatorial treatment viability readouts were analysed and visualized using SynergyFinder 2.0 (lanevski et al., 2020). The degree of synergy between inhibitors of interest was determined by comparing the observed impact against the expected drug response, calculated using the Bliss independence reference model. The Bliss model implies that the two medications have independent effects and that the expected combination effect may be estimated based on the likelihood of independent events (Bliss, 1939).

### 2.2.10 shRNA-mediated knockdown of *NPM-ALK*<sup>+T</sup> cell lines

The short hairpin RNA (*shRNA*) plasmids mentioned in **Table 14** were used in order to generate and investigate single knockdown models, as well as double knockdown-knockout models to mimic the *in vivo* double knockout models. The mCherry fluorescent marker is genetically connected to the Neomycin resistance cassette and is used as a readout of successful target cell infection (**Figure 12**).



**Figure 12: Schematic map of pLENC vector**

Schematic map of validated constitutive (*pMSCV*) retroviral *shRNA* expression vector with optimised backbone, featuring different Neomycin resistance cassette and mCherry fluorescent markers (Fellmann et al., 2013).

#### 2.2.10.1 Plasmid transfection to Plat-E cells

Virus supernatants were produced using Plat-E cells that were separately transfected with a *pLENC* retroviral vector containing the following *shRNAs*: *shCdk6*, *shStat5a*, *shStat5b* and *shRenilla* (*shRen*) (**Table 14**). The transfection was done using Turbofect according to the

manufacturer's instruction. In brief, Plat-E cells were grown in 10-cm-dishes with 10 ml of complete DMEM media until the cells reached 70–80% confluency. 20 µg of the desired viral vector and 40 µl Turbofect were resuspended in 2 ml of serum-free DMEM (Sigma Aldrich), mixed thoroughly and set for 15 min incubation at RT. After the incubation, the mix was added dropwise to the Plat-E cells, rocked to mix and incubated o/n at 37°C. The next day the viral DMEM media was replaced by 7 ml of target cell medium (complete RPMI) and incubated o/n. After 24 and 48 h, the viral supernatants were harvested, filtered (0.45 µm), and the Plat-E cells were again incubated o/n with 7 ml of fresh complete RPMI media.

#### **2.2.10.2 Target cell infection**

Target cells were spin-infected with virus supernatant on each of the following two days. The target cells were grown for two days after passage.  $4 \times 10^6$  cells were resuspended in 500 µl of complete RPMI medium and seeded in one well of a 6-well-plate (Corning). In the next step, 2.5 ml of the filtered virus supernatant, supplemented with Polybrene (1:500, Thermo Scientific), was added to the cells, and the spin infection was performed at 600 g for 1 h. After the spin infection was completed, the plate was placed in the incubator at 37°C for 24 h. The same procedure was repeated the following day on the infected cells with a fresh dose of the viral supernatant. The cells were incubated at 37°C for 24 h before monitored for mCherry expression using fluorescence microscopy. In the following days, mCherry-positive (mCherry<sup>+</sup>) cells were regularly monitored by flow cytometry and eventually fluorescence-associated cell sorting (FACS)-sorted to achieve a pure population.

#### **2.2.11 Generation of Ba/F3 NPM-ALK-expressing cell line**

The IL-3-dependent murine B-cell progenitor cell line Ba/F3 was used for testing the NPM-ALK construct *in vitro*. The *pMSCV-NPM-ALK-IRES-GFP* vector, previously described by Gu et al. (2004), was used for the generation of NPM-ALK-expressing Ba/F3 cells.

##### **2.2.11.1 IL-3 deprivation**

IL-3 deprivation of Ba/F3 cell lines was performed to ensure the IL-3 dependence of parental Ba/F3 cells. The cells were washed twice and resuspended in RPMI medium without IL-3 or lower concentrations of IL-3 (R&D Systems). Cells were monitored over 14 days by SYTOX™ viability staining (Invitrogen) analysed by flow cytometry at respective time points.

### **2.2.11.2 Virus production and target cell infection**

Viral supernatants were produced as previously described (2.2.10.1), with the difference of using the *pMSCV* vector containing the NPM-ALK transgene. The target cell infection was also performed as previously described (2.2.10.2) with the following changes. In brief,  $3 \times 10^6$  Ba/F3 cells were resuspended in 500  $\mu$ l of complete RPMI medium and seeded in one well of a 6-well-plate (Corning) for the infection. The target cell medium, as well as the viral supernatant, were additionally supplemented with recombinant murine IL-3 (2 ng/ml, R&D Systems) during the infection. The viral supernatant was removed 24 h after the second spin infection, and the cells were resuspended in complete RPMI medium without IL-3.

### **2.2.11.3 Testing NPM-ALK construct *in vitro***

The cells were grown in complete RPMI medium with or without IL-3 (2 ng/ml, R&D Systems) for 14 days, regularly monitored via flow cytometry and SYTOX™ viability staining (Invitrogen). Furthermore, transgene expression analysis was performed via Western blotting or RNA expression analysis.

### **2.2.12 *Ex vivo* NPM-ALK-mediated transformation of BM cells**

The *pMSCV-NPM-ALK-IRES-GFP* vector was used for the NPM-ALK-mediated transformation of single-cell suspensions of BM cells. Viral supernatants were produced as previously described (2.2.10.1), with the difference of using the *pMSCV* vector containing the NPM-ALK transgene. The target cell infection was also performed as previously described (2.2.10.2) with the following changes: The viral supernatant was additionally supplemented with recombinant murine IL-3 (R&D Systems), IL-6 (IMP), IL-7 (StemCell Technologies) (all 10 ng/ml) and stem cell factor (SCF, 1:60, Preprotech) during the infection. The viral supernatant was removed 24 h after the second spin infection, and the cells were resuspended in complete RPMI medium without cytokines.

### **2.2.13 Colony formation assay (CFA)**

Following *ex vivo* NPM-ALK-mediated transformation of BM cells (2.2.12)  $1 \times 10^4$  green fluorescent protein (GFP)-positive (GFP<sup>+</sup>) cells were seeded in 2.5 ml of growth factor-free methylcellulose (StemCell Technologies) and plated on cell culture dishes with a diameter of 35 mm (Corning). Formed colonies (GFP<sup>+</sup>) were analysed under the fluorescent microscope after 21 days of incubation by colony counting per dish, and the pictures were taken using the

ChemiDoc™ Touch Imaging System (BioRad). Next, the colonies were liquefied with PBS and analysed via flow cytometry for total cell numbers and surface markers as previously described (2.2.14.1).

### **2.2.14 Flow cytometry**

Surface marker and intracellular flow cytometry were used in order to characterise cellular components of thymic lymphomas, thymi and established cancer cell lines. The analyses were performed on the CytoFLEX or the CytoFLEX S instrument (Beckman Coulter) and quantified with the CytEXPERT software (Beckman Coulter), if not indicated otherwise.

#### **2.2.14.1 Surface marker flow cytometry**

Single-cell suspensions of organs or cell lines were stained with antibodies conjugated to different fluorophores. For each staining, a master mix containing the desired antibodies was prepared (1:100 dilution in 2% FCS (Capricorn) in PBS). All antibodies used in this study are listed in (**Table 12**). The cell suspension was incubated 1:1 with the respective antibodies (1:200 final dilution) for 30–60 min, protected from light at 4°C. Unbound antibodies were removed by another washing step with PBS, cells were resuspended in 100–200 µl PBS and were analysed via flow cytometry. Compensations were done with single-antibody-stained cells, and FMOs (fluorescence minus one) were included for gating purposes.

#### **2.2.14.2 SYTOX viability analysis**

Cells were washed and incubated with the SYTOX dye (1:2,000) for 10 min at RT in the dark. The incubation was immediately followed by the measurement, performed using the CytoFLEX S flow cytometer and the results were analysed with the CytEXPERT software (Beckman Coulter).

#### **2.2.14.3 Cell cycle analysis**

Cell cycle analysis was performed with propidium iodide (PI) fluorescent DNA intercalating agent. For each sample, 500 µl of PI buffer was mixed well with PI dye (1:50) and RNase (10 mg/ml). Single-cell suspensions of organs or cell lines were washed once with PBS, and 100 µl cells were incubated with the propidium iodide staining mixture for 30 min at 37°C. The stained cells were then washed and analysed by flow cytometry.

#### **2.2.14.4 Apoptosis analysis**

Annexin-V/DAPI staining was performed for analysis of apoptosis. All steps were performed in Annexin-V Binding Buffer (1x). Single-cells suspensions were washed and resuspended in binding buffer. 100 µl of the cell suspension was incubated with 2 µl of fluorochrome-conjugated Annexin-V for 15 min in the dark at RT. The cells were then washed, centrifuged at 500 g for 5 min and resuspended in 100 µl of the Binding Buffer containing 2 µg/ml DAPI. After a 15 min incubation in the dark, the stained cells were analysed by flow cytometry.

#### **2.2.14.5 Intracellular staining**

Intracellular staining of STAT3, STAT5, pY-STAT3, pY-STAT5 on cell lines was carried out using the antibodies described in (**Table 12**). Cells were washed once with PBS and fixed by 2% formaldehyde (Sigma Aldrich)/PBS at 37°C for 10 min. Cells were permeabilized with 90% ice-cold methanol (Sigma Aldrich) in wash/stain buffer for 30 min at 4°C. Cells were washed twice with the wash/stain buffer and incubated with e.g., phosphoryated-STAT5-APC antibodies (diluted in wash/stain buffer) on ice, in the dark for 90 min. After two washing steps with incubation on ice for 10 min samples were analysed via flow cytometry.

#### **2.2.14.6 FACS sorting**

FACS sorting thymocytes or thymic lymphoma cell lines were performed at 4°C on a FACSAriaII (BD Biosciences) equipped with a 488, 561, 633 and 395 nm laser and FACSDiva software (BD Biosciences). *Ex vivo* thymocytes were stained with CD4, CD8, TER-119 and THY1.2 antibodies. TER-119<sup>-</sup>, THY1.2<sup>+</sup> DN or DP cells were sorted in FACS tubes. A purity check of the sorted samples resulted in 99% purity of the respective cell type. (Single-cell) sorts of cell lines (e.g., mCherry<sup>+</sup>) were directly sorted into U-shaped 96-well-plates (Capricorn).

#### **2.2.15 Western blotting**

##### **2.2.15.1 Protein extraction**

Cell pellets were obtained by 5 min centrifugation at 1,200 rpm from single-cell suspensions of murine organs or cell lines and washed once with ice-cold PBS. The pellets were resuspended in 150–350 µl of ice-cold 1x Laemmli lysis buffer, supplemented with protease inhibitor cocktail (Roche, 1:20) and the Sodium Orthovanadate phosphatase inhibitor (Sigma

Aldrich, 1:200). Protein lysates were vigorously vortexed (IKA) for 5 seconds, followed by a 5 min incubation at 95°C in a termoshaker (Eppendorf) at 600 rpm and 15 min sonication (Bandelin).

### 2.2.15.2 Protein concentration measurement

The protein concentration was measured using the BCA assay (Pierce-Thermo Scientific). Therefore, 5 µl of the protein lysates were added to 45 µl of ddH<sub>2</sub>O (MiliQ). After addition of 200 µl BCA reagent (1:50 mixture of Buffer A and Buffer B), the flat-bottom 96-well-plate (Corning) was incubated at 37°C in the dark for 15 min. The absorbance was measured at 595 nm using the EnSpire plate reader (Perkin Elmer) and concentrations were calculated from a corresponding BSA (Roth) standard curve (0–2 µg/ml). Protein extracts were stored at –20°C before use, they were thawed on ice incubated at 95°C for 5 min.

### 2.2.15.3 Preparing polyacrylamide gels

For all Western blots, a 5% stacking and an 8–10% separation polyacrylamide gels were prepared. For each polyacrylamide gel, the separation gel recipe was scaled-up for 20 ml. A gel pouring apparatus from the mini-PROTEAN System (Biorad) was assembled per manufacturer's instructions. First, all components of the separation gel, finishing with TEMED (Sigma Aldrich), were thoroughly mixed in a 50 ml falcon tube (Fisher Scientific). The mixture was immediately poured between the glass plates of the gel pouring apparatus (Biorad) and sealed with propan-2-ol (Roth). After 20 min incubation time, the propan-2-ol was removed, the stacking gel mixture was prepared as described for the separation gel, mixed well and immediately poured on top of the separation gel. Finally, a comb of interest from the Mini-PROTEAN System (Biorad) was inserted, and the gel was left to polymerize for 20 min.

**Table 16: Recipe for stacking and separation gels**

Component	5% Stacking gel	8% Separation	10% Separation
ddH <sub>2</sub> O	8.4 ml	9.3 ml	7.9 ml
1.5 mM Tris pH8.8	/	5.0 ml	5.0 ml
0.5 mM Tris pH6.8	3.7 ml	/	/
30% Acrylamide	2.5 ml	5.3 ml	6.7 ml
10% SDS	150 µl	200 µl	200 µl
10% APS	150 µl	200 µl	200 µl

TEMED	15 $\mu$ l	20 $\mu$ l	20 $\mu$ l
-------	------------	------------	------------

#### 2.2.15.4 SDS-PAGE and immunoblotting

Samples were thawed on ice, and 10–30  $\mu$ g of the protein extracts were mixed with 4x Laemmli protein loading buffer. Before loading, samples were briefly vortexed (IKA) and heated up to 95°C for 5 min on a shaking heating block (Eppendorf). For later determination of the correct bands, 8  $\mu$ l of a pre-stained molecular weight standard (protein ladder 10–180 kDa; Thermo Scientific) was loaded. The samples (20–40  $\mu$ l) were loaded on 8–10% polyacrylamide gels depending on the size of the protein of interest. Gels were run in 1x SDS-PAGE running buffer in Mini Format 1-D electrophoresis systems (BioRad) at 70 V for 1 h and then increased to 100 V until the desired protein separation grade. Proteins were transferred onto PVDF membranes (Merck) by wet blotting o/n at 4°C in 1x transfer buffer (16 h at 200 mA and 2 h at 400 mA) using a Trans-Blot® Cell (BioRad).

#### 2.2.15.5 Probing the PVDF membrane

After blotting, membranes were either washed for 15 min in 1x pY-TBST buffer or treated with the Signal Enhancer (Thermo Scientific) per manufacturer's instructions before incubated in 5% milk powder pY-TBST blocking solution for 1 h at room temperature on a shaker (Labnet International). After three 10 min washing steps, the membranes were incubated with primary antibody solutions (**Table 9**) (diluted in 3% BSA in 1x pY-TBST) at 4°C overnight. After overnight incubation, the membranes were washed 3 times with pY-TBST for 10 min, then further incubated with HRP-conjugated secondary antibody (diluted 1:10,000 in 3% BSA in 1x TBST, **Table 10**) at room temperature for 1 h on a shaker (Labnet International). The membrane was again washed three times with pY-TBST for 10 min. To detect antibody binding, membranes were incubated with the ECL substrate solution A+B (Clarity™ Western ECL substrate BioRad) in a 1:1 ratio. The ECL solution acting as a substrate for the peroxidase leads to the formation of chemiluminescence within 3-5 min incubation at RT. Chemiluminescence was detected using the ChemiDoc™ Touch Imageing System (BioRad). Protein levels were quantified using the ImageLab software.

#### 2.2.15.6 Stripping and re-probing PVDF membranes

Stripping and re-probing were utilised to remove already existing signals from PVDF membranes, allowing us to look at other target protein. The membranes were placed upside

down in a microwave-stabile plastic dish with plenty of ddH<sub>2</sub>O and microwaved the membrane at 800W for 15 min. The membranes were briefly washed with 1x pY-TBST buffer, incubated with 5% milk powder pY-TBST blocking solution for 45 min at RT on a shaker (Labnet International), washed three times with 1x pY-TBST for 10 min and incubated with primary antibody solutions (**Table 9**) (diluted in 3% BSA in 1x pY-TBST) at 4°C overnight. If possible, the membranes were incubated with primary antibodies, which required a different secondary antibody for the analysis, to avoid background signals. After the overnight incubation, the analysis was performed as previously described (2.2.15.5).

### 2.2.16 Co-immunoprecipitation (co-IP)

Co-immunoprecipitation of STAT5A and STAT5B was performed to analyse the specific protein-protein interactions of STAT5. The anti-STAT5A and anti-STAT5B antibody mentioned in **Table 11**, were used for the IP.

50 ml of the radioimmunoprecipitation (RIPA) buffer were supplemented with the protease inhibitor cocktail (1 Complete Tablet, Roche).  $6 \times 10^7$  cells were collected, washed and pelleted for each target cell line. The pellet was lysed with 500  $\mu$ l supplemented RIPA buffer and incubated on a shaker for 1 h at 4°C. The lysate was centrifuged at 14,000 g for 45 min, and the protein concentration was measured via the BCA assay (Pierce-Thermo Scientific) as previously described (2.2.15.2). For each IP reaction, 3  $\mu$ g of either anti-STAT5A or anti-STAT5B antibody was added to 1000  $\mu$ g protein lysate. The volume was added up to 300  $\mu$ l with the supplemented RIPA buffer, and the reactions were incubated at 4°C o/n on a rotating shaker. In order to have a comparison for the co-immunoprecipitate, whole lysate samples were prepared (input).

For each sample, 30  $\mu$ l of magnetic beads (BioRad) were used. The beads were washed three times with supplemented RIPA buffer on a magnetic rack (SureBeads™, Bio-Rad). The beads were added to each antibody bound sample, appropriately sealed with parafilm and incubated on a rotating shaker (Stuart) for 2 h at 4°C. Next, the sample tubes were again put on the magnetic rack, and the supernatant containing unbound protein was collected (supernatant). The immunoprecipitated samples were washed three times with supplemented RIPA buffer using the magnetic rack. The bound protein was eluted from the magnetic beads with 30  $\mu$ l of 4x Laemmli loading buffer and heated up at 95°C for 5 min (Eppendorf). The magnetic beads

were discarded, and the eluant was collected (immunoprecipitant) for Western blotting (as described 2.2.15).

## 2.2.17 mRNA expression analysis

### 2.2.17.1 mRNA extraction

For RNA extraction, the RNeasy Mini Kit (Qiagen) was used according to the manufacturer's protocol. In brief, the cell pellets were kept on ice after being removed from  $-80^{\circ}\text{C}$ , where they were directly lysed in an appropriate amount of Buffer RLT Plus, supplemented with 1:100  $\beta$ -mercaptoethanol (Sigma Aldrich). The samples were then further processed by the manufacturer's guidelines. The RNA was eluted in 30  $\mu\text{l}$  of RNase free water (Qiagen), the concentration and the purity were measured using a nanodrop photometer (Nanodrop One; Thermo Scientific). The RNA samples were stored at  $-80^{\circ}\text{C}$ . Only after receiving satisfactory results (concentration  $> 50 \text{ ng}/\mu\text{l}$  and  $A_{260}/A_{280} > 2.0$ ), could the RNA be stored at  $-80^{\circ}\text{C}$  or directly used for cDNA synthesis.

### 2.2.17.2 cDNA synthesis

cDNA synthesis was performed using the iScript™ cDNA Synthesis Kit (BioRad). Between 100 and 500  $\mu\text{g}$  of the target RNA was used for cDNA synthesis, depending on the RNA availability. The reactions were prepared per manufacturer's instructions as described in **Table 17**. The thoroughly mixed complete reaction mix was incubated in a thermal cycler (MyCycler; BioRad) using manufacturer's guidelines:  $25^{\circ}\text{C}$  for 5 min,  $46^{\circ}\text{C}$  for 20 min,  $95^{\circ}\text{C}$  for 1 min and  $4^{\circ}\text{C}$  for hold. Depending on the amount of RNA used for the cDNA synthesis, the cDNA was then usually diluted 1:5 with RNase free water (Qiagen) and stored at  $-20^{\circ}\text{C}$ .

**Table 17: iScript cDNA synthesis reaction mix**

Reagent	Volume per reaction
5x iScript RT reaction mix	4 $\mu\text{l}$
iScript reverse transcriptase	1 $\mu\text{l}$
RNA	100–500 ng
ddH <sub>2</sub> O	Fill up to 20 $\mu\text{l}$

### 2.2.17.3 Quantitative real time PCR

Gene-specific forward and reverse primers for SYBR Green real-time qPCR were designed with online tools and then synthesized by Microsynth Inc. Upon arrival, the primers were resuspended in RNase free water (Qiagen) to achieve 10  $\mu$ M solutions and stored at -20 °C. The qPCR reactions were set up in triplicates, in a 96-well-plate (4titude), using PowerUp SYBR Green PCR Master Mix (BioRad) according to the manufacturer's instructions. A non-template control (NTC) was included for each target gene. The polymerization was performed and analysed using a CFX96 Touch™ Real-Time PCR Detection System (BioRad), the standard protocol used was: (1) 95°C for 3 min, (2) 95°C for 10 sec, (3) 58°C or 60°C for 10 sec, (4) 72°C for 30 sec, (5) repeat step 2–4 for 39 additional cycles, (6) 60°C for 10 sec and (7) 0.5°C per cycle until 95°C. The utilised primers are listed in **Table 7**. The relative mRNA expression of the genes of interest was determined by normalising to the expression of the *Rplp0* housekeeping gene, which served as an internal control. The analysis was performed with the CFX Manager™ software (BioRad).

**Table 18: qPCR reaction mix**

Reagent	Volume per reaction
10 $\mu$ M Primer mix (forward and reverse)	0,4 $\mu$ l
Sybergreen mix qPCR Master Mix	10 $\mu$ l
ddH <sub>2</sub> O	7,6 $\mu$ l
cDNA	2 $\mu$ l

### 2.2.18 Statistical analysis and reproducibility

Unless indicated otherwise, all experiments were performed in technical and biological triplicates. Sample sizes and animal numbers were determined from pilot laboratory experiments and previously published literature.

Statistical calculations were performed using GraphPad Prism 8.00 (GraphPad Software) and reported as mean values  $\pm$  SEM. Pairwise comparisons between two normally distributed groups were performed using an unpaired two-tailed Student's t-test. For testing whether the population means of several groups are equal, the Kruskal-Wallis test was performed (the non-parametric equivalent of the analysis of variance), followed by Dunn's multiple comparison test, which was applied for pairwise comparison of subgroups when the Kruskal-Wallis test

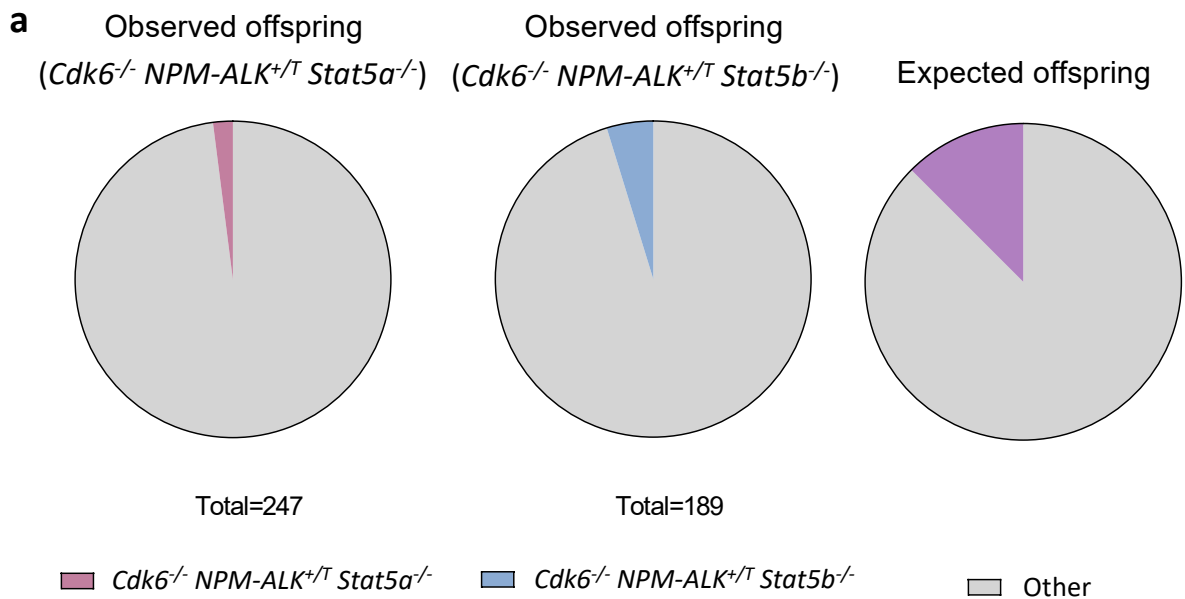
was positive. The log-rank test was performed for the Kaplan-Meier survival analysis. For statistical analysis of contingency tables (e.g., thymic lymphoma incidence), we used the Chi-square test.

Data points excluded were only those that were clear outlier due to technical problems in assays done in triplicate experiments. P-value <0.05 was accepted as statistically significant and p-values are considered as follows: \* p-value < 0.05; \*\* p-value < 0.01; \*\*\* p-value < 0.001, \*\*\*\* p-value < 0.0001.

### 3 Results

#### 3.1 Combined absence of CDK6 and STAT5A or STAT5B inhibits NPM-ALK-driven thymic lymphoma development

Our group provided several hints that CDK6 interferes with STAT5-driven diseases (Scheicher et al., 2015; Uras et al., 2019). Based on the observation that the transgenic NPM-ALK model (Chiarle et al., 2003) develops thymic lymphomas significantly later in the absence of CDK6 (K. Kollmann et al., 2013), we asked the question whether STAT5A or STAT5B also interplay. Therefore, we crossed NPM-ALK transgenic mice with *Cdk6*<sup>-/-</sup> (Malumbres et al., 2004) *Stat5a*<sup>-/-</sup> (Liu et al., 1997) or *Cdk6*<sup>-/-</sup> and *Stat5b*<sup>-/-</sup> (Udy et al., 1997) mice. These combined mice were viable and fertile. However, *Cdk6*<sup>-/-</sup> *NPM-ALK*<sup>+T</sup> *Stat5a*<sup>-/-</sup> and *Cdk6*<sup>-/-</sup> *NPM-ALK*<sup>+T</sup> *Stat5b*<sup>-/-</sup> mice are born at a submendelian ratio (**Figure 13a**). The observed occurrence of *Cdk6*<sup>-/-</sup> *NPM-ALK*<sup>+T</sup> *Stat5a*<sup>-/-</sup> and *Cdk6*<sup>-/-</sup> *NPM-ALK*<sup>+T</sup> *Stat5b*<sup>-/-</sup> offspring are 2.02% and 4.76%, respectively, which is significantly lower than the expected 12.5% (**Figure 13b**).



**b**

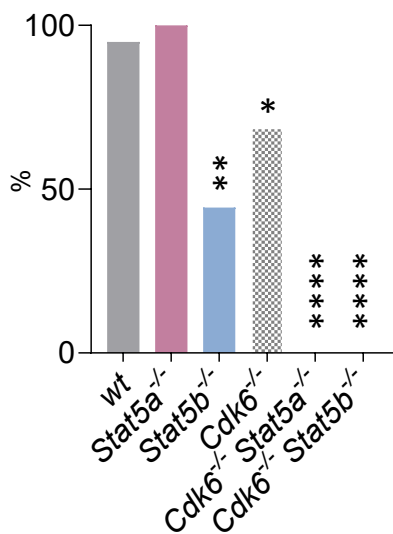
Genotype	Expected	Observed	p-value	Significance
<i>Cdk6</i> <sup>-/-</sup> <i>NPM-ALK</i> <sup>+T</sup> <i>Stat5a</i> <sup>-/-</sup>	12.5 %	2.02 %	<0,0001	****
<i>Cdk6</i> <sup>-/-</sup> <i>NPM-ALK</i> <sup>+T</sup> <i>Stat5b</i> <sup>-/-</sup>	12.5 %	4.76 %	0,0006	***

**Figure 13: *Cdk6*<sup>-/-</sup> *NPM-ALK*<sup>+T</sup> *Stat5a*<sup>-/-</sup> and *Cdk6*<sup>-/-</sup> *NPM-ALK*<sup>+T</sup> *Stat5b*<sup>-/-</sup> are born at a submendelian ratio**

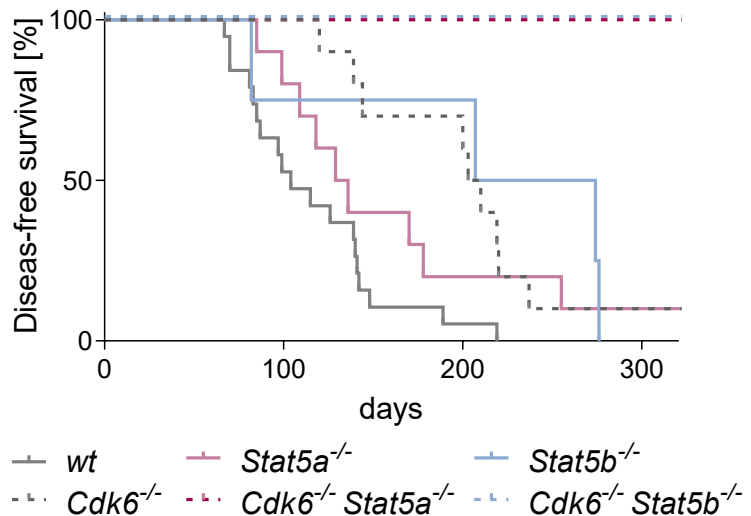
Offspring data collected from *Cdk6*<sup>-/-</sup> *NPM-ALK*<sup>+T</sup> *Stat5a*<sup>+/+</sup> (or *Stat5b*<sup>+/+</sup>) and *Cdk6*<sup>-/-</sup> *NPM-ALK*<sup>+T</sup> *Stat5a*<sup>-/+</sup> (or *Stat5b*<sup>-/+</sup>) matings. **a)** Pie chart of observed offspring proportions from the *Stat5a* (n = 189) and *Stat5b* (n = 247) matings, highlighting the observed *Cdk6*<sup>-/-</sup> *NPM-ALK*<sup>+T</sup> *Stat5a*<sup>-/-</sup> and *Cdk6*<sup>-/-</sup> *NPM-ALK*<sup>+T</sup> *Stat5b*<sup>-/-</sup> offspring respectively, and the expected offspring proportions for both matings at weaning day 21. **b)** Table showing expected and observed birthing rates of *Cdk6*<sup>-/-</sup> *NPM-ALK*<sup>+T</sup> *Stat5a*<sup>-/-</sup> and *Cdk6*<sup>-/-</sup> *NPM-ALK*<sup>+T</sup> *Stat5b*<sup>-/-</sup> mice. Levels of significance were obtained by a two-tailed binomial test for comparing the observed distribution with the expected Mendelian distribution.

To determine the implications of STAT5A/B and CDK6 in the context of NPM-ALK-driven lymphomagenesis, we followed disease development of *NPM-ALK*<sup>+T</sup> – from now on referred to as *NPM-ALK*<sup>+</sup> – *wt*, *Cdk6*<sup>-/-</sup>, *Stat5a*<sup>-/-</sup>, *Stat5b*<sup>-/-</sup>, *Cdk6*<sup>-/-</sup> *Stat5a*<sup>-/-</sup> and *Cdk6*<sup>-/-</sup> *Stat5b*<sup>-/-</sup> mice for more than one year. While wild type (*wt*) and *Stat5a*<sup>-/-</sup> mice developed a thymic lymphoma with almost 100% penetrance, *Stat5b*<sup>-/-</sup> and *Cdk6*<sup>-/-</sup> mice only developed a thymic lymphoma in 45% and 65% of cases, respectively (**Figure 14a**). The *wt* mice, on average, displayed a median survival of 104 days of age, while the absence of STAT5A slightly prolonged the disease-free survival to 132.5 days. The lower thymic lymphoma incidence of *Cdk6*<sup>-/-</sup> or *Stat5b*<sup>-/-</sup> mice is also reflected in significantly prolonged survival of mice developing a thymic lymphoma to 206.5 and 240 days, respectively. Strikingly, the combined absence of CDK6 and STAT5A or STAT5B prohibited NPM-ALK-driven transformation of thymi – not a single mouse developed a thymic tumour within more than one year of analysis (**Figure 14b-c**).

**a** Thymic lymphoma incidence



**b**



**c**

Genotype	Median Survival (days)	p-value	Significance
<i>wt</i>	104	NA	NA
<i>Stat5a</i> <sup>-/-</sup>	132.5	0.0937	ns
<i>Stat5b</i> <sup>-/-</sup>	240.5	0.0197	*
<i>Cdk6</i> <sup>-/-</sup>	206.5	0.0006	***
<i>Cdk6</i> <sup>-/-</sup> <i>Stat5a</i> <sup>-/-</sup>	NA	<0.0001	****
<i>Cdk6</i> <sup>-/-</sup> <i>Stat5b</i> <sup>-/-</sup>	NA	<0.0001	****

**Figure 14: The concomitant absence of CDK6 and STAT5A or STAT5B prevents NPM-ALK-driven transformation**

**a)** Incidence of thymic lymphoma development in the respective *NPM-ALK*<sup>+</sup> genotypes: *wt* (n = 19), *Stat5a*<sup>-/-</sup> (n = 17), *Stat5b*<sup>-/-</sup> (n=9), *Cdk6*<sup>-/-</sup> (n = 17), *Cdk6*<sup>-/-</sup> *Stat5a*<sup>-/-</sup> (n = 5) and *Cdk6*<sup>-/-</sup> *Stat5b*<sup>-/-</sup> (n=12). Levels of significance were obtained by a Chi-square test. **b)** Survival of *NPM-ALK*-transgenics in the Kaplan-Meier plot showing no thymic lymphoma development of *NPM-ALK*<sup>+</sup> *Cdk6*<sup>-/-</sup> *Stat5a*<sup>-/-</sup> and *Cdk6*<sup>-/-</sup> *Stat5b*<sup>-/-</sup> mice within one year of analysis (n = 5–19/genotype). **c)** Table depicting median survival for each genotype, with corresponding p-values and significance levels, calculated using the log-rank test. \* p < 0.05, \*\* p < 0.01, \*\*\* p < 0.001, and \*\*\*\* p < 0.0001.

To confirm the observed phenotype, we analysed H&E-stained thymi samples of *NPM-ALK*<sup>+</sup> *wt*, *Cdk6*<sup>-/-</sup>, *Stat5a*<sup>-/-</sup> and *Stat5b*<sup>-/-</sup> mice at the ageing experiment endpoint – development of thymic lymphoma – in addition to age-matched thymi samples from *NPM-ALK*<sup>+</sup> *Cdk6*<sup>-/-</sup> *Stat5a*<sup>-/-</sup> and *Cdk6*<sup>-/-</sup> *Stat5b*<sup>-/-</sup> mice. The analysis of histology revealed that all *NPM-ALK*<sup>+</sup> *Cdk6*<sup>-/-</sup>, *Stat5a*<sup>-/-</sup>, *Stat5b*<sup>-/-</sup> samples were more similar to the *NPM-ALK*<sup>+</sup> *wt* thymic tissue, while *NPM-ALK*<sup>+</sup> *Cdk6*<sup>-/-</sup> *Stat5b*<sup>-/-</sup> thymic samples were more similar to the control healthy thymic tissue obtained from age-matched *NPM-ALK*<sup>-</sup> *Cdk6*<sup>-/-</sup> *Stat5b*<sup>-/-</sup> mice (**Figure 15**). Additionally, *NPM-ALK*<sup>+</sup> *Cdk6*<sup>-/-</sup> *Stat5b*<sup>-/-</sup> and *NPM-ALK*<sup>-</sup> *Cdk6*<sup>-/-</sup> *Stat5b*<sup>-/-</sup> thymic tissues appear to retain histological features of healthy thymic tissue – separation of the medulla and cortex. Ki67 IHC staining revealed that *NPM-ALK*<sup>+</sup> *wt*, *Stat5a*<sup>-/-</sup> and *Stat5b*<sup>-/-</sup> thymic tissues appear to be in a higher proliferative state compared to *NPM-ALK*<sup>+</sup> *Cdk6*<sup>-/-</sup>, *Cdk6*<sup>-/-</sup> *Stat5b*<sup>-/-</sup> and the healthy control – *NPM-ALK*<sup>-</sup> *Cdk6*<sup>-/-</sup> *Stat5b*<sup>-/-</sup> thymic tissue.

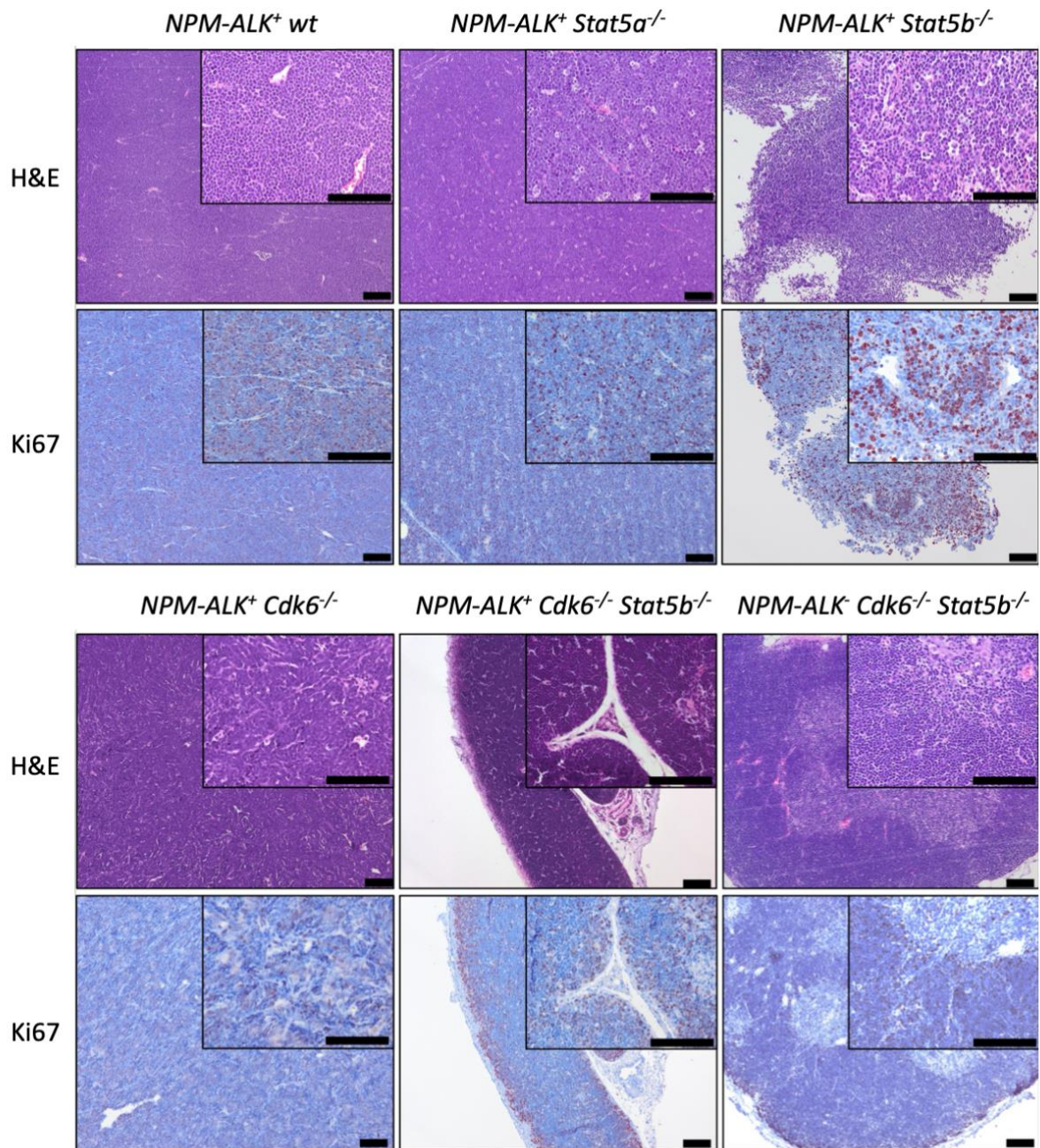


**Figure 15: H&E staining of experiment endpoint samples**

Representative phase-contrast images of H&E- and Ki67-stained thymi samples of *NPM-ALK<sup>+</sup> wt*, *Cdk6<sup>-/-</sup>*, *Stat5a<sup>-/-</sup>*, *Stat5b<sup>-/-</sup>* and *Cdk6<sup>-/-</sup> Stat5b<sup>-/-</sup>* mice at ageing experiment endpoint. As controls, we include age-matched H&E-stained thymi samples from *NPM-ALK<sup>-</sup> Cdk6<sup>-/-</sup> Stat5b<sup>-/-</sup>* mice. The scale bar always represents 100 μm.

### 3.2 NPM-ALK is present in *NPM-ALK<sup>+</sup> Cdk6<sup>-/-</sup> Stat5a<sup>-/-</sup>* and *NPM-ALK<sup>+</sup> Cdk6<sup>-/-</sup> Stat5b<sup>-/-</sup>* thymi

To exclude the suppression of transgenic NPM-ALK in double knockout thymi as a potential reason for the lack of lymphoma onset, we investigated NPM-ALK protein levels in *NPM-ALK<sup>+</sup> Cdk6<sup>-/-</sup> Stat5a<sup>-/-</sup>* and *Cdk6<sup>-/-</sup> Stat5b<sup>-/-</sup>* mice. Western blotting of 8–10-week-old *NPM-ALK<sup>+</sup> Cdk6<sup>-/-</sup> Stat5a<sup>-/-</sup>* and *Cdk6<sup>-/-</sup> Stat5b<sup>-/-</sup>* murine thymi samples confirmed that the ALK protein levels are not affected in the combined absence of CDK6 and STAT5A or CDK6 and STAT5B (Figure 16). We concluded that NPM-ALK is expressed in *Cdk6<sup>-/-</sup> Stat5a<sup>-/-</sup>* and *Cdk6<sup>-/-</sup> Stat5b<sup>-/-</sup>* mice, excluding impaired expression as a reason for the lack of ALK-driven tumours.

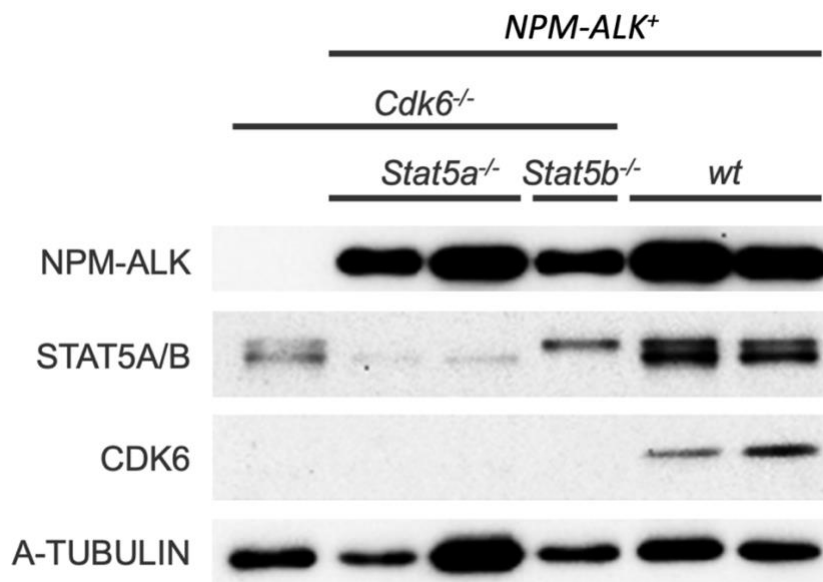


**Figure 16: NPM-ALK protein is present in the thymi of *NPM-ALK<sup>+</sup> Cdk6<sup>-/-</sup> Stat5a<sup>-/-</sup>* and *Cdk6<sup>-/-</sup> Stat5b<sup>-/-</sup>* mice**

Representative immunoblot showing NPM-ALK transgene expression in *NPM-ALK<sup>+</sup> Cdk6<sup>-/-</sup> Stat5a<sup>-/-</sup>* (n = 2), *Cdk6<sup>-/-</sup> Stat5a<sup>-/-</sup>* (n = 1), and *wt* murine thymi (n = 2). An age-matched transgene-negative *Cdk6<sup>-/-</sup>* murine thymus was used as negative control. A-TUBULIN was used as the loading control.

### 3.3 *NPM-ALK<sup>+</sup> Cdk6<sup>-/-</sup> Stat5a<sup>-/-</sup>* and *NPM-ALK<sup>+</sup> Cdk6<sup>-/-</sup> Stat5b<sup>-/-</sup>* thymi have an unaltered cell-type composition

Next, we investigated the thymic tissue as a potential cause for the absent thymic lymphomagenesis in *NPM-ALK<sup>+</sup> Cdk6<sup>-/-</sup> Stat5a<sup>-/-</sup>* and *Cdk6<sup>-/-</sup> Stat5b<sup>-/-</sup>* mice. Due to the high number of genotypes and mouse breeding limitations, we focused on the more severe phenotype (*NPM-ALK<sup>+</sup> Stat5b<sup>-/-</sup>* and *Cdk6<sup>-/-</sup> Stat5b<sup>-/-</sup>*). As CDK6 and STAT5B are implicated in

T cell development, we analysed the cellular composition of thymi at eight weeks of age. No significant alteration in the main cell types – double-negative (DN, CD4<sup>-</sup>CD8<sup>-</sup>), double-positive (DP, CD4<sup>+</sup>CD8<sup>+</sup>), CD8<sup>+</sup> and CD4<sup>+</sup> thymocytes – was observed (**Figure 17a-b**). The most immature cells can be further subdivided into DN1–4 stages based on CD25 and CD44 expression – also here the genotypes did not differ significantly (**Figure 17c**). We concluded that there are no gross changes in T cell development in *Cdk6*<sup>-/-</sup> *Stat5b*<sup>-/-</sup> mice, which could interfere with ALK-driven tumorigenesis.

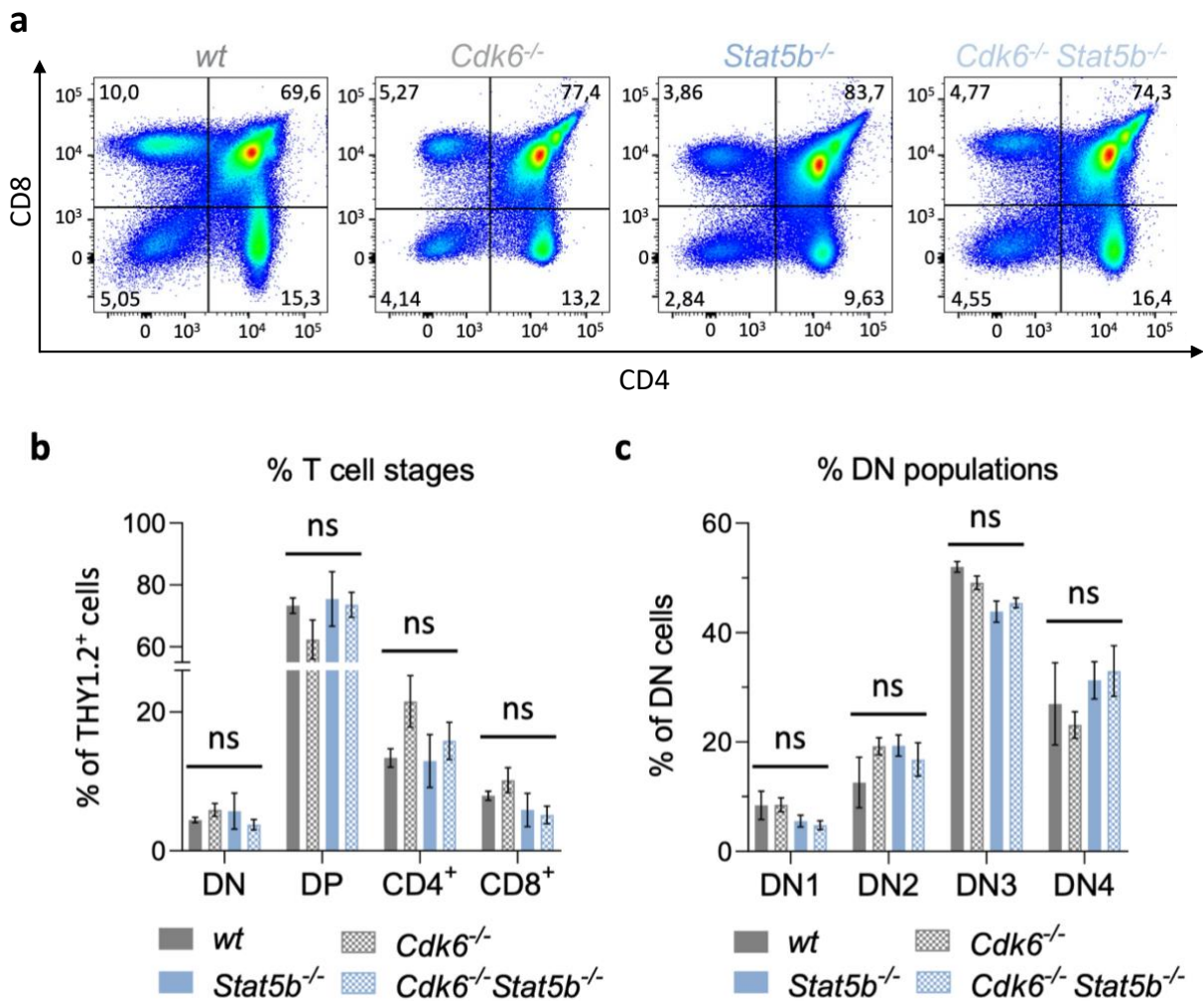


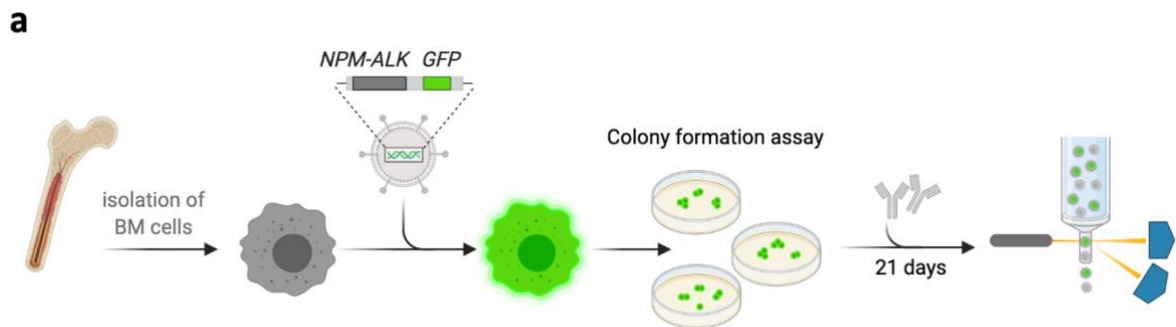
**Figure 17: No significant changes in thymic cell populations in the absence of CDK6 and/or STAT5B in the NPM-ALK transgenic model**

**a**) Representative dot plots and **b**) quantification of thymi composition of 8-week-old mice analysed via flow cytometry. CD4/CD8 expression on TER-119/THY1.2<sup>+</sup> thymocytes is shown (n = 4/genotype). The T cell stages are shown as they develop during thymus maturation. **c**) Quantification of further gating on the DN cells to classify in DN1–4 based on CD25 and CD44 expression (n = 4/genotype). Levels of significance were calculated by Kruskal-Wallis tests, followed by Dunn's multiple comparison test. The error bars represent mean values ± standard error of the mean (SEM).

In summary, NPM-ALK-expressing *Stat5b*<sup>-/-</sup> *Cdk6*<sup>-/-</sup> and *Stat5a*<sup>-/-</sup> *Cdk6*<sup>-/-</sup> mice exert largely unaltered thymic cell composition but lack entirely thymic lymphoma onset. Consequently, we hypothesised that the combined action of CDK6 and STAT5A or STAT5B is required for NPM-ALK-driven transformation.

### 3.4 *Cdk6*<sup>-/-</sup> *Stat5a*<sup>-/-</sup> and *Cdk6*<sup>-/-</sup> *Stat5b*<sup>-/-</sup> BM cells fail to undergo NPM-ALK-mediated transformation

To substantiate our *in vivo* findings, we next investigated the effect of *Cdk6* and *Stat5a* or *Stat5b* deficiency on *ex vivo* NPM-ALK-mediated transformation (**Figure 18a**). BM cells were infected with a retrovirus encasing the NPM-ALK-IRES-GFP vector and were plated in growth factor-free methylcellulose. A similar infection efficiency, varying from 5–7% (not shown), was observed among the genotypes. While the absence of *Stat5a* or *Stat5b* did not have a substantial effect on colony numbers, *Cdk6* deficiency strikingly reduced the number of colonies. Hardly any colonies were derived from NPM-ALK-infected *Cdk6*<sup>-/-</sup> and *Stat5a*<sup>-/-</sup> or *Stat5b*<sup>-/-</sup>-deficient BM cells, revealing a severe disadvantage during transformation (**Figure 18b and 18c**). These observations further substantiated the presumption that the combinations of CDK6 and STAT5A or CDK6 and STAT5B are required for NPM-ALK mediated transformation.



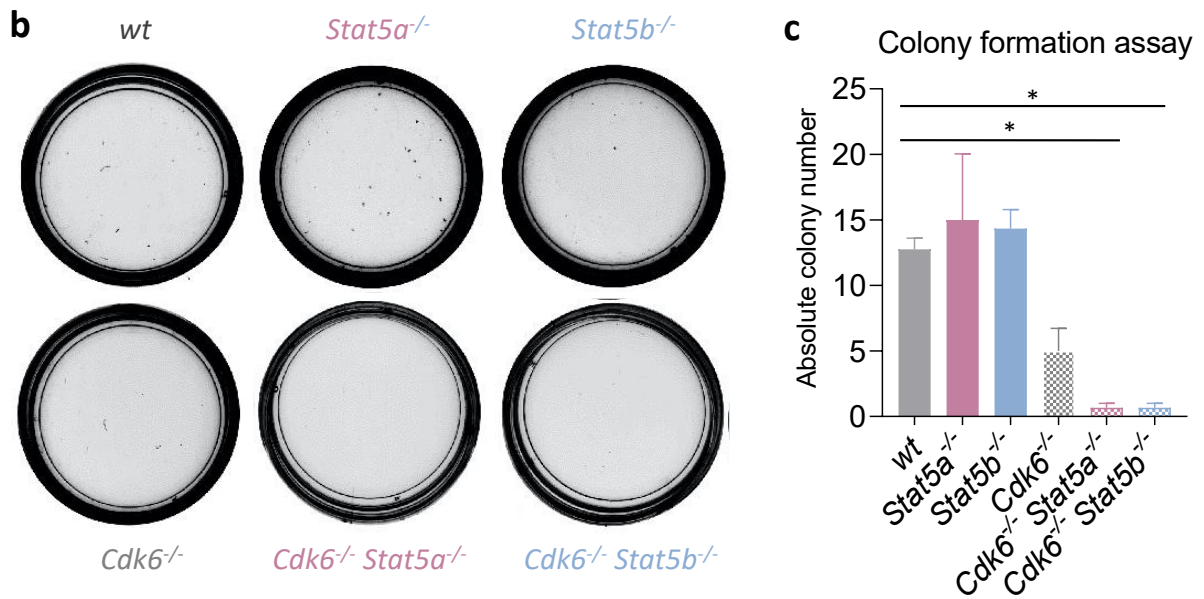


**Figure 18: *Cdk6*<sup>-/-</sup> *Stat5a*<sup>-/-</sup> and *Cdk6*<sup>-/-</sup> *Stat5b*<sup>-/-</sup> BM cells fail to transform during ex vivo NPM-ALK-infection**

**a)** Experimental setup scheme of ex vivo NPM-ALK-mediated transformation ( $n \leq 3$ ). NPM-ALK-infected wt ( $n = 4$ ), *Stat5a*<sup>-/-</sup> ( $n = 3$ ), *Stat5b*<sup>-/-</sup> ( $n = 3$ ), *Cdk6*<sup>-/-</sup> ( $n = 3$ ), *Cdk6*<sup>-/-</sup> *Stat5a*<sup>-/-</sup> ( $n = 2$ ) and *Cdk6*<sup>-/-</sup> *Stat5b*<sup>-/-</sup> ( $n = 2$ ) BM cells were plated in growth factor-free methylcellulose. After an incubation of 21 days, the colonies were liquified and analysed via flow cytometry for GFP fluorescent and CD11b, CD3, THY1.2, TER-119, KIT, spinocerebellar ataxia type 1 (SCA-1) surface marker expression. **b)** Representative pictures of the CFA are depicted. **c)** Quantification of GFP<sup>+</sup> colonies of the CFA. The bar graph summarises the data obtained from the biological replicates ( $n \geq 2$ ). Error bars represent mean  $\pm$  SEM. Levels of significance were calculated using Kruskal–Wallis test followed by Dunn’s multiple comparison test. \*  $p < 0.05$ .

The differences in the colony numbers were reflected by the absolute number of GFP<sup>+</sup> cells stemming from the methylcellulose assay. A strikingly lower number of GFP<sup>+</sup> cells were obtained from *Cdk6*<sup>-/-</sup>, *Cdk6*<sup>-/-</sup> *Stat5a*<sup>-/-</sup> and *Cdk6*<sup>-/-</sup> *Stat5b*<sup>-/-</sup> cells (**Figure 19a**), with *Cdk6*<sup>-/-</sup> *Stat5b*<sup>-/-</sup> showing the most drastic effect. We further analysed the transformed GFP<sup>+</sup> cells for their surface marker expression. The NPM-ALK infected GFP<sup>+</sup> cells displayed no expression of any lineage-specific marker (including CD11b, CD3, THY1.2 or TER-119; not shown) but expressed KIT<sup>+</sup> and SCA-1<sup>+</sup>, both markers for haematopoietic stem/progenitor cells (**Figure 19b**). Due to the low numbers of transformed GFP<sup>+</sup> cells in the *Cdk6*<sup>-/-</sup> *Stat5a*<sup>-/-</sup> and *Cdk6*<sup>-/-</sup> *Stat5b*<sup>-/-</sup> samples, we were unable to obtain reliable measurements of the SCA-1 median fluorescence intensity (MFI). Nevertheless, we observed a significant positive correlation between SCA-1 expression and the absolute number of colonies (**Figure 19c**). Regardless of the genotype, 56.3% of the colony number variance is explained by SCA-1 expression. BM cells carrying a *Cdk6* and *Stat5a* or *Stat5b* deficiency failed to undergo

NPM-ALK-mediated transformation. This experiment confirmed in another cellular system that both CDK6 and STAT5A or STAT5B have to be expressed to allow for NPM-ALK-mediated transformation.

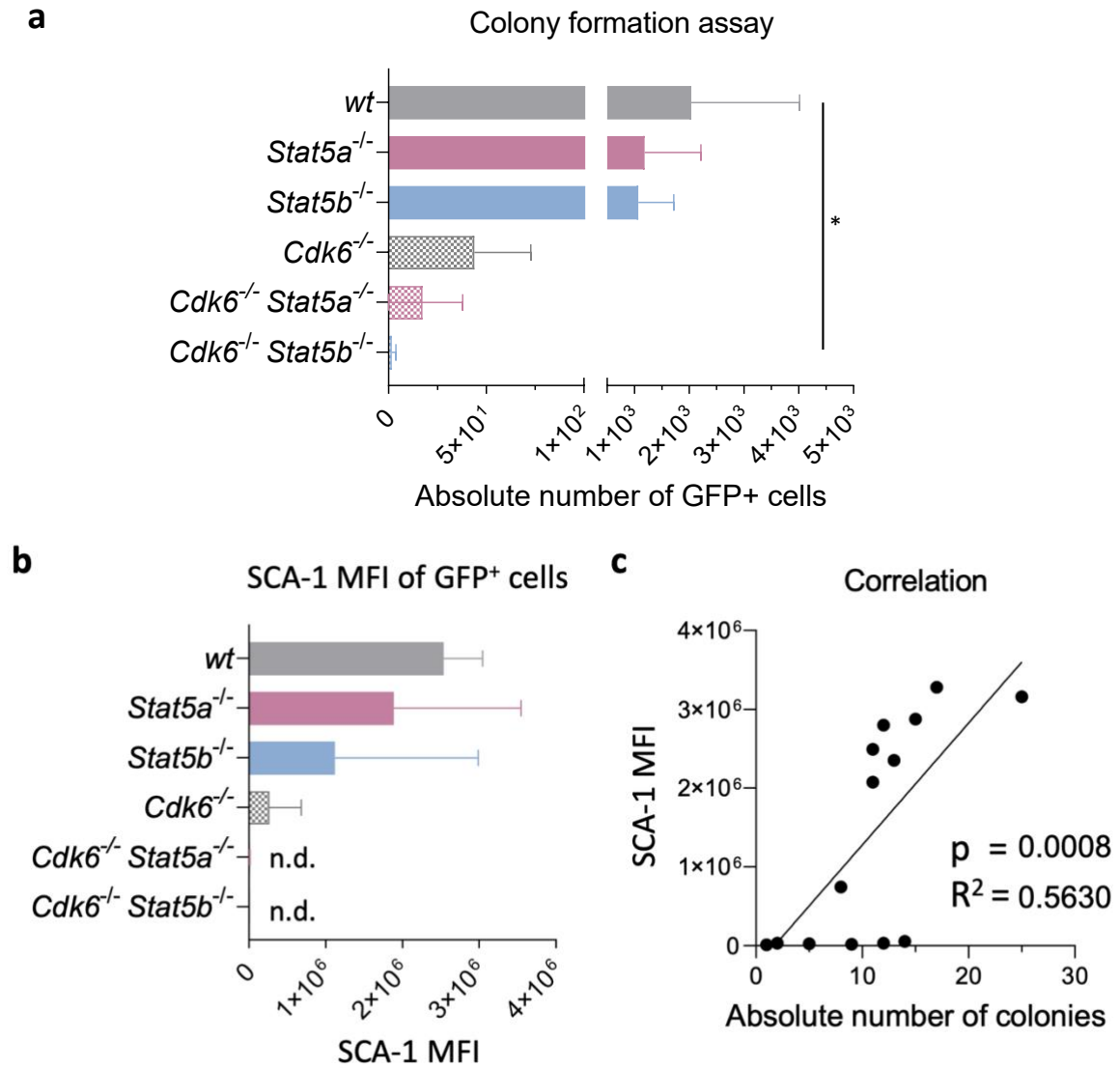


**Figure 19: Colony formation is positively correlated with SCA-1 expression on GFP<sup>+</sup> cells**

**a)** The absolute number of GFP<sup>+</sup> cells obtained from the CFA per genotype (n = 2–4/genotype). Error bars represent mean ± SEM. **b)** Background-subtracted SCA-1 MFI of GFP<sup>+</sup> cells per genotype (n = 2–4/genotype). Error bars represent mean ± SEM. **c)** Correlation of normalised SCA-1 MFI value and the absolute number of colonies in the CFA. The p-value was calculated under the null hypothesis of »Slope is significantly non-zero«. \* p < 0.05.

### 3.5 Generation of primary murine *NPM-ALK*<sup>+</sup> cell lines

To investigate the molecular consequences of CDK6 and STAT5A/B on already transformed *NPM-ALK*<sup>+</sup> thymic lymphomas, we established cell lines from thymic lymphomas of *NPM-ALK*<sup>+</sup> *wt*, *Cdk6*<sup>-/-</sup>, *Stat5a*<sup>-/-</sup> and *Stat5b*<sup>-/-</sup> mice. Due to the failure of *NPM-ALK*<sup>+</sup> *Cdk6*<sup>-/-</sup> *Stat5a*<sup>-/-</sup> and *Cdk6*<sup>-/-</sup> *Stat5b*<sup>-/-</sup> mice establishing a thymic lymphoma, we were unable to generate *NPM-ALK*-expressing double knockout cell lines. Through the span of 8 months, we successfully established between 2–7 cell lines per genotype by culturing thymic lymphoma cells of the *NPM-ALK*<sup>+</sup> mice *in vitro* (**Figure 20a**). Regardless of the genotype, the primary cell lines were successfully established with a 40–50% probability rate (**Figure 20b**).

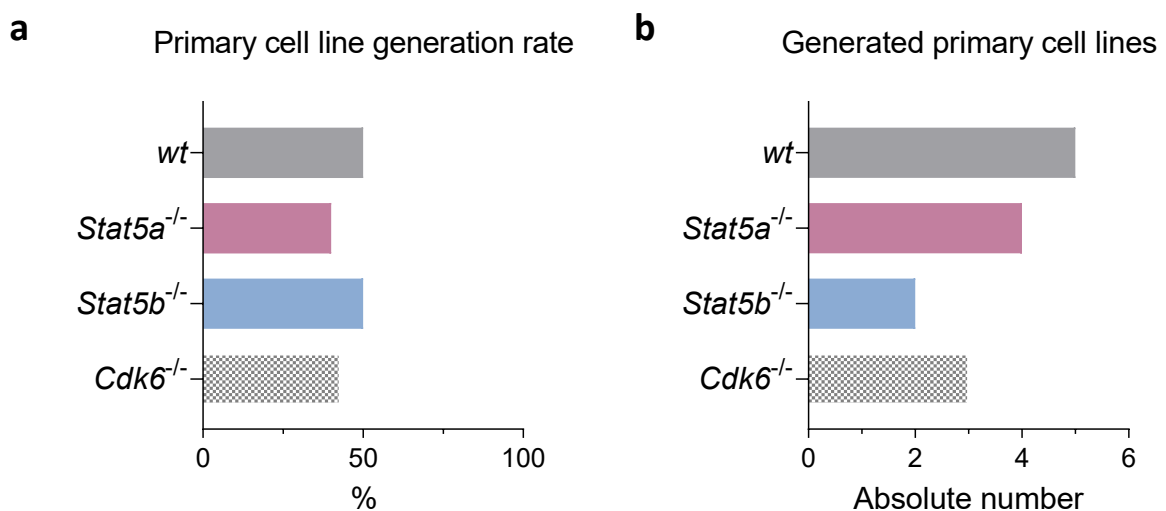


**Figure 20: Numbers of established primary murine cell lines**

**a)** Absolute number and **b)** the relative quantification of the established cell lines compared to the total number of primary thymic lymphomas that were subjected to *in vitro* outgrowth for *NPM-ALK*<sup>+</sup> *wt* (n = 10), *Cdk6*<sup>-/-</sup> (n = 7), *Stat5a*<sup>-/-</sup> (n = 10), *Stat5b*<sup>-/-</sup> (n = 4) genotypes.

### 3.6 *NPM-ALK*<sup>+</sup> *Stat5a*<sup>-/-</sup> and *Stat5b*<sup>-/-</sup> cells regain the expression of transcriptionally silenced *Cdk6*

We performed another a further attempt to generate CDK6/STAT5A/B double-knockout *NPM-ALK*-expressing cell lines. We investigated the consequences of *shRNA*-mediated *Cdk6* knockdown on the established murine *NPM-ALK*<sup>+</sup> *wt*, *Stat5a*<sup>-/-</sup> and *Stat5b*<sup>-/-</sup> cell lines (**Figure 21a**). We successfully retrovirally infected *NPM-ALK*<sup>+</sup> *wt*, *Stat5a*<sup>-/-</sup> and *Stat5b*<sup>-/-</sup> cells with *shRNAs* against *Renilla* (used as control) and *Cdk6* with similar infection rates of 3–5% (**Figure 21b**). The % mCherry<sup>+</sup> cells stagnated for the first 14 days – independent of the genotype – after which the % *shRenilla* infected cells enriched in the population, while the % of *shCdk6* infected cells declined. The *Cdk6* knocked-down *NPM-ALK*<sup>+</sup> *wt* cells (*NPM-ALK*<sup>+</sup> *wt* + *shCdk6*)

recovered over time, while the % mCherry<sup>+</sup> Cdk6 knocked-down *Stat5a*<sup>-/-</sup> and *Stat5b*<sup>-/-</sup> cells (*NPM-ALK*<sup>+</sup> *Stat5a*<sup>-/-</sup> + *shCdk6* and *NPM-ALK*<sup>+</sup> *Stat5b*<sup>-/-</sup> + *shCdk6*) continued to decline but persisted in low numbers.

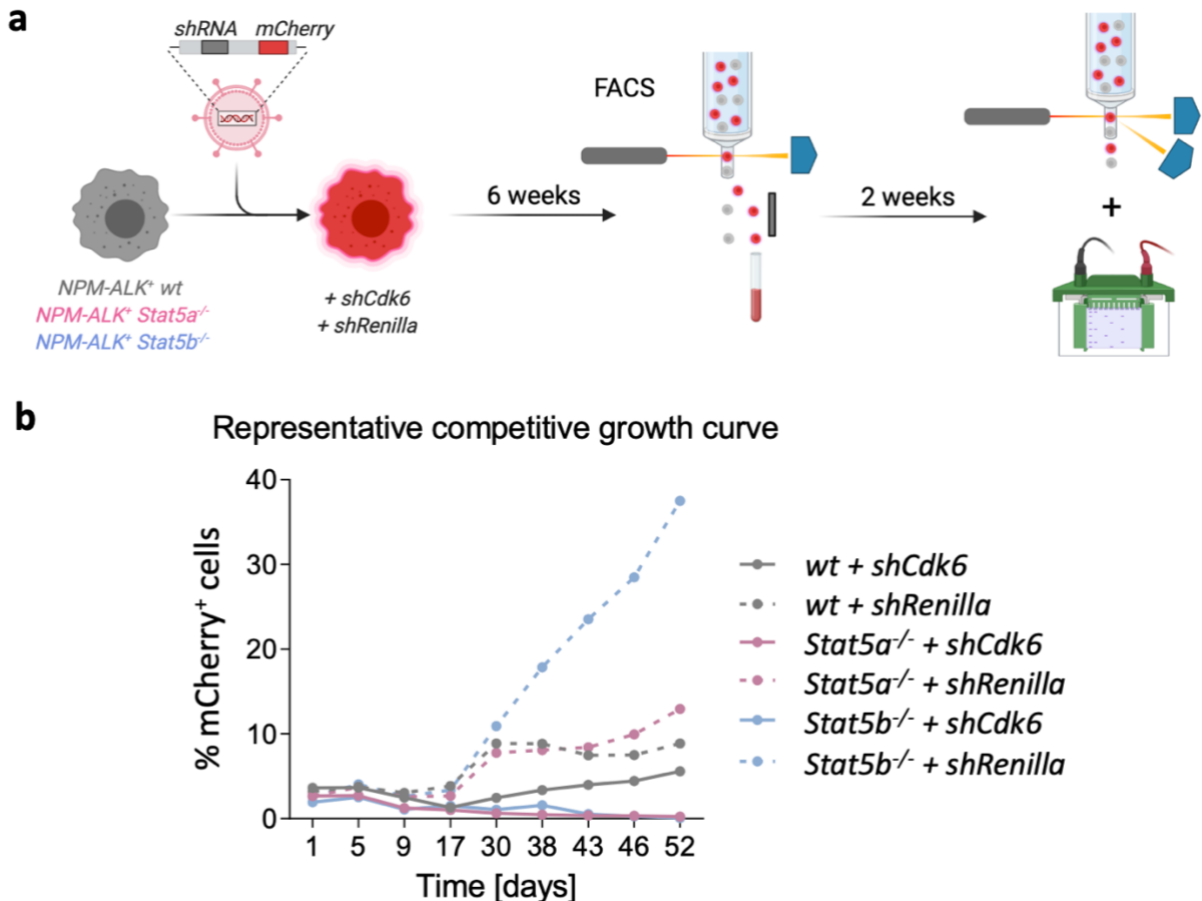


**Figure 21: *shCdk6* infected *NPM-ALK*<sup>+</sup> cells display a growth disadvantage compared to *shRenilla* controls**

**a)** Experimental setup of *shRNA*-mediated knockdown of Cdk6 and Renilla, followed by sorting of mCherry<sup>+</sup> cells and CDK6 knockdown validation by Western blotting.  
**b)** Representative competitive growth curve of *shRNA* infected cells (n = 1/genotype).

After maintaining a population of *Stat5a*<sup>-/-</sup> or *Stat5b*<sup>-/-</sup> cells carrying a *Cdk6* knockdown (mCherry<sup>+</sup>) for six weeks, the mCherry<sup>+</sup> cells were FACS-sorted, cultured for 14 days and regularly checked for the expression of the fluorescent marker. The mCherry expression of the *shCdk6* infected cell lines behaved similarly to their controls. The majority of the newly established cell lines maintained the mCherry expression, with the exception of one *Stat5a*<sup>-/-</sup> cell line, where both *shRNA* infected derivatives appeared to be losing the fluorescent marker (**Figure 22a**). This observation caused us to further investigate and validate the *shRNA*-

mediated *Cdk6* knockdown in those cell lines. The knockdown efficiency of *Cdk6* was validated in *NPM-ALK<sup>+</sup> wt cells*, which showed a substantial depletion of the CDK6 protein. Although the *shCdk6*-infected *NPM-ALK<sup>+</sup> Stat5a<sup>-/-</sup>* or *Stat5b<sup>-/-</sup>* cells also showed a very high % of mCherry<sup>+</sup> cells (identical to their *shRenilla* controls), they failed to downregulate CDK6 expression (**Figure 22b-c**).

Summing up, all our experimental approaches indicate that it is not possible to generate an NPM-ALK-driven cell line deficient in both *Cdk6* and *Stat5a* or *Stat5b*.

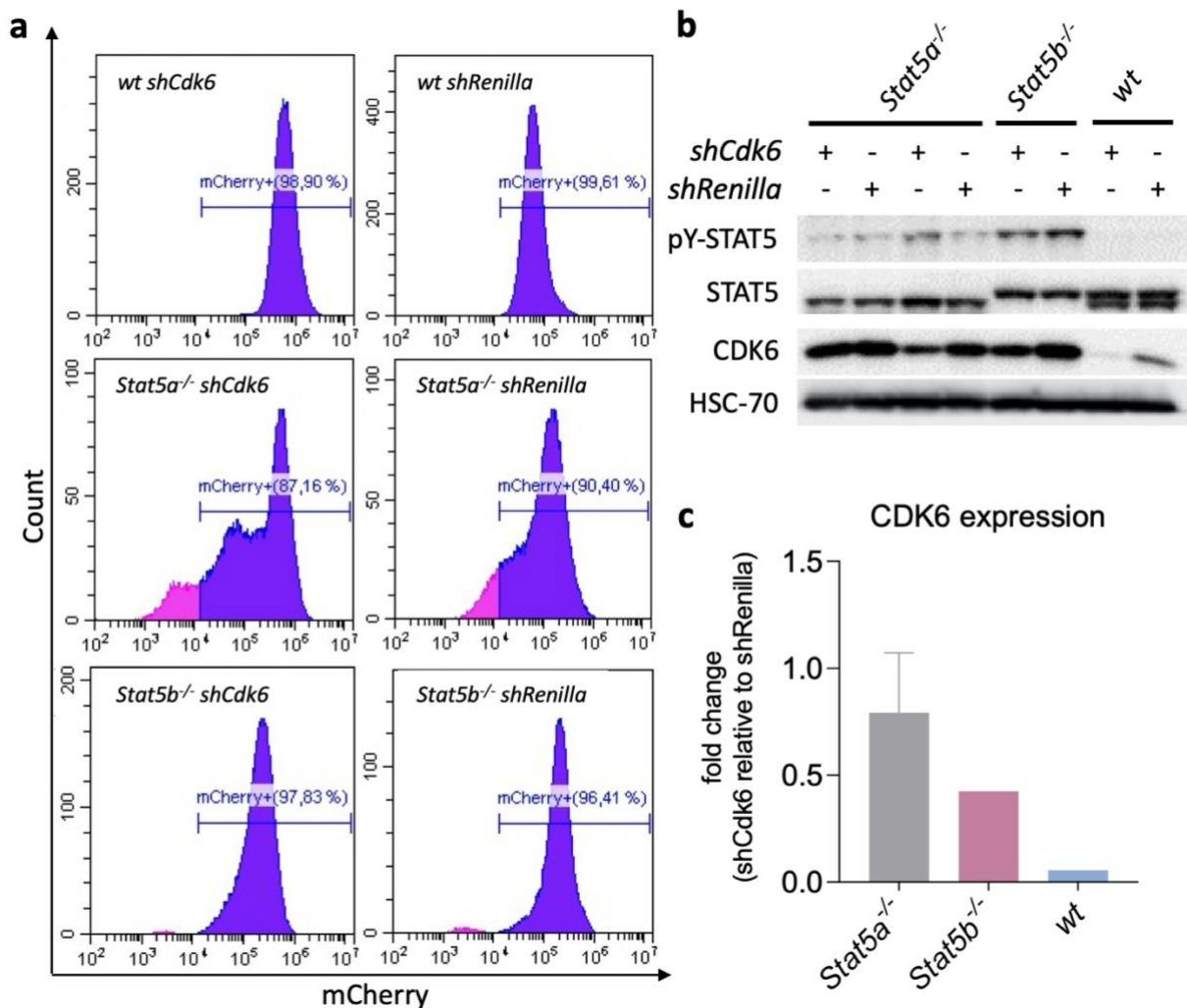


**Figure 22: *shRNA*-mediated knockdown of *Cdk6* is incompatible with *Stat5a* or *Stat5b* loss**

**a**) Representative flow cytometry histograms showing % mCherry<sup>+</sup> cells of live *shRNA* (against *Cdk6* and *Renilla*) infected and purity-sorted *NPM-ALK<sup>+</sup> wt*, *Stat5a<sup>-/-</sup>* and *Stat5b<sup>-/-</sup>* cells. **b**) Representative immunoblots and **c**) quantification showing CDK6 expression in *shRNA* (*Cdk6* and *Renilla*) infected and purity-sorted *NPM-ALK<sup>+</sup> wt*, *Stat5a<sup>-/-</sup>* and *Stat5b<sup>-/-</sup>* cell lines. The heat shock protein 70 (HSC-70) was used as a loading control.

Taken together, we conclude that a deficiency in *Cdk6* and *Stat5a* or *Stat5b* not only prevents lymphomagenesis in *NPM-ALK*<sup>+</sup> mice but is also incompatible to establish transformed murine *NPM-ALK*<sup>+</sup> ALCL cell lines.

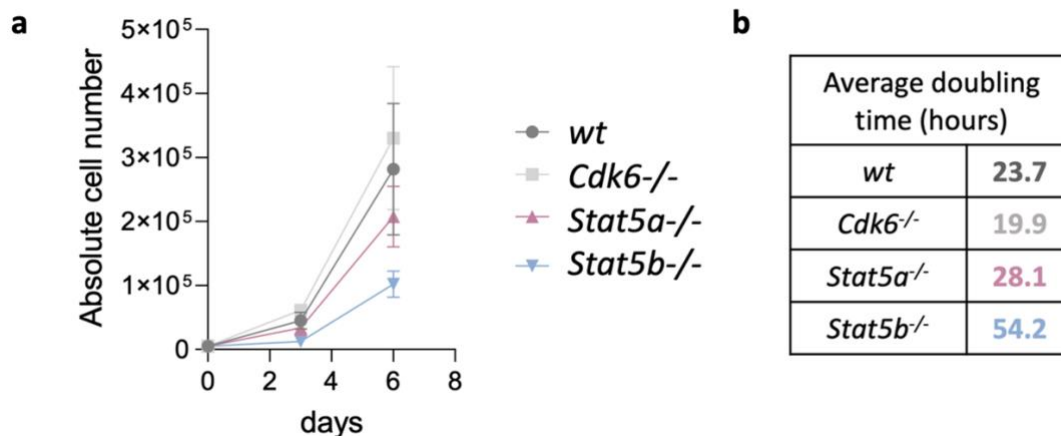
### 3.7 *NPM-ALK*<sup>+</sup> cell line characterisation

As we were unable to generate an *NPM-ALK*<sup>+</sup> *Cdk6*<sup>-/-</sup> and *Stat5a*<sup>-/-</sup> or *Stat5b*<sup>-/-</sup> double-knockout model, we investigated the consequences of single *Stat5a*, *Stat5b* or *Cdk6* deficiency in *NPM-ALK*<sup>+</sup> cell lines.

#### 3.7.1 The absence of STAT5A or STAT5B results in a proliferation defect

It is important to note that at the time of the following analysis, we were limited with the number of established cell lines. Compared to *NPM-ALK*<sup>+</sup> *wt* cell lines, the loss of STAT5A or STAT5B in *NPM-ALK*<sup>+</sup> cells confers a growth disadvantage, where STAT5B loss displays a more drastic phenotype. Contradictory to our expectation of *NPM-ALK*<sup>+</sup> *Cdk6*<sup>-/-</sup> cell lines having a growth disadvantage (later disease onset and lower incidence), we observed a trend that the *NPM-ALK*<sup>+</sup> *Cdk6*<sup>-/-</sup> cell lines proliferate faster than *NPM-ALK*<sup>+</sup> *wt* cell lines (**Figure 23a-b**).

To further address the observed growth differences of *NPM-ALK*<sup>+</sup> cell lines, a cell limiting dilution assay was performed. This revealed a severe growth disadvantage of *NPM-ALK*<sup>+</sup> *Stat5a*<sup>-/-</sup> and *Stat5b*<sup>-/-</sup> cell lines compared to *NPM-ALK*<sup>+</sup> *wt* and *Cdk6*<sup>-/-</sup> cell lines (**Figure 23c**). The effect was more prominent in low cell number dilutions, as depicted by the absolute cell count and fold-change of *NPM-ALK*<sup>+</sup> *Stat5a*<sup>-/-</sup> and *Stat5b*<sup>-/-</sup> relative to *NPM-ALK*<sup>+</sup> *wt* cell numbers (**Figure 23d**). Our observations indicate that the growth disadvantage of *NPM-ALK*<sup>+</sup> *Stat5a*<sup>-/-</sup> and *Stat5b*<sup>-/-</sup> cells is firmly dependent on cell density.



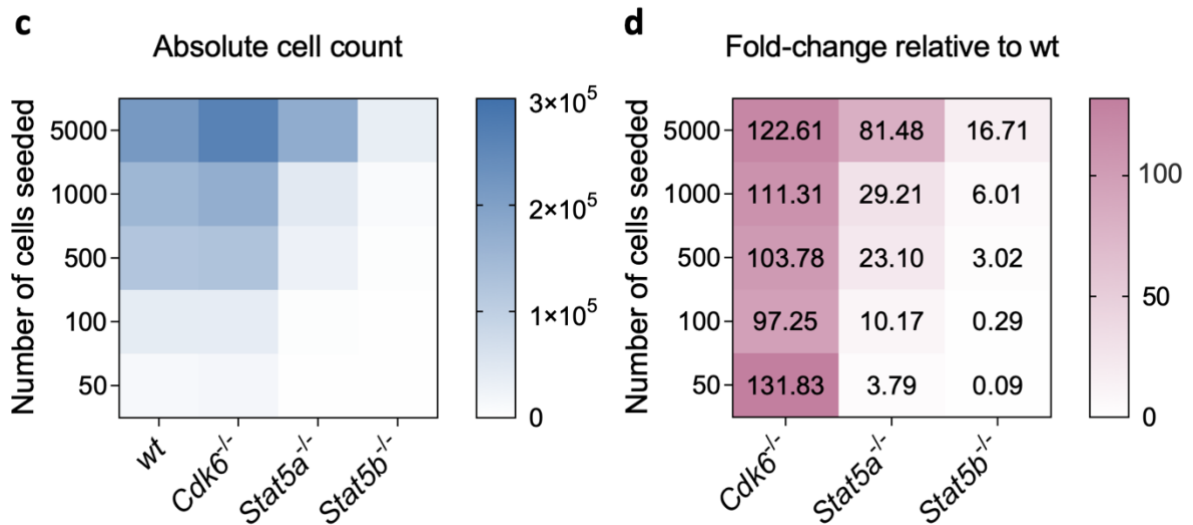


**Figure 23: *NPM-ALK<sup>+</sup> Stat5a<sup>-/-</sup>* and *Stat5b<sup>-/-</sup>* cell lines display a growth disadvantage compared to *NPM-ALK<sup>+</sup> wt***

**a)** Growth curve analysis and **b)** the calculated average cell doubling time of *NPM-ALK<sup>+</sup> wt*, *Cdk6<sup>-/-</sup>*, *Stat5a<sup>-/-</sup>* and *Stat5b<sup>-/-</sup>* cell lines ( $n = 2/\text{genotype}$ , mean $\pm$ SEM) from day 0 to day 3. 5,000 cells were seeded per genotype per well in 96-well-plates for each biological replicate and monitored over a period of six days. **c)** Cell dilution assay for *NPM-ALK<sup>+</sup> wt*, *Cdk6<sup>-/-</sup>*, *Stat5a<sup>-/-</sup>* and *Stat5b<sup>-/-</sup>* ( $n = 2/\text{genotype}$ ). 50, 100, 500, 1,000 and 5,000 cells were seeded for each biological replicate of each genotype, and absolute cell counts were obtained after seven days in culture. Heatmap illustrating the average absolute cell counts per genotype. **d)** Heatmap illustrating the fold change of absolute average cell numbers per genotype relative to those of *NPM-ALK<sup>+</sup> wt* cells.

### 3.7.2 Cell cycle shift and increased apoptosis in *Stat5b<sup>-/-</sup>* cells

Next, we determined if the observed growth defect of *NPM-ALK<sup>+</sup> Stat5a<sup>-/-</sup>* and *Stat5b<sup>-/-</sup>* cells is attributable to a change in cell cycle state or due to a higher rate of apoptosis. *NPM-ALK<sup>+</sup> Stat5a<sup>-/-</sup>* and *Stat5b<sup>-/-</sup>* cells harbour a cell cycle disadvantage (**Figure 24a-c**): The % of cells in S and G2/M phase trend indicate a delayed cell cycle entry, where *Stat5b<sup>-/-</sup>* cells displayed a more severe phenotype. The quantification of the sub-G0/G1 phase shows an increase in apoptosis/cell cycle arrest in *NPM-ALK<sup>+</sup> Stat5a<sup>-/-</sup>* and *Stat5b<sup>-/-</sup>* cells (**Figure 24d**). The Annexin-V/DAPI staining confirmed an increase of primary apoptosis and secondary necrosis in *Stat5a<sup>-/-</sup>* and *Stat5b<sup>-/-</sup>* cells (**Figure 24e-i**). However, due to limited sample numbers, no statistically significant changes in cell cycle phase distribution and apoptosis were depictable. We concluded that the severity of the growth disadvantage imposed on the cells by a *Stat5a* and *Stat5b* deficiency is most likely due to a decrease in cell cycle progression and an increase in apoptosis.

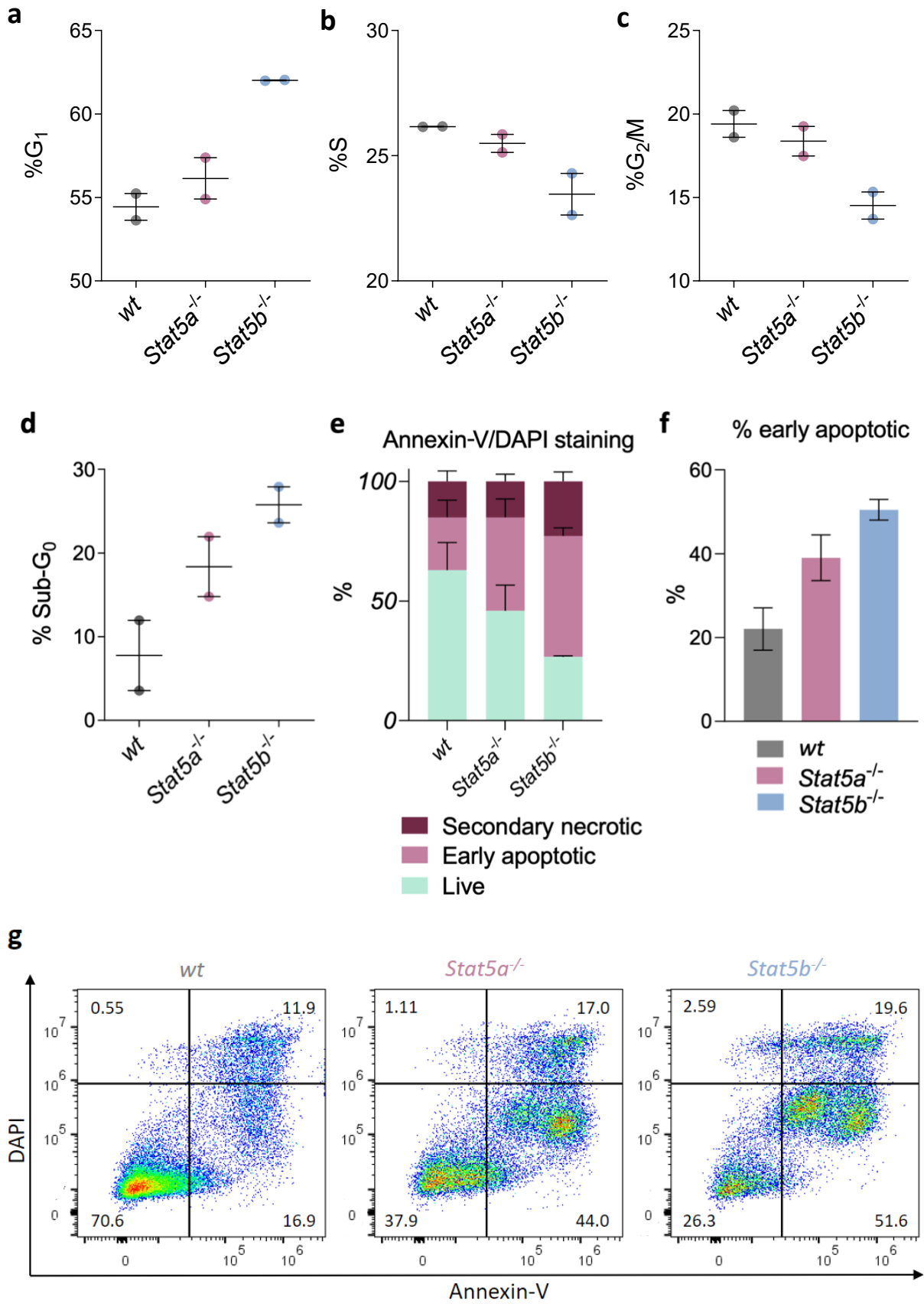


**Figure 24: *NPM-ALK*<sup>+</sup> *Stat5a*<sup>-/-</sup> and *Stat5b*<sup>-/-</sup> cells display a growth disadvantage and undergo increased apoptosis**

5,000 cells of *NPM-ALK*<sup>+</sup> *wt*, *Stat5a*<sup>-/-</sup> and *Stat5b*<sup>-/-</sup> (n = 2/genotype) cell lines were seeded per well in 96-well-plates for each biological replicate in technical triplicates. The cells were used for cell cycle and Annexin-V/DAPI analysis five days (120 h) after the start of the experiment. Quantification of cell cycle phase distributions analysis: **a)** % cells in the G0/G1-, **b)** S-, **c)** G2/M- and **d)** sub-G0/G1-phase. **e)** Annexin-V/DAPI staining showing the distribution of living (Annexin-V<sup>-</sup>/DAPI<sup>-</sup>), early apoptotic (Annexin-V<sup>+</sup>/DAPI<sup>-</sup>) and secondary necrotic (DAPI<sup>+</sup>) cells (n = 2/genotype). **f)** Quantification of % early apoptotic cells (Annexin-V<sup>+</sup>/DAPI<sup>-</sup>) per genotype. **g-i)** Representative flow cytometry plots Annexin-V/DAPI analysis for each genotype.

**3.7.3 Conditioned medium rescues the growth defect of *Stat5a*<sup>-/-</sup> or *Stat5b*<sup>-/-</sup> cell lines**

Figure **23c** and **d** showed that the severe growth defect by *Stat5a* or *Stat5b* deficiency is highly dependent on the cell density. This prompted us to investigate whether factors secreted by the cells influence cell growth and whether these factors are genotype-dependent. Therefore, we tested the effect of conditioned medium (complete RPMI medium obtained from dense cell culture dish) on *Stat5a*- and *Stat5b*-deficient cells. *NPM-ALK*<sup>+</sup> *wt*-conditioned medium resulted in higher *NPM-ALK*<sup>+</sup> *wt*, *Stat5a*<sup>-/-</sup> and *Stat5b*<sup>-/-</sup> cell numbers, rescuing the *Stat5a*<sup>-/-</sup> growth defect to *wt* level and increasing the *Stat5b*<sup>-/-</sup> cell number up to 3.5-fold after five days (**Figure 25a**). The rescue effect of conditioned medium was higher with cells seeded at a lower density and was more pronounced in *Stat5b*<sup>-/-</sup> cells compared to *Stat5a*<sup>-/-</sup> cells (**Figure 25b**).

To test the genotype dependency of the secreted factors, we repeated the cell dilution experiment with various medium conditions, including complete RPMI medium (normal medium), *wt*-, *Stat5a*<sup>-/-</sup>- and *Stat5b*<sup>-/-</sup>-conditioned medium. The rescue was possible with *wt*-, *Stat5a*<sup>-/-</sup>- or *Stat5b*<sup>-/-</sup>-conditioned medium (**Figure 25c**), but to a lower extent with *Stat5b*<sup>-/-</sup>-conditioned medium. Based on recent studies by Prutsch et al. (2019), we additionally tested whether the addition of IL-10 rescues the growth defect in non-dense cultures (**Figure 25c**). However, the addition of IL-10 neither improved the effects of normal nor *Stat5b*<sup>-/-</sup>-conditioned medium on cell growth – at least at the concentration tested (10 ng/ml) (**Figure 25c**).

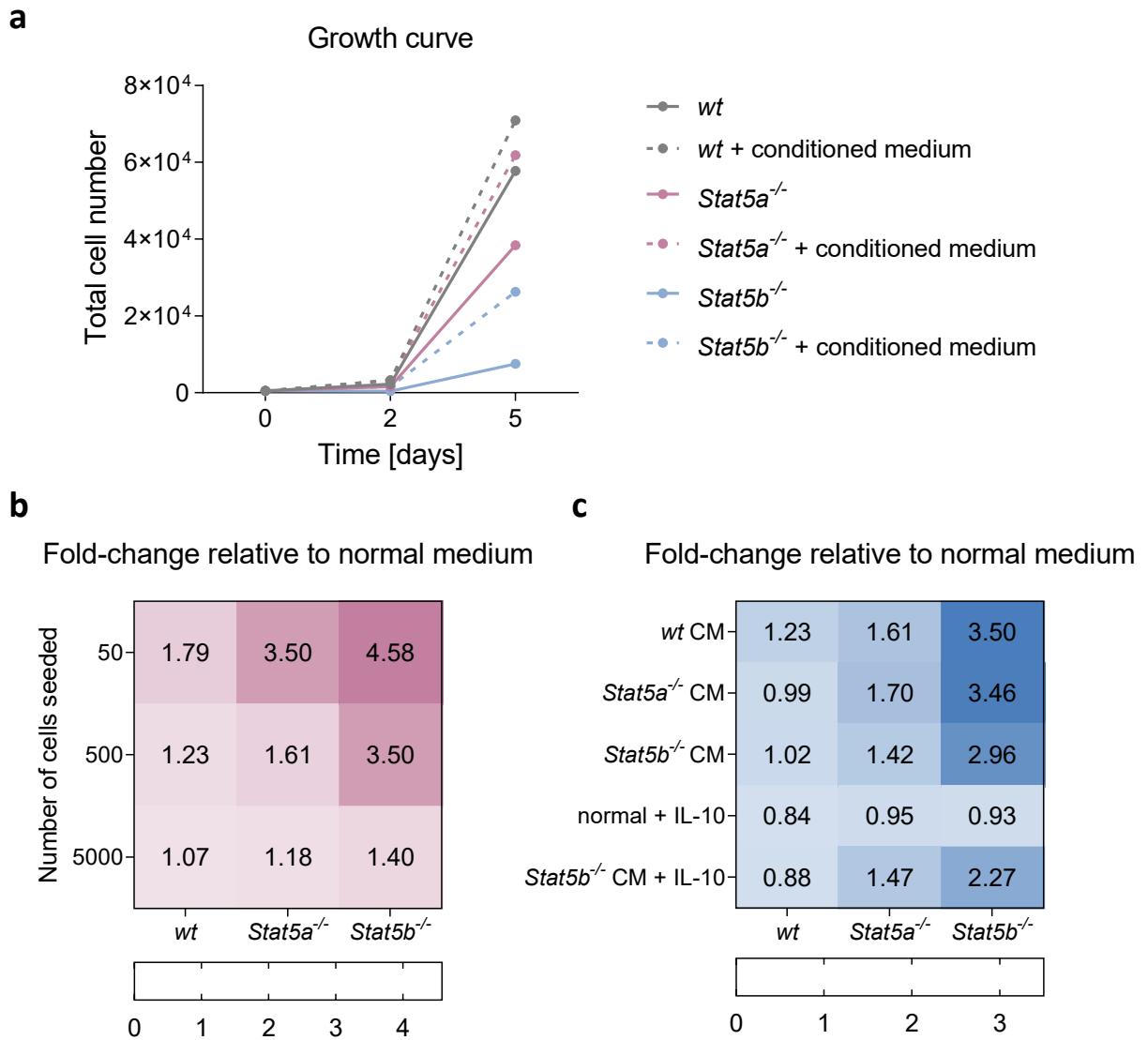


**Figure 25: The growth disadvantage of *NPM-ALK*<sup>+</sup> *Stat5a*<sup>-/-</sup> and *Stat5b*<sup>-/-</sup> is partially rescued by conditioned medium**

Limited dilution assay with 50, 500 and 5,000 cells of *NPM-ALK*<sup>+</sup> *wt*, *Stat5a*<sup>-/-</sup> and *Stat5b*<sup>-/-</sup> ( $n = 1/\text{genotype}$ ) cell lines were seeded per well in 96-well-plates. The cells were incubated in normal or conditioned complete RPMI-medium. The cells were monitored over a period of five days. **a**) Competitive growth analyses represented in absolute cell numbers. **b**) Absolute cell number fold-change of *wt*-conditioned medium incubated cells compared to normal RPMI medium at day 5 of the analysis. **c**) Absolute cell number fold-change of respective conditioned medium treated cells compared to normal RPMI medium at day 5 of the analysis for seeded cell density of 500.

### 3.7.4 Increased pY-STAT3/5 levels in the absence of CDK6

Knowing that the *Stat5a* or *Stat5b* deficiency leads to a growth disadvantage and increased rate of apoptosis in *NPM-ALK*<sup>+</sup> cells, we next interrogated the consequence of *Cdk6* deficiency.

By overcoming their disadvantage in thymic lymphoma onset (**Figure 14b**), the generated *NPM-ALK<sup>+</sup> Cdk6<sup>-/-</sup>* cell lines on average decrease their cell doubling time and tend to perform better in limiting cell dilution assays compared to *NPM-ALK<sup>+</sup> wt cells* (**Figure 23b-d**). We quantified tyrosine-phosphorylated STAT3 (pY-STAT3) and STAT5 (pY-STAT5) -levels in the generated *Cdk6<sup>-/-</sup>* cell lines by intracellular flow cytometry. *Cdk6<sup>-/-</sup>* cells exhibited higher levels of pY-STAT3 and pY-STAT5 compared to *wt cells* (**Figure 26**). pY-STAT3 levels were also increased in *Stat5a<sup>-/-</sup>* and *Stat5b<sup>-/-</sup>* compared to *wt cells*, while pY-STAT5 levels were increased exclusively in *Cdk6<sup>-/-</sup>* cells.

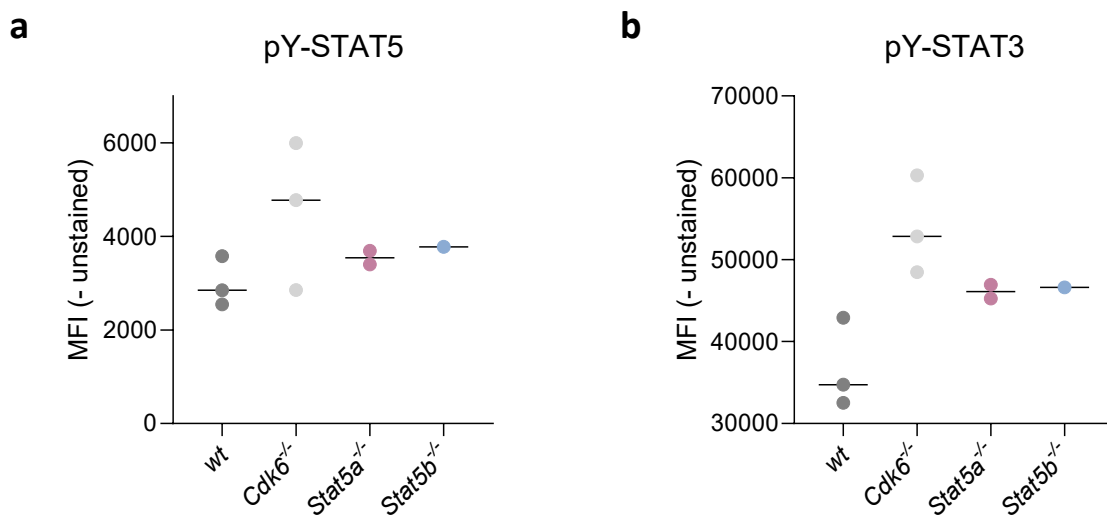


**Figure 26: Transformed *Cdk6<sup>-/-</sup>* cell lines harbour increased levels of pY-STAT5 and pY-STAT3**

**a)** pY-STAT5A/B and **b)** pY-STAT3 levels of generated *wt* (n = 3), *Cdk6<sup>-/-</sup>* (n = 3), *Stat5a<sup>-/-</sup>* (n = 2) and *Stat5b<sup>-/-</sup>* (n = 1) cell lines derived from primary thymic lymphomas, determined by intracellular flow cytometry staining.

Next, we asked whether increased pY-STAT3/5 levels are already present in non-diseased thymic tissue. We found *NPM-ALK<sup>+</sup> Cdk6<sup>-/-</sup>* thymi to have higher pY-STAT5 levels compared to *wt*, *Cdk6<sup>-/-</sup>* and *NPM-ALK<sup>+</sup> wt cells* (**Figure 27a**). The increase in pY-STAT5 levels cannot be attributed to an overall increase in total STAT5 levels (**Figure 27b**). Conversely, we instead found a trend of decreased total STAT5 levels in *NPM-ALK<sup>+</sup>* cells. The pY-STAT5/total STAT5 ratio underlines the increased pY-STAT5 levels in *Cdk6*-deficient *NPM-ALK<sup>+</sup>* cells (**Figure 27c**).

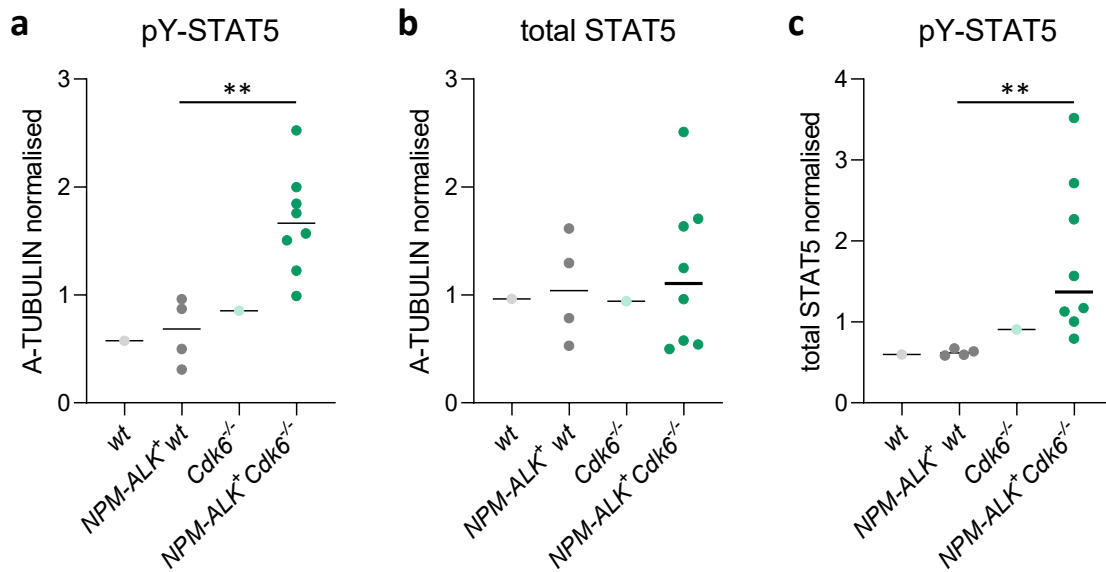


**Figure 27: Healthy *NPM-ALK<sup>+</sup> Cdk6<sup>-/-</sup>* thymic tissue express high levels of pY-STAT5**

Quantification of **a)** pY-STAT5A/B and **b)** STAT5A/B immunoblot analysis normalised to A-TUBULIN in wt (n = 1), *Cdk6<sup>-/-</sup>* (n = 1), *NPM-ALK<sup>+</sup> wt* (n = 4) and *NPM-ALK<sup>+</sup> Cdk6<sup>-/-</sup>* (n = 8) thymic tissue. **c)** Normalised pY-STAT5A/B levels relative to total STAT5A/B levels in wt (n = 1), *Cdk6<sup>-/-</sup>* (n = 1), *NPM-ALK<sup>+</sup> wt* (n = 2) and *NPM-ALK<sup>+</sup> Cdk6<sup>-/-</sup>* (n = 4) thymic tissue. Each data point represents a biological replicate. Levels of significance were calculated using an unpaired two-tailed Student's t-test. \*\* p < 0.01.

### 3.8 Pharmacological inhibition of *NPM-ALK<sup>+</sup>* cell lines

As a next step, we aimed to translate the observed phenotype and genotypic vulnerabilities into novel treatment opportunities.

#### 3.8.1 *Stat5a*, *Stat5b* or *Cdk6* deficiency does not sensitise *NPM-ALK<sup>+</sup>* cells to ALK inhibition

First, we determined the sensitivity of the cell lines to ALK inhibitors. Treating cell lines with increasing concentrations of Crizotinib or Alecetinib showed that *NPM-ALK<sup>+</sup> Stat5a<sup>-/-</sup>* and *Stat5b<sup>-/-</sup>* cell lines react similarly to ALK inhibition compared to *NPM-ALK<sup>+</sup> wt* cell lines (**Figure 28a**). At lower cell densities, *NPM-ALK<sup>+</sup> Cdk6<sup>-/-</sup>* cells appear to react less to ALK inhibition compared to *wt* cells (higher IC<sub>50</sub>). Nevertheless, when seeding the cells at a slightly higher density, there is no observable difference in the IC<sub>50</sub> upon Crizotinib or Alecetinib treatment between *Cdk6<sup>-/-</sup>* and *wt NPM-ALK<sup>+</sup>* cells (**Figure 28b-c**).

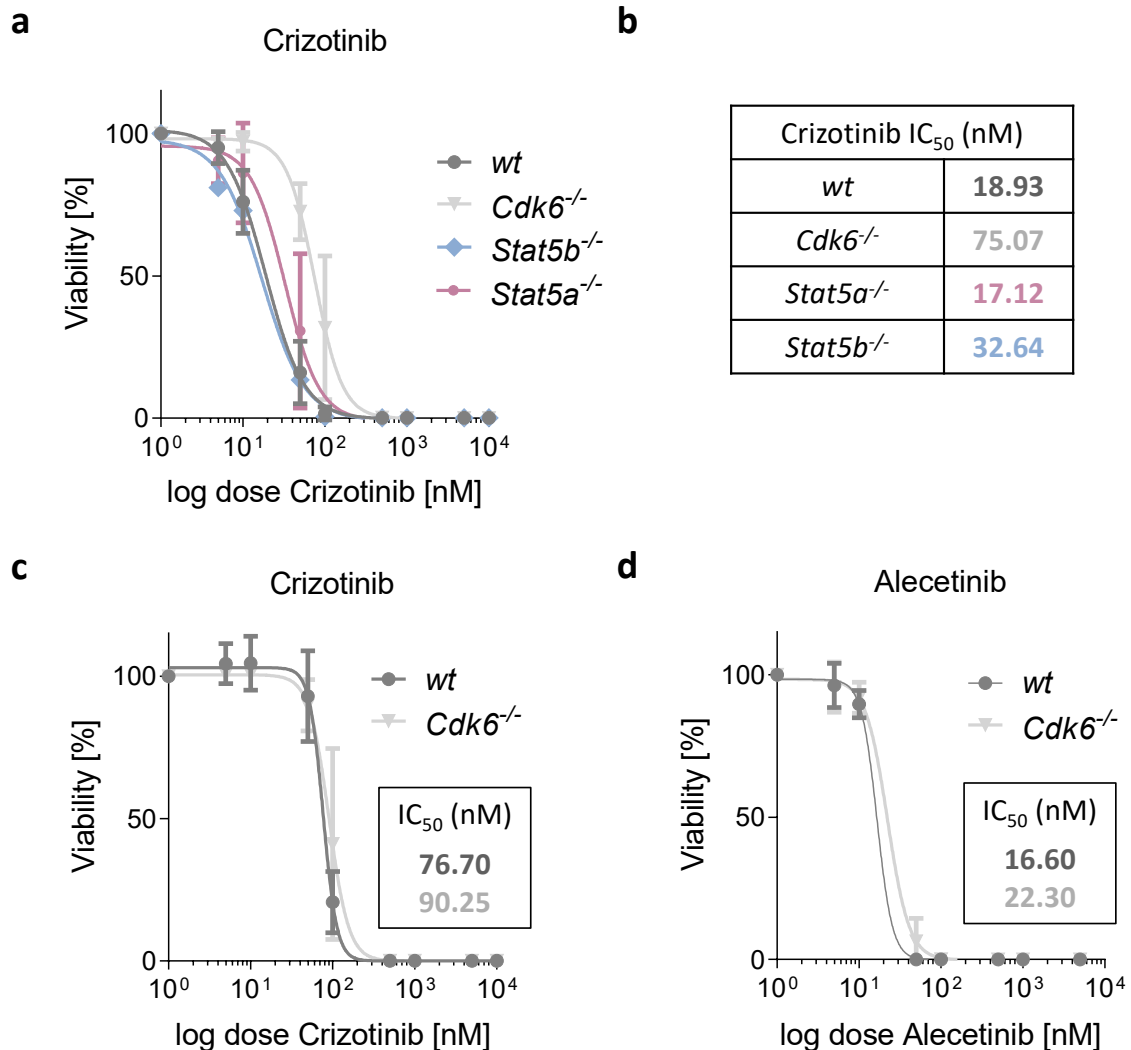


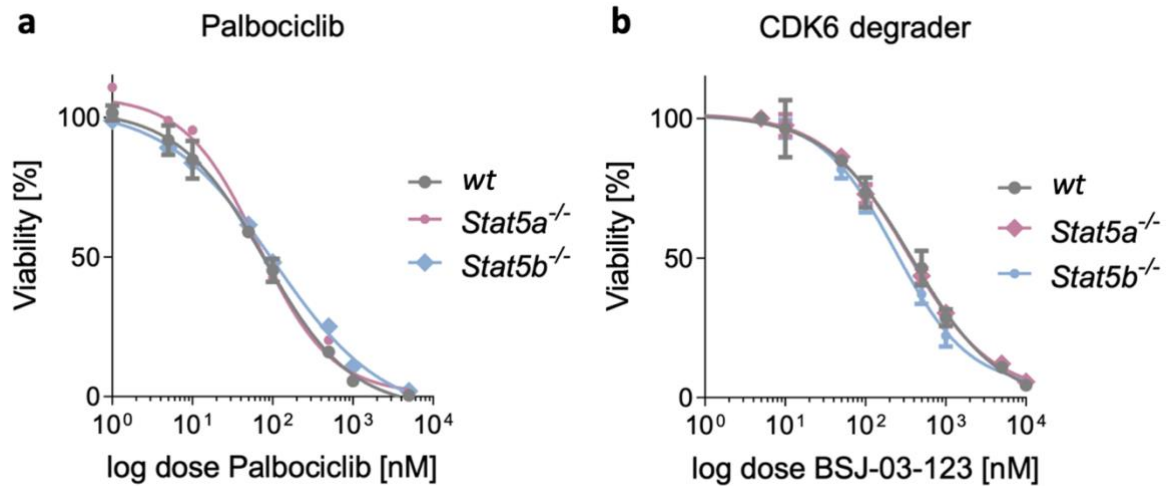
**Figure 28: All *NPM-ALK*<sup>+</sup> genotypes react similarly to ALK inhibition**

Determination of IC<sub>50</sub> via the CellTiter-Glo cell viability assay. The cells were seeded in 96-well-plates and treated with increasing concentrations of ALK-inhibitors in technical triplicates. The response was recorded after 72 hours and normalised to the DMSO treated control. **a**) 5,000 cells of *NPM-ALK*<sup>+</sup> *wt* (n = 3), *Cdk6*<sup>-/-</sup> (n = 3), *Stat5a*<sup>-/-</sup> (n = 2) and *Stat5b*<sup>-/-</sup> (n = 1) cell lines were seeded per well and treated with increasing concentrations of Crizotinib. **b**) Table depicting calculated IC<sub>50</sub> values for Crizotinib per each genotype. **c**) 10,000 cells of *NPM-ALK*<sup>+</sup> *wt* and *Cdk6*<sup>-/-</sup> cell lines (n = 2/genotype) were seeded per well and treated with increasing concentrations of Crizotinib or d) Alecetinib. The depicted viability assay also shows calculated IC<sub>50</sub> values.

**3.8.2 *Stat5a* or *Stat5b* deficiency fails to sensitise *NPM-ALK*<sup>+</sup> cells to kinase inhibition or degradation of CDK6**

To mimic the phenotype observed *in vivo* (*Cdk6*<sup>-/-</sup> *Stat5a*<sup>-/-</sup> or *Cdk6*<sup>-/-</sup> *Stat5b*<sup>-/-</sup>) via pharmacological perturbations, we treated the *wt*, *Stat5a*<sup>-/-</sup> and *Stat5b*<sup>-/-</sup> cells with a CDK6

kinase inhibitor or CDK6 degrader. The CDK6 inhibitor Palbociclib or the CDK6 degrader BSJ-03-123 displayed no statistically significant difference in cell viability or  $IC_{50}$  values (**Figure 29a-b**). As observed in other cellular systems used in our group (unpublished data by B. Schmalzbauer or T. Brandstoetter, data not shown), the CDK6 degrader BSJ-03-123 does not entirely diminish CDK6 protein levels (**Figure 29c-d**).



Palbociclib $IC_{50}$ (nM)	
<i>wt</i>	79.49
<i>Stat5a</i> <sup>-/-</sup>	66.15
<i>Stat5b</i> <sup>-/-</sup>	104.3

BSJ-03-123 $IC_{50}$ (nM)	
<i>wt</i>	379.2
<i>Stat5a</i> <sup>-/-</sup>	336.3
<i>Stat5b</i> <sup>-/-</sup>	235.6

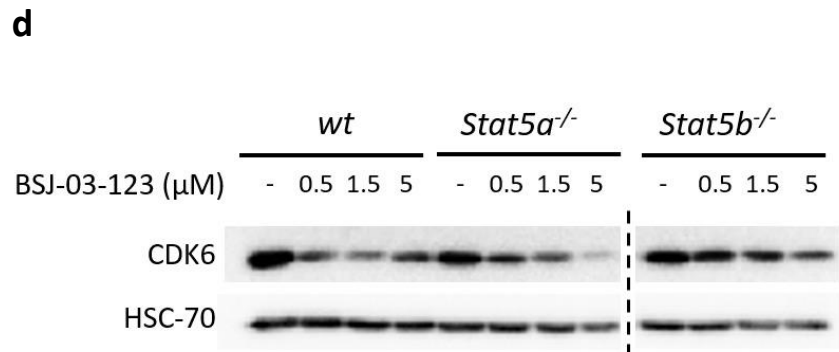
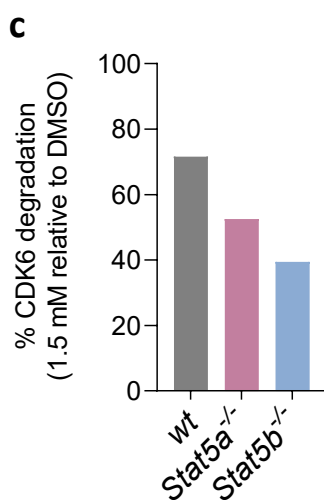
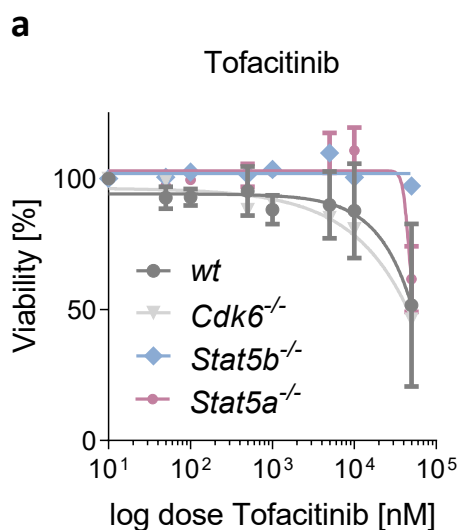


**Figure 29: No genotype difference is observed in response to CDK6 inhibitor or degrader treatment**

Determination of  $IC_{50}$  via the CellTiter-Glo cell viability assay. **a)** 10,000 cells of *NPM-ALK<sup>+</sup> wt* (n = 2, mean + SEM), *Stat5a<sup>-/-</sup>* (n = 1) and *Stat5b<sup>-/-</sup>* (n = 1) cell lines were seeded per well of 96-well-plate and treated with increasing concentrations of Palbociclib in technical triplicates. The response was recorded after 72 h and normalised to the DMSO treated control. **b)** Similarly, 10,000 cells of *NPM-ALK<sup>+</sup> wt*, *Stat5a<sup>-/-</sup>* and *Stat5b<sup>-/-</sup>* (n = 1/genotype) cell lines were seeded per well of 96-well-plate and treated with increasing concentrations of the BSJ-03-123 CDK6 degrader in technical triplicates. The degrader dose was re-administered every 24 h until the response was recorded after 72 h and normalised to the DMSO treated control. Table depicting calculated  $IC_{50}$  values for Palbociclib and BSJ-03-123 for each genotype, respectively. **c)** Immunoblot of CDK6 and HSC-70 in *NPM-ALK<sup>+</sup> wt*, *Stat5a<sup>-/-</sup>* and *Stat5b<sup>-/-</sup>* (n = 1/genotype) cell lines after 24 h treatment with 0.5  $\mu$ M, 1.5  $\mu$ M or 5  $\mu$ M of the BSJ-03-123 CDK6 degrader and DMSO as control. **d)** Quantification of CDK6 expression normalised to HSC-70.

**3.8.3 Cdk6 deficiency fails to sensitise *NPM-ALK<sup>+</sup>* cells to (pan-)JAK inhibition**

*NPM-ALK* has been shown to activate STAT5 through JAK2 (Nieborowska-Skorska et al., 2001). Therefore, we investigated whether the absence of *Stat5a*, *Stat5b* or *Cdk6* in the *NPM-ALK<sup>+</sup>* transformed cell lines influence JAK inhibitor sensitivity. After initial treatment of *wt*, *Cdk6<sup>-/-</sup>*, *Stat5a<sup>-/-</sup>* and *Stat5b<sup>-/-</sup>* cells with the JAK inhibitors Tofacitinib (**Figure 30a**) and Ruxolitinib (data not shown), we observed that the cells are not responding to the treatment. We repeated the experiment with a relevant subset of genotypes (*wt*, *Cdk6<sup>-/-</sup>*) together with the human *NPM-ALK<sup>-</sup>* ALCL control cell line Mac2A (**Figure 30b-d**). Indeed, the Mac2A cell line responded to JAK inhibition, while the *wt* and *Cdk6<sup>-/-</sup>* cell lines only responded at a very high  $IC_{50}$ , with no difference between the genotypes. We conclude that the established *NPM-ALK<sup>+</sup>* cell lines are insensitive to JAK1/2/3 inhibition.



**b**

$IC_{50}$ ( $\mu$ M)	Tofacitinib	Ruxolitinib
<i>wt</i>	49.5	7.54
<i>Cdk6<sup>-/-</sup></i>	50.7	9.97
Mac2A	0.77	0.08

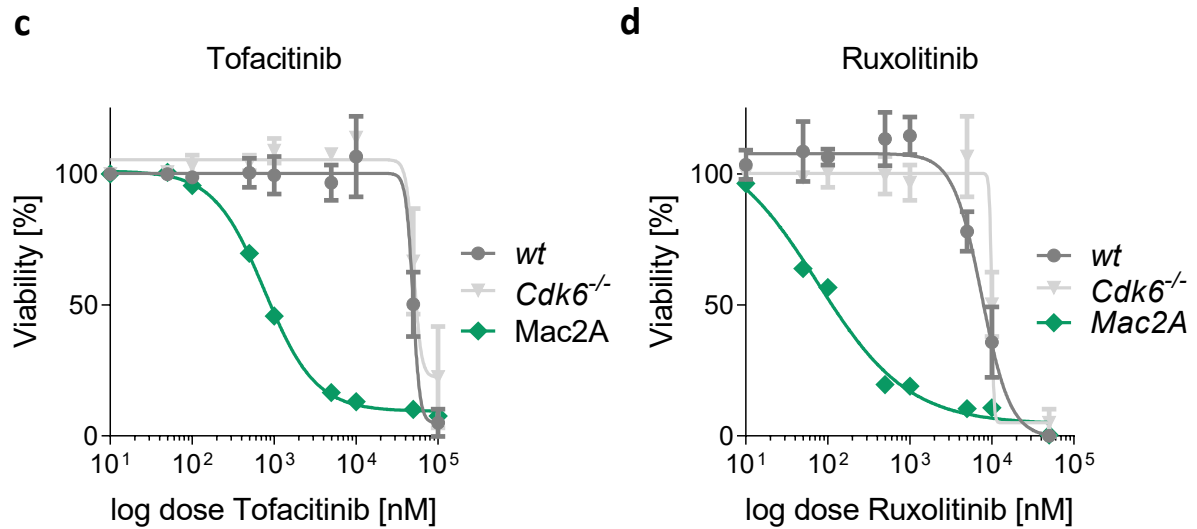


**Figure 30: *NPM-ALK*<sup>+</sup> cell lines are not sensitive to JAK-inhibition**

Determination of  $IC_{50}$  via the CellTiter-Glo cell viability assay. Cells were seeded in 96-well-plates and treated with increasing concentrations of JAK-inhibitors in technical triplicates. The response was recorded after 72 h and normalised to the DMSO treated control. **a)** 10,000 cells of *NPM-ALK*<sup>+</sup> wt (n = 3), *Cdk6*<sup>-/-</sup> (n = 3), *Stat5a*<sup>-/-</sup> (n = 2) and *Stat5b*<sup>-/-</sup> (n = 1) cell lines were seeded per well and treated with increasing concentrations of Tofacitinib. **b)** Table depicting calculated  $IC_{50}$  values for Tofacitinib and Ruxolitinib for *NPM-ALK*<sup>+</sup> wt, *Cdk6*<sup>-/-</sup> and Mac2A cells. 10,000 cells of the Mac2A and *NPM-ALK*<sup>+</sup> wt, *Cdk6*<sup>-/-</sup> (n = 2/genotype) cell lines were seeded per well and treated with increasing concentrations of **c)** Tofacitinib or **d)** Ruxolitinib.

### 3.8.4 PDGFR inhibition

Based on the work of Laimer et al. (2012), showing that the AP-1 family members JUN and JUNB promote lymphoma development and tumour dissemination through transcriptional regulation of platelet-derived growth factor receptor (PDGFR), we next interrogated the inhibition of the PDGFR on *NPM-ALK*<sup>+</sup> cell lines. The *NPM-ALK*<sup>+</sup> cell lines did not display any difference between genotypes in their response to PDGFR inhibitors (**Figure 31**). All genotypes reacted to Imatinib and Crenolanib only at very high concentrations. The high  $IC_{50}$  indicates the insensitivity of our *NPM-ALK*<sup>+</sup> cell lines to PDGFR inhibition.

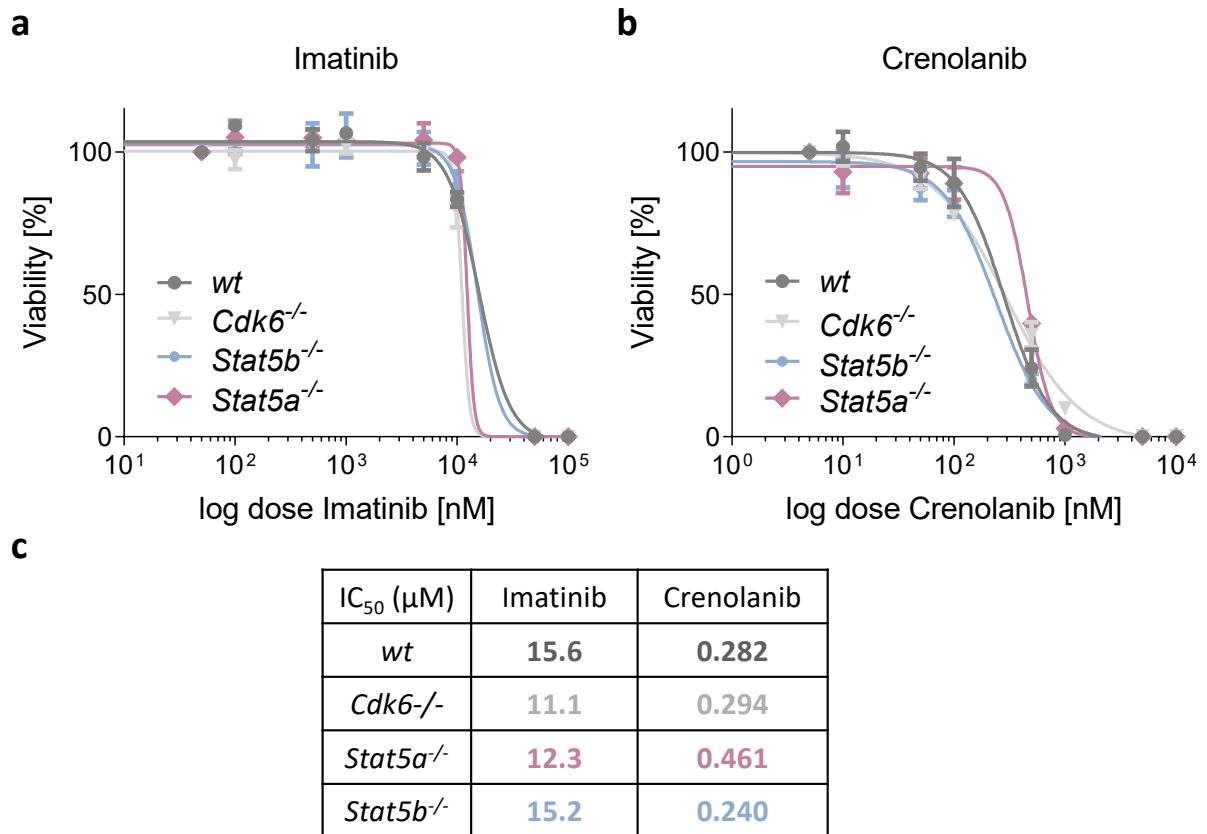


**Figure 31: *NPM-ALK*<sup>+</sup> cells lines do not respond to PDGFR inhibition**

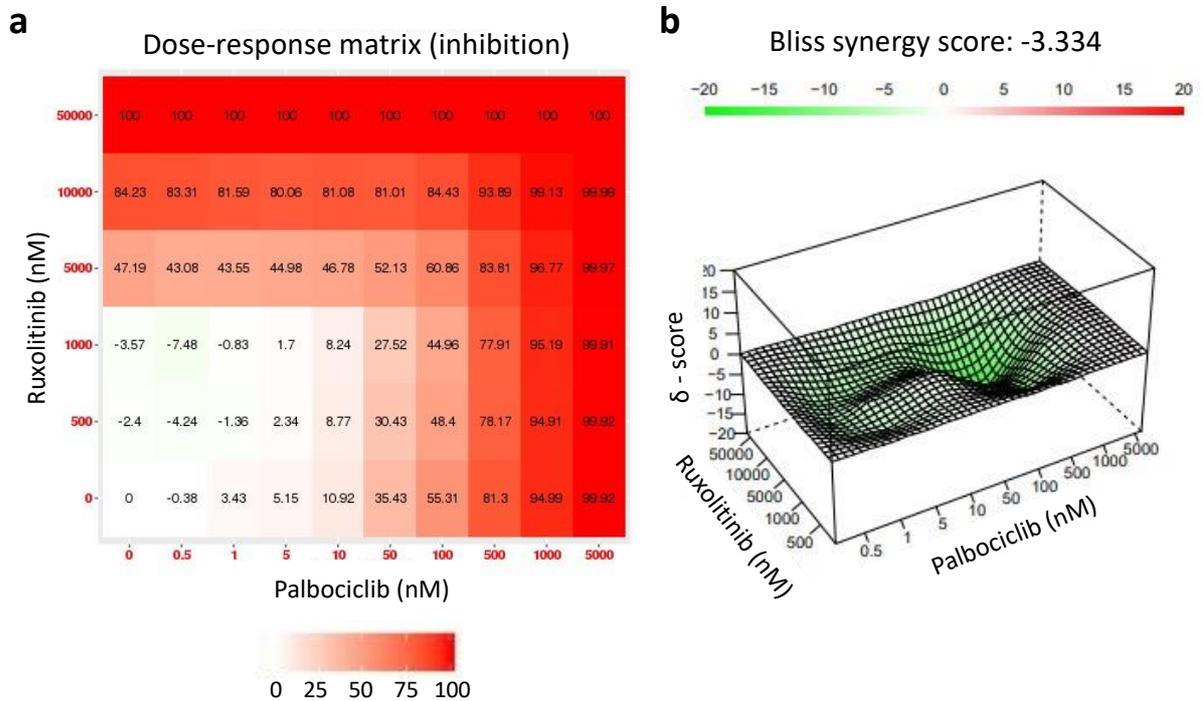
Determination of IC<sub>50</sub> via the CellTiter-Glo cell viability assay. 10,000 cells of *NPM-ALK*<sup>+</sup> wt, *Cdk6*<sup>-/-</sup>, *Stat5a*<sup>-/-</sup> and *Stat5b*<sup>-/-</sup> (n = 1/genotype) cell lines were seeded per well of 96-well-plate and treated with increasing concentrations of **a**) Imatinib and **b**) Crenolanib (PDGFR inhibitors) in technical triplicates (mean + SEM). The response was recorded after 72 h and normalised to the DMSO treated control. **c**) Table depicting calculated IC<sub>50</sub> values for Imatinib and Crenolanib per genotype.

### 3.9 Pharmacological perturbations of CDK6 and STAT5 activation do not result in synergistic effects

Failing to observe sensitisation of established transformed murine *Stat5a*<sup>-/-</sup>, *Stat5b*<sup>-/-</sup> or *Cdk6*<sup>-/-</sup> cell lines to ALK, JAK, PDGFR and CDK6 inhibition as well as CDK6 degradation, we further elucidated the independent or converged pathways orchestrated by CDK6 and STAT5A/B proteins in *NPM-ALK*-transformed cells. We hypothesised that the established *Cdk6*<sup>-/-</sup>, *Stat5a*<sup>-/-</sup> and *Stat5b*<sup>-/-</sup> cell lines develop compensatory mechanisms, thereby becoming independent of the targeted pathways. We aimed to determine whether the combined pharmacological inhibition of CDK6 and STAT5 activation has a synergistic effect on “non-compensated” murine cell lines established from primary *NPM-ALK*<sup>+</sup> wt thymic lymphomas.

### 3.9.1 Combined inhibition of JAK1/2 and CDK6

As clinical-grade direct STAT5 inhibitors are not available, we first used the JAK1/2 inhibitor Ruxolitinib to target the STAT5 axis. However, this is not an ideal setting as it is not clear whether NPM-ALK directly phosphorylates STAT5A or STAT5B circumventing JAK activation. Nevertheless, we combined the Ruxolitinib treatment with the CDK6 kinase inhibitor Palbociclib. The combined CDK6 and JAK1/2 kinase inhibition resulted in a slightly additive but not synergistic effect (**Figure 32a-b**). Next, we investigated the combinatorial effects of Ruxolitinib and the CDK6 degrader BSJ-03-123. Similarly, the combined degradation of CDK6 and JAK1/2 kinase inhibition display only a slightly additive effect (**Figure 32c-d**).



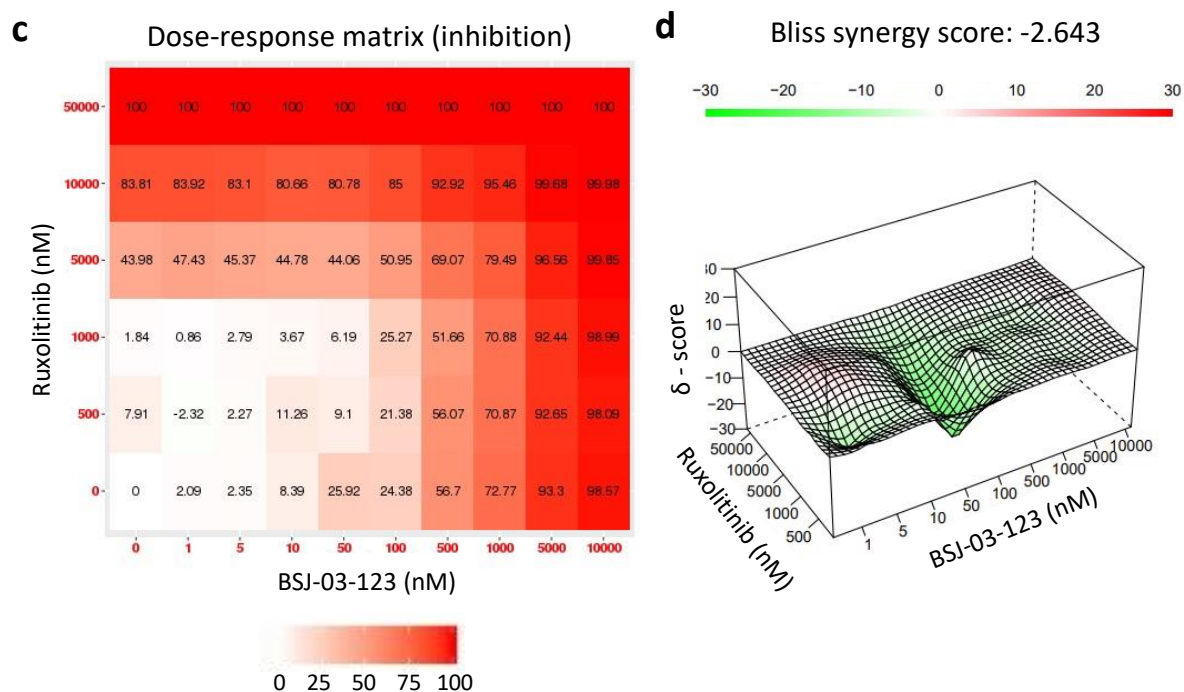


**Figure 32: Kinase inhibition or degradation of CDK6 combined with JAK1/2 kinase inhibition results in an additive but not a synergistic effect**

Determination of combinatorial inhibition effects on murine wt *NPM-ALK*<sup>+</sup> cell lines. 10,000 cells of *NPM-ALK*<sup>+</sup> wt (n = 2) were seeded per well of 96-well-plate and treated with increasing concentrations of inhibitors or degraders. The BSJ-03-123 dose was re-administered every 24 h until the response was recorded after 72 h and normalised to the DMSO treated control. The CellTiter-Glo viability assay was used as a readout for determining the inhibition elicited by the combinatorial treatment. The Bliss synergy score is calculated as the difference between expected and observed drug response under the hypothesis of the independent action of drugs and no synergy. Averaged dose-response matrix (inhibition) of **a**) Ruxolitinib-Palbociclib and **c**) Ruxolitinib-BSJ-03-123 combinatorial treatments. 3D Synergy plots visualising the Bliss synergy score of the **b**) Ruxolitinib-Palbociclib and **d**) Ruxolitinib-BSJ-03-123 combinatorial treatment. (Antagonism: -20 to -10, Additivity: -10 to 10, Synergy: 10 to 20).

### 3.9.2 Targeting ALK alongside CDK6

Due to the above-mentioned caveat of direct or indirect phosphorylation of STAT5A or STAT5B by NPM-ALK, we decided to repeat the experiment by targeting NPM-ALK alongside CDK6. Therefore, we combined the ALK inhibitor Crizotinib with the CDK6 kinase inhibitor Palbociclib and the CDK6 degrader BSJ-03-123. Again, combining CDK6 kinase inhibition or degradation with ALK kinase inhibition resulted in an additive but not synergistic effect (**Figure 33**).

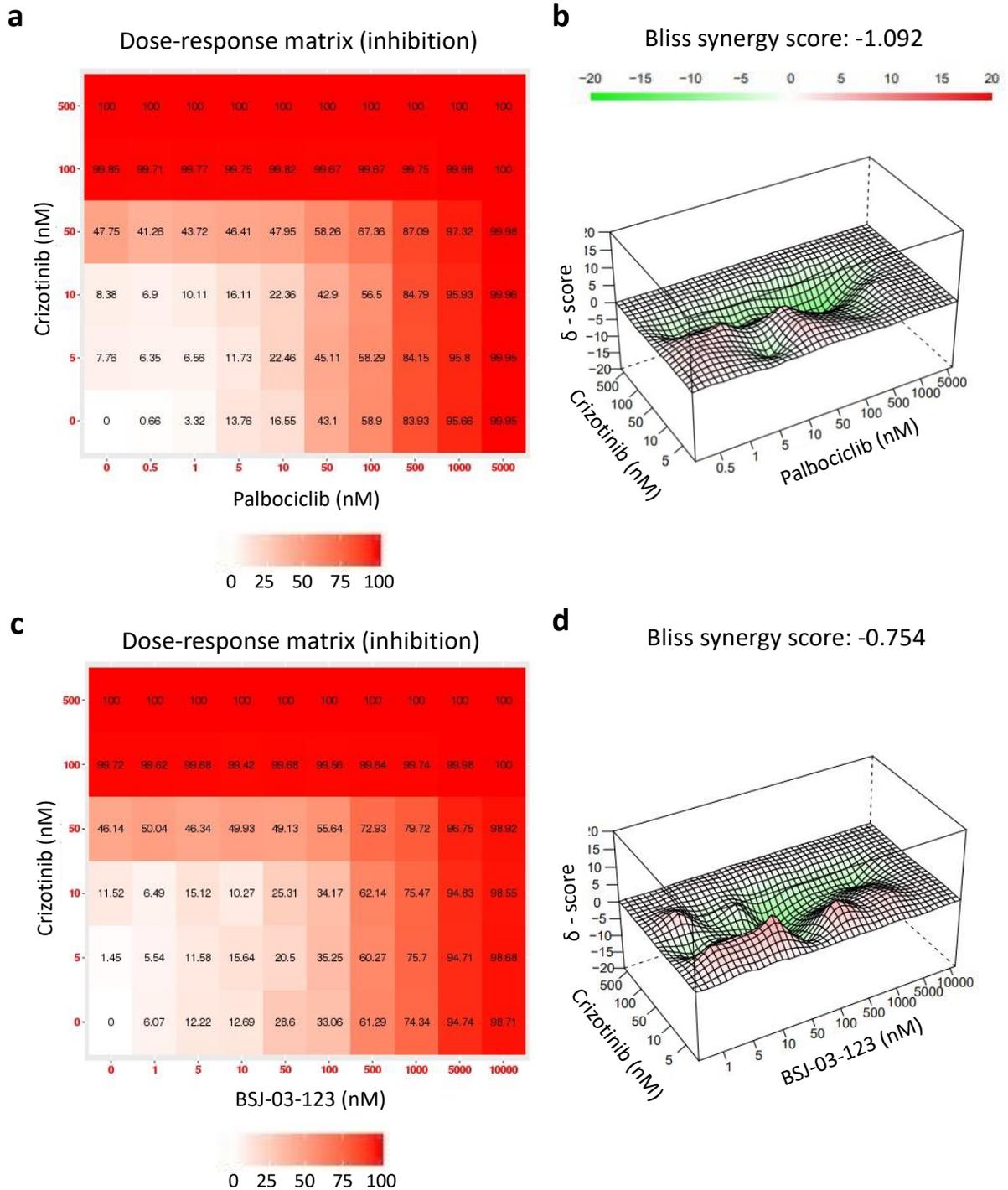


**Figure 33: Kinase inhibition or degradation of CDK6 combined with ALK inhibition results in an additive but not a synergistic effect**

Determination of combinatorial inhibition effects on murine *wt* *NPM-ALK*<sup>+</sup> cell lines. 10,000 cells of *NPM-ALK*<sup>+</sup> *wt* (n = 2) were seeded per well of 96-well-plate and treated with increasing concentrations of inhibitors or degraders. The BSJ-03-123 dose was re-administered every 24 h until the response was recorded after 72 h and normalised to the DMSO treated control. The CellTiter-Glo viability assay was used as a readout for determining the inhibition elicited by the combinatorial treatment. The Bliss synergy score is

calculated as the difference between expected and observed drug response under the hypothesis of the independent action of drugs and no synergy. Averaged dose-response matrix (inhibition) of **a)** Crizotinib-Palbociclib and **c)** Crizotinib-BSJ-03-123 combinatorial treatments. 3D Synergy plots visualising the Bliss synergy score of the **b)** Crizotinib-Palbociclib and **d)** Crizotinib-BSJ-03-123 combinatorial treatment. (Antagonism: -20 to -10, Additivity: -10 to 10, Synergy: 10 to 20).

When comparing the synergy scores of different combinatorial treatments, we observe that the Crizotinib combinatorial treatments resulted in a higher synergy score compared to Ruxolitinib combinatorial treatments, indicating higher additivity of the drugs (**Figure 34**). A similar trend was also observed with CDK6 degradation combinatorial treatments, which displayed higher additivity compared to kinase inhibitory (Palbociclib) combinatorial treatments. Crizotinib-BSJ-03-123 combinatorial treatment displayed the highest Bliss synergy score, indicating that best inhibition is achieved by targeting CDK6 kinase-dependent and independent functions, together with ALK-mediated signalling.

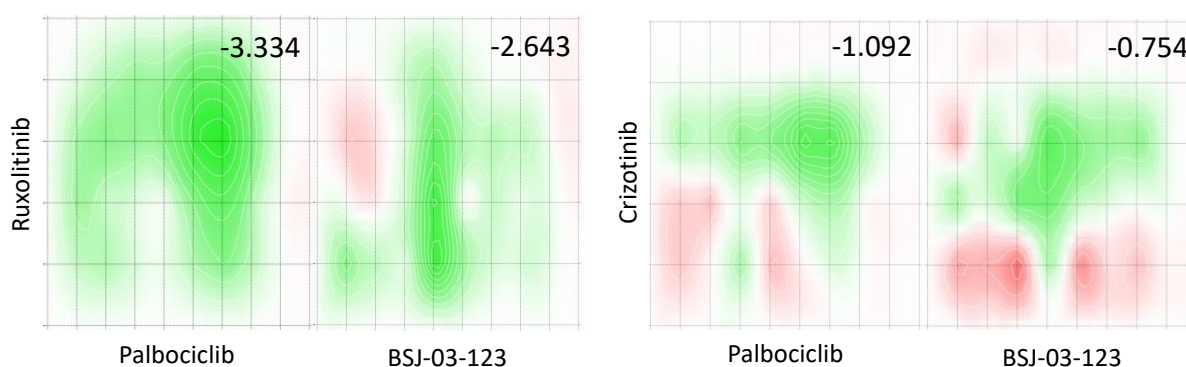


**Figure 34: ALK inhibitor Crizotinib and the CDK6 degrader BSJ-03-123 show the highest Bliss synergy score.**

2D Synergy plots visualising the Bliss synergy score of various drug combinations (Antagonism: -20 to -10, Additivity: -10 to 10, Synergy: 10 to 20).

### 3.10 ALK- or pan-JAK-inhibition diminishes pY-STAT5 levels

Combinatorial treatments utilising CDK6 inhibitors or degraders and inhibitors of STAT5 activation did not result in synergistic inhibitory effects in NPM-ALK-transformed cells. We postulate that synergy was not observed due to incomplete inhibition of kinase-dependent and -independent functions of CDK6, as well as incomplete inhibition of the STAT5 activation axis. As a next step, we further interrogated STAT5 activation in *NPM-ALK<sup>+</sup> wt cells* upon pharmacological perturbation. Compared to DMSO-treated controls, ALK inhibitors Crizotinib and Alecetinib diminished pY-STAT5 levels before affecting p-ALK or pY-STAT3 levels

(**Figure 35**). High concentrations of the JAK1/2 inhibitor Ruxolitinib inhibited the majority of STAT5 phosphorylation, leaving a small portion of pY-STAT5 intact. However, PDGFR inhibitor Crenolanib, BCR-ABL inhibitor Imatinib (also targets KIT and PDGFR), and pan-JAK inhibitor (JAK1/2/3) Tofacitinib did not have a detrimental effect on pY-STAT5 levels of all three *NPM-ALK<sup>+</sup> wt* cell lines at the tested concentrations. We thus conclude, that ALK-inhibition diminished pY-STAT5 levels to a higher degree than pan-JAK inhibition.

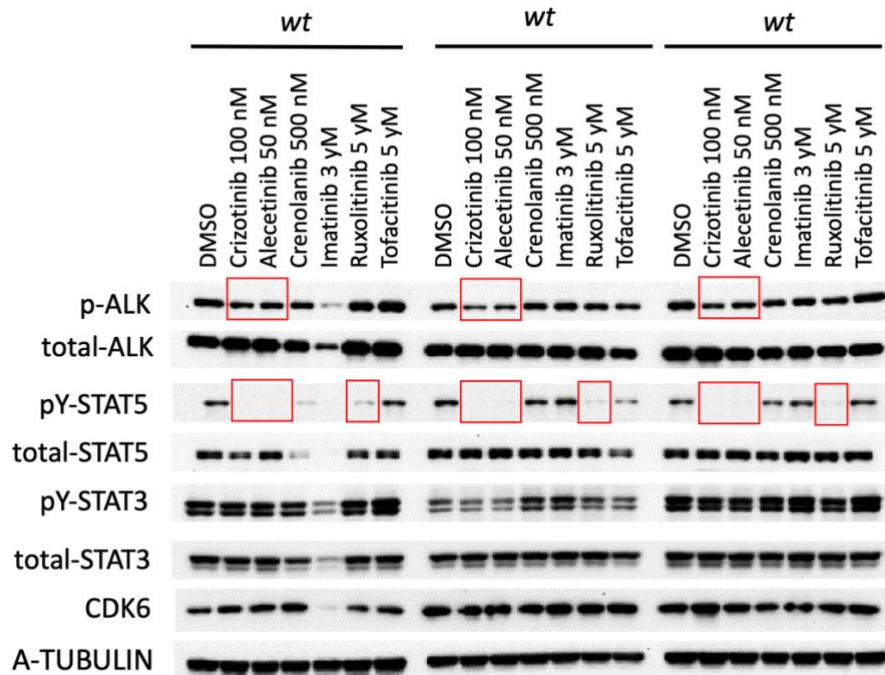


**Figure 35: *NPM-ALK* inhibitors diminish pY-STAT5 levels**

Immunoblot of p-ALK, total ALK, pY-STAT5A/B, total STAT5A/B, pY-STAT3, total STAT3 and A-TUBULIN in *NPM-ALK<sup>+</sup> wt* ( $n = 3$ ) cell lines after 4 h treatment with 100 nM Crizotinib, 50 nM Alecetininib, 500 nM Crenolanib, 3  $\mu$ M Imatinib, 5  $\mu$ M Ruxolitinib, 5  $\mu$ M Tofacitinib and DMSO as control. The used drug concentrations were chosen according to the  $IC_{50}$  on *NPM-ALK<sup>+</sup> wt* cells.

### 3.11 *NPM-ALK* – directly and indirectly – phosphorylates STAT5 proteins

The effect of ALK- and JAK-inhibitors on pY-STAT5 levels caused us to further interrogate mechanisms of how *NPM-ALK* phosphorylates STAT5 proteins. It was shown that *NPM-ALK* indirectly phosphorylates STAT5 proteins via JAK2 (Nieborowska-Skorska et al., 2001). However, based on our observations that pan-JAK inhibition fails to completely diminish pY-STAT5 levels in *NPM-ALK<sup>+</sup>* cells, we hypothesised that *NPM-ALK* also directly phosphorylates STAT5 proteins. In order to test our hypothesis, we needed a system of parental – *NPM-ALK*-negative – cells in addition to an *NPM-ALK* expressing sub-cell line. For

this purpose, Ba/F3 cells were infected with a retrovirus containing the NPM-ALK-transgene and processed as depicted in **Figure 36a**. After seven days in culture, we obtained a pure population of NPM-ALK expressing Ba/F3 cells (**Figure 36b**). The NPM-ALK-infected Ba/F3 cells were IL-3-independent, while parental Ba/F3 cells depend on IL-3 (**Figure 36c**). The immunoblot depicts differences in protein levels after NPM-ALK infection of Ba/F3 cells (**Figure 36d**). We validated NPM-ALK expression in NPM-ALK-infected Ba/F3 by pY- and total-ALK immunoblotting, indicating a strong presence of the transgene. Furthermore, the NPM-ALK-infected Ba/F3 cells exhibit an overall similar signalling pattern – pY- and total-STAT3/5 levels – compared to the established murine NPM-ALK-expressing (NPM-ALK<sup>+</sup>) wt cell line.

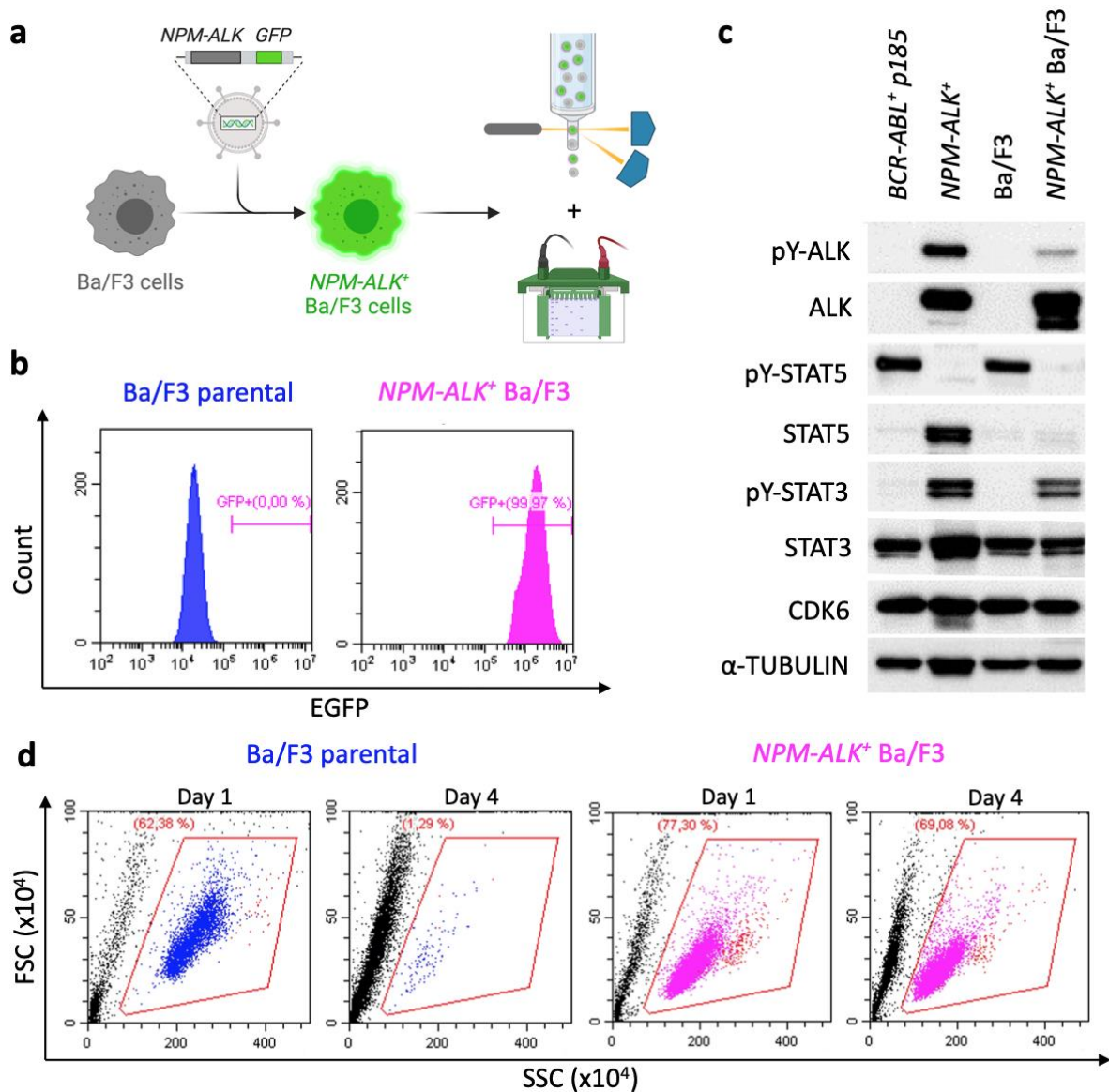


**Figure 36: NPM-ALK-infected parental Ba/F3 cell line exhibits increased protein levels of the transgene**

**a)** Parental Ba/F3 cell line experimental setup scheme. **b)** Representative flow cytometry histograms of parental and NPM-ALK-infected Ba/F3 at day 7 post-infection. **c)** Representative flow cytometry plots of parental and NPM-ALK<sup>+</sup> Ba/F3 cells at day 0 and day 4 after IL-3-deprivation. **d)** Immunoblot of p-ALK, total ALK, pY-STAT5A/B, total STAT5A/B, pY-STAT3, total STAT3, CDK6 and A-TUBULIN in parental Ba/F3 and NPM-ALK<sup>+</sup> Ba/F3 cells, including a positive (*NPM-ALK<sup>+</sup> wt cell line*) and negative (*BCR-ABL p185 cell line*) control.

After confirming NPM-ALK expression in the Ba/F3 cells, IC<sub>50</sub> values for JAK-inhibitors Ruxolitinib and Tofacitinib were determined. From the cell viability assay, we observed that the IC<sub>50</sub> value is highly dependent on the addition of IL-3 to the cell culture medium. The addition of IL-3 to the culture of NPM-ALK<sup>+</sup> Ba/F3 cells increased the IC<sub>50</sub> concentration of Ruxolitinib by 6-fold (**Figure 37a**). A similar effect was observed after Tofacitinib treatment (**Figure 37b**), indicating that IL-3 holds an important role when interrogating pY-STAT5 levels.

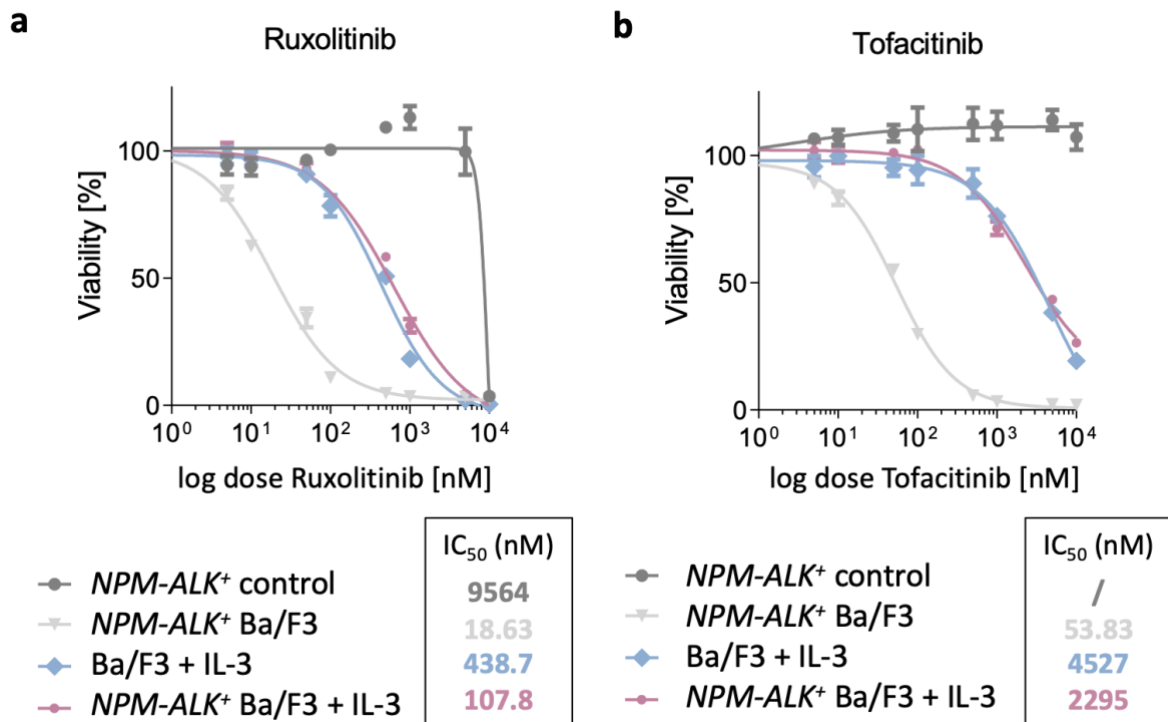


**Figure 37: IC<sub>50</sub> concentration of Ba/F3 cells is highly dependent on the addition of IL-3**  
Determination of IC<sub>50</sub> via the CellTiter-Glo cell viability assay. The cells were seeded in 96-well-plates and treated with increasing concentrations of JAK-inhibitors in technical triplicates. The response was recorded after 72 h and normalised to the DMSO treated control. **a)** 5,000 cells were seeded per well of the parental Ba/F3 cell line in the presence of IL-3, NPM-ALK<sup>+</sup> Ba/F3 cell line with and without IL-3, as well as an *NPM-ALK<sup>+</sup> wt* control cell line and treated with increasing concentrations of **a)** Ruxolitinib and **b)** Tofacitinib.

Due to the incomplete inhibition of pY-STAT5 levels following JAK1/2-inhibition, we further investigated the mechanism of STAT5 phosphorylation. Based on the high volatility of the

IC<sub>50</sub> concentration, we included multiple controls when interrogating pY-STAT5 levels in Ba/F3 cells with and without NPM-ALK (**Figure 38a**). In a starved state, NPM-ALK increases the baseline pY-STAT5 levels (**Figure 38b**). Upon the addition of Ruxolitinib, the pY-STAT5 levels of the Ba/F3 parental cells are strongly diminished, while Ba/F3 cells expressing NPM-ALK still contain high levels of pY-STAT5. A similar observation was made when parental Ba/F3 and NPM-ALK-expressing Ba/F3 cells were cultured in IL-3. The addition of IL-3 strikingly increased pY-STAT5 levels in NPM-ALK<sup>+</sup> Ba/F3 cells, while parental Ba/F3 displayed a slight increase in pY-STAT5. Ruxolitinib completely diminished pY-STAT5 levels of IL-3-cultured Ba/F3 cells, while NPM-ALK-expressing cells sustained 20-fold higher pY-STAT5 levels. In summary, the presence of NPM-ALK drastically increased baseline pY-STAT5 levels in NPM-ALK-expressing Ba/F3 cells, which retained high pY-STAT5 levels after Ruxolitinib treatment. Since Ruxolitinib inhibits the IL-3/JAK2 signalling axis, as well as the NPM-ALK-mediated STAT5 phosphorylation via JAK1/2, we concluded that STAT5 is phosphorylated by NPM-ALK at least partly JAK1/2-independent. In other words, we conclude that STAT5 is also directly phosphorylated by NPM-ALK.

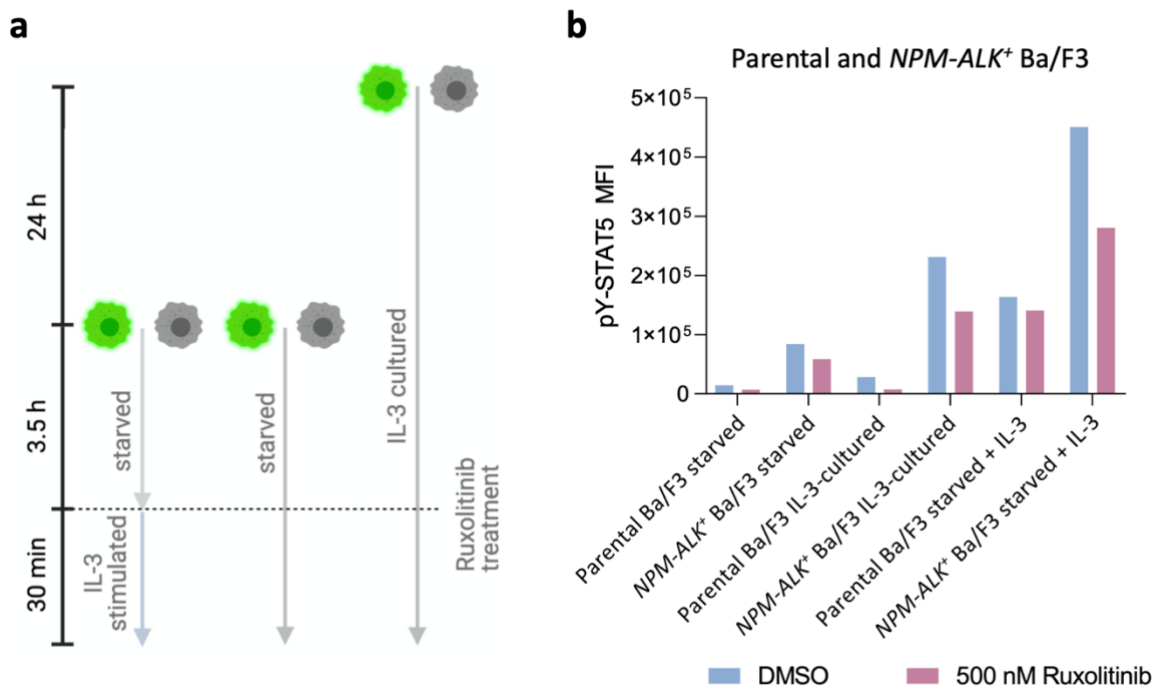


**Figure 38: NPM-ALK phosphorylates STAT5 directly and indirectly via JAK2**

**a)** Experimental schematic depicting the treatment timeline. **b)** Quantification of flow-cytometry intracellular staining of pY-STAT5 levels in parental Ba/F3 and NPM-ALK<sup>+</sup> Ba/F3 cells in 3 different conditions (starved, IL-3 cultured and starved followed by IL-3 stimulation) upon Ruxolitinib treatment and DMSO as control.

### 3.12 STAT5A and STAT5B physically interact with CDK6

To further investigate the function of the concomitant *Cdk6* and *Stat5a* or *Stat5b* dependency, we interrogated physical interactions between the two proteins in transformed *wt* *NPM-ALK*<sup>+</sup> cells (**Figure 39**). Co-immunoprecipitation revealed that both STAT5A and STAT5B physically interact with CDK6 in *NPM-ALK*<sup>+</sup> cell lines. By including *Cdk6*<sup>-/-</sup> cells as a control, we excluded unspecific antibody binding. This data indicates the existence of an essential CDK6-STAT5A or -STAT5B protein complex in *NPM-ALK*<sup>+</sup> cells.

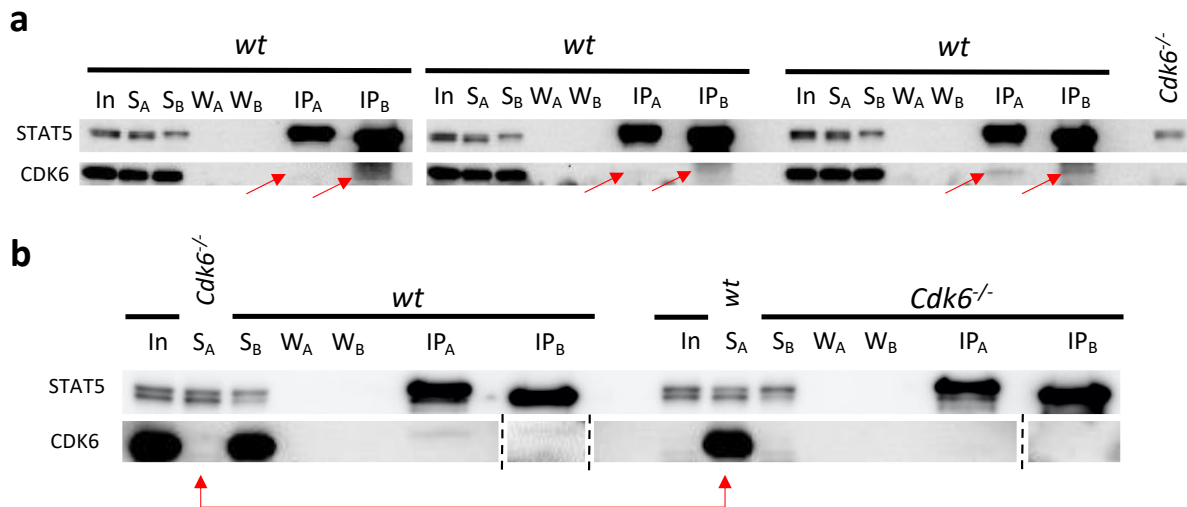


**Figure 39: CDK6 physically associates with STAT5A and STAT5B**

**a)** Co-immunoprecipitation assays in *NPM-ALK*<sup>+</sup> cell lines (n = 3). Protein extracts were immunoprecipitated with anti-STAT5A and anti-STAT5B antibody and immunoblotted with an anti-STAT5 and anti-CDK6 antibody. An *NPM-ALK*<sup>+</sup> *Cdk6*<sup>-/-</sup> control was added to exclude unspecific antibody binding of anti-CDK6 antibody for immunoblotting.

**b)** Co-immunoprecipitation assays in *NPM-ALK*<sup>+</sup> *wt* and *Cdk6*<sup>-/-</sup> cell line (n = 1/genotype). Protein extracts were immunoprecipitated with anti-STAT5A and anti-STAT5B antibody and immunoblotted with an anti-STAT5 and anti-CDK6 antibody. An *NPM-ALK*<sup>+</sup> *Cdk6*<sup>-/-</sup> cell line was added as a negative control – in the absence of CDK6, STAT5A and STAT5B co-immunoprecipitate. Loaded: input (In), supernatant from anti-STAT5A antibody (S<sub>A</sub>), supernatant from anti-STAT5B antibody (S<sub>B</sub>), wash of magnetic-bead-bound STAT5A immunoprecipitate complex (W<sub>A</sub>), wash of magnetic-bead-bound STAT5B immunoprecipitate (W<sub>B</sub>), immunoprecipitate of anti-STAT5A antibody (IP<sub>A</sub>) and immunoprecipitate of anti-STAT5B antibody (IP<sub>B</sub>).

## 4 Discussion

NPM-ALK is an oncogenic fusion protein driving more than 70% of all ALCL cases. 40–65% of ALCL patients develop resistance to first-line chemotherapy or ALK-inhibition (Huang et al., 2018), driving the need for further targeted treatment opportunities for relapsed or resistant ALCL. We show that the combined absence of CDK6 and STAT5A or STAT5B inhibits NPM-ALK-mediated malignant transformation, thereby preventing thymic lymphoma development. Our results also suggest that their combined deletion prohibits NPM-ALK tumour progression, predisposing their combined inhibition for pharmaceutical interventions. We found STAT5A and STAT5B to physically interact with CDK6, indicative of a transcriptional complex essential for NPM-ALK-mediated malignant transformation. We were not able to replicate this effect with existing pharmacological inhibitors. One potential explanation is the direct phosphorylation of STAT5A/B by NPM/ALK, which we demonstrated in a Ba/F3 model.

### 4.1 STAT5A and STAT5B display oncogenic properties in NPM-ALK<sup>+</sup> lymphoma

*NPM-ALK<sup>+</sup> Stat5a<sup>-/-</sup>* mice display a slightly delayed thymic lymphoma onset compared to *NPM-ALK<sup>+</sup> wt* mice, which is even further increased in the absence of STAT5B. We speculate that this is due to a higher expression of STAT5B than STAT5A in T cells (A. Villarino et al., 2016). Zhang et al. (2007) claimed that – in human ALK<sup>+</sup> T cell lymphoma cell lines – STAT5B shows oncogenic potential, while STAT5A acts as a tumour suppressor. However, our investigated murine *NPM-ALK<sup>+</sup>* model has revealed literature-opposing effects, where both STAT5A and STAT5B show oncogenic potential, as their absence delays the onset of murine *NPM-ALK<sup>+</sup>* thymic lymphomas. In addition to known discrepancies between the murine and human immune and haematopoietic systems (Mestas & Hughes, 2004; Parekh & Crooks, 2013), we speculate that opposing effects were observed due to different experimental settings – *in vitro* human cell lines (Zhang et al., 2007) vs *in vivo* mouse models (**Figure 14**). Zhang et al. (2007) highlighted the tumour suppressor functions of STAT5A based on its inhibitory potential of NPM-ALK; however, no other indications for the opposing roles of STAT5A/B have yet been described in T cells. Another explanation may be provided by the *Stat5a*-deficient environment of our constitutive knockout mouse models influencing the disease. Excluding the environmental effects by utilising a thymocyte specific depletion of *Cdk6*, *Stat5a* or *Stat5b* or transplantation of disease initiating cells into a *wt* environment would provide us with definite

cell-intrinsic effects. Irrespective, we conclude that STAT5A and STAT5B act redundantly in the context of the NPM-ALK-CDK6-STAT5 oncogene axis.

## 4.2 CDK6 and STAT5A or STAT5B deficiencies are incompatible in NPM-ALK-driven transformation and disease

We found an inability of *NPM-ALK<sup>+</sup> Cdk6<sup>-/-</sup> Stat5a<sup>-/-</sup>* or *Stat5b<sup>-/-</sup>* mice to develop a thymic lymphoma and *NPM-ALK<sup>-</sup> Cdk6<sup>-/-</sup> Stat5a<sup>-/-</sup>* or *Stat5b<sup>-/-</sup>* BM cells to undergo *ex vivo* NPM-ALK-mediated transformation. The first indication for the incompatibility of the combined *Cdk6* and *Stat5a* or *Stat5b* deficiency was the submendelian ratio of *NPM-ALK<sup>+</sup> Cdk6<sup>-/-</sup>* and *Stat5a<sup>-/-</sup>* or *Stat5b<sup>-/-</sup>* mice at weaning. We postulate that some mice die during embryonic development or early after birth, and the survivors potentially developed compensatory mechanisms. The cause of the submendelian ratios could be further investigated by analysing the offspring at embryonic day 18.5 (E18.5) to determine if combined STAT5A/B and CDK6 deficiency causes perinatal lethality, and which potential compensatory mechanisms take place to allow for complete embryogenesis. Since all three knockout models used are whole-body (constitutive) knockouts, it is hard to speculate which defect may cause this embryonic or perinatal lethality if STAT5A or STAT5B absence is combined with CDK6 loss. Nevertheless, we propose that the submendelian ratio may occur as a result of impaired glucose metabolism or insulin signalling, which has to be further investigated for confirmation. Despite the roles of STAT5A/B and CDK6 in T cell development (Villarino et al., 2016; Nivarthi et al., 2015; Pham et al., 2018; Maurer et al., 2020; Malumbres et al., 2004; Hu et al., 2019; Hu et al., 2011), the cellular composition of thymi isolated from *NPM-ALK<sup>+</sup>* double-knockout mice did not significantly differ from those of single *NPM-ALK<sup>+</sup> Cdk6<sup>-/-</sup>* or *Stat5b<sup>-/-</sup>* mice. Hence, we exclude that differences in the thymi are the sole reason for the absence of thymic lymphomas in the double knockout mice. In addition, we concluded that the compensatory mechanisms do not extend to NPM-ALK mediated transformation.

The incompatibility of a *Cdk6* and *Stat5a* or *Stat5b* deficiency was also demonstrated utilising *shRNA*-mediated knockdown of *Cdk6* in *NPM-ALK<sup>+</sup> Stat5a<sup>-/-</sup>* or *Stat5b<sup>-/-</sup>* cells. Despite getting mCherry<sup>+</sup> (the fluorescence marker for the *Cdk6 shRNA*) *NPM-ALK<sup>+</sup> Stat5a<sup>-/-</sup>* or *Stat5b<sup>-/-</sup>* cells – indicative of a successful *Cdk6 shRNA* expression – we proved that these cells counteracted and regained CDK6 expression or prevented its silencing. We assume that the cells, which down-regulated *Cdk6* expression did not survive. The data suggest that the concomitant absence of CDK6 and STAT5A or STAT5B might also play significant roles in disease

maintenance (e.g., proliferation and survival). Therefore, combined pharmacological interventions targeting CDK6 and STAT5A/B in established NPM-ALK<sup>+</sup> ALCL represents a potential treatment strategy.

### **4.3 The absence of CDK6 triggers compensatory mechanisms in NPM-ALK<sup>+</sup> cells**

The substantial disadvantage of *Cdk6*<sup>-/-</sup> cells in NPM-ALK mediated transformation indicates that the absence of CDK6 leads to more drastic consequences compared to *Stat5a* or *Stat5b* deficiencies. In contrast, established *Cdk6*<sup>-/-</sup> thymic lymphoma cell lines proliferate the fastest indicative of a novel developed secondary event in those *Cdk6*<sup>-/-</sup> cell lines or alternatively, indicative of a difference in their immunosuppression in mice. Our group previously observed that CDK6 drives a complicated transcriptional program in haematopoietic cells to block p53 and that cells lacking CDK6 kinase capabilities must mutate p53 to acquire a fully transformed immortalised state (Bellutti et al., 2018). We can therefore assume that our *Cdk6*<sup>-/-</sup> cell lines have most likely acquired additional mutations (e.g., silencing tumour suppressors) to by-pass their *Cdk6* deficiency. Further insight into the necessary “hits” could be gained by genome sequencing of established *Cdk6*<sup>-/-</sup> cell lines, which was beyond the scope of this thesis.

We found increased pYSTAT5 levels in established NPM-ALK<sup>+</sup> *Cdk6*<sup>-/-</sup> murine cell lines. Elevated STAT5 activation in *Cdk6*<sup>-/-</sup> compared to *wt* haematopoietic cells has also been observed in other haematopoietic cell types ((Uras et al., 2019); unpublished data by B. Maurer, S. Kollmann, K. Kollmann). Hence, this effect seems to be NPM-ALK-independent and applicable for various cell types. This effect is already present in the thymi of 10-12-week-old NPM-ALK<sup>+</sup> *Cdk6*<sup>-/-</sup> mice, already exhibiting hyperplastic thymi indicative of early stages of transformation. We speculate that STAT5 (hyper)activation might be a compensatory mechanism for a *Cdk6* deficiency and that the additional absence of STAT5A or STAT5B prevents this “rescue” during transformation.

### **4.4 Cytokines facilitate growth and survival of transformed NPM-ALK<sup>+</sup> *Stat5a*<sup>-/-</sup> and *Stat5b*<sup>-/-</sup> cells in overcoming their proliferation disadvantage**

We demonstrated that *Stat5a* or *Stat5b* deficiency results in a proliferation defect (delayed cell cycle entry and increased rate of apoptosis) of NPM-ALK<sup>+</sup> cell lines, which is more pronounced at lower cell densities. The effect is partially overcome when seeded in higher densities or

when cultured in conditioned medium, indicating the existence of autocrine cytokine production. Specific cytokines may lead to further signalling, promoting survival and proliferation. To further address which cytokines are secreted by our *NPM-ALK*<sup>+</sup> thymic lymphoma cell lines, a proteome profiler murine cytokine array on conditioned medium of *NPM-ALK*<sup>+</sup> *wt*, *Stat5a*<sup>-/-</sup> and *Stat5b*<sup>-/-</sup> thymic lymphoma cell lines would provide us with first insights. We would gain an indication of differentially secreted cytokines, where the cytokines secreted in higher quantities by the *NPM-ALK*<sup>+</sup> *wt* cells compared to *Stat5a*<sup>-/-</sup> or *Stat5b*<sup>-/-</sup> cell lines represent potential rescue candidates of the *Stat5a*<sup>-/-</sup> or *Stat5b*<sup>-/-</sup>-specific proliferation defect.

This observation could also be applicable *in vivo*: During transformation, already transformed thymocytes are sparsely seeded throughout the thymus. This “limiting cytokine” environment may cause a latent disease state, enhancing genotype-dependent effects (e.g., later disease onset). When the transformed cells reach a specific density, the disease seems to drastically progress – leading to fast-developing symptoms in mice. We speculate that a certain cytokine threshold is required in the lymphoma microenvironment, which leads to a fast disease progression by allowing the *NPM-ALK*<sup>+</sup> *Stat5a*<sup>-/-</sup> and *Stat5b*<sup>-/-</sup> cells to overcome their proliferation disadvantages.

We speculate that during later disease stages, a cytokine-dependent reinforcement loop forms, possibly signalling over JAK2-STAT5 or otherwise synergising with growth-factor-receptor-mediated STAT5 activation (via KIT, EGFR, PDGFR, Fibroblast growth factor receptor (FGFR), Mesenchymal-epithelial transition factor (MET) receptor, AXL receptor tyrosine kinase (AXL), etc.), to promote disease progression. A similar autocrine signalling mechanism has recently been proposed as a resistance mechanism of *ALK*<sup>+</sup> ALCL cells towards *ALK* inhibition. Elevated IL-10 receptor and IL-10 levels induce STAT3 signalling, rendering cells independent of STAT3 activation by *ALK* (Prokoph et al., 2020). Our preliminary experiment of IL-10 stimulation did not positively affect the proliferation of the *NPM-ALK*<sup>+</sup> *Stat5a*<sup>-/-</sup> or *Stat5b*<sup>-/-</sup> cells. We hypothesise that either different cytokines are involved in the rescue effect or too high IL-10 concentrations used in the experimental setting led to over-activation. Therefore, we cannot exclude positive effects of IL-10 concentrations. To conclude, JAK inhibitor treatment should be tested and considered as a possible option to prevent the formation of cytokine-mediated positive reinforcement loops.

## 4.5 Targeting of CDK6 and STAT5 in transformed *NPM-ALK*<sup>+</sup> cells

We followed up on our *shRNA*-mediated *Cdk6* knockdown with pharmacological perturbations targeting CDK6 and STAT5 activation in established *NPM-ALK*<sup>+</sup> *wt*, *Cdk6*<sup>-/-</sup>, *Stat5a*<sup>-/-</sup> and *Stat5b*<sup>-/-</sup> cell lines. Against our expectations, the absence of CDK6, STAT5A or STAT5B failed to sensitise *NPM-ALK*<sup>+</sup> cells to ALK or pan-JAK inhibition. Interestingly, all *NPM-ALK*<sup>+</sup> cell lines appeared insensitive to pan-JAK inhibition.

### 4.5.1 *NPM-ALK* directly phosphorylates STAT5A/B, thereby contributing to JAK-inhibitor insensitivity

The used JAK inhibitors were not sufficient to mimic the effects of *Stat5a* or *Stat5b* deficiency in *NPM-ALK*<sup>+</sup> *Cdk6*<sup>-/-</sup> cells. As Ruxolitinib only inhibits JAKs in active conformations (Zhou et al., 2014), we speculate that the insensitivity may occur due to heterodimerisation between JAK2 and JAK1 or TYK2, resulting in persistence and reactivation of JAK-STAT signalling (Koppikar et al., 2012). We hypothesise direct phosphorylation of STAT5A/B by ALK – as it has been shown for STAT3 (Zamo et al., 2002) – explaining why *Cdk6*<sup>-/-</sup> *NPM-ALK*<sup>+</sup> cells tolerate JAK inhibition.

To investigate the direct STAT5A/B phosphorylation by *NPM-ALK*, we used the Ba/F3 *NPM-ALK* expressing system. The high levels of pY-STAT5 after inhibiting JAK1/2 signalling argues for ALK's ability to directly phosphorylate STAT5A/B.

IL-3 stimulation in *NPM-ALK*-expressing Ba/F3 cells leads to an unproportionate increase in pY-STAT5 levels, indicating a higher sensitivity to IL-3 or synergistic interaction between *NPM-ALK* and IL-3 mediated signalling. The higher sensitivity or synergistic interaction might additionally contribute to the cells' insensitivity to JAK-inhibition. Murine *NPM-ALK*<sup>+</sup> thymic lymphoma cell lines also do not react with a complete pY-STAT5 diminishment to JAK1/2 inhibition via Ruxolitinib, indicating that *NPM-ALK* directly activates STAT5 or by means other than via JAK1/2. High residual pY-STAT5 levels and insensitivity of *NPM-ALK*<sup>+</sup> murine cell lines to Tofacitinib (JAK1/2/3 inhibitor) treatment insinuate that STAT5 activation also does not occur via JAK3 signalling. However, alternative STAT5 phosphorylation may occur via *NPM-ALK*-mediated activation of a JAK2-TYK2 heterodimer, as STAT5 has been described as their downstream effector in some cell types (Parham et al., 2002). As Crizotinib diminishes pY-STAT5 levels to a higher degree than pan-JAK inhibitors, we hypothesise that the main alternative mechanism of STAT5 activation takes place through

direct phosphorylation by ALK. In summary, we postulate that Ruxolitinib failed to sensitise *NPM-ALK<sup>+</sup> Cdk6<sup>-/-</sup>* cells to the inhibition of STAT5 activation, as NPM-ALK can directly phosphorylate STAT5 by-passing the canonical JAK-STAT pathway (**Figure 40**).

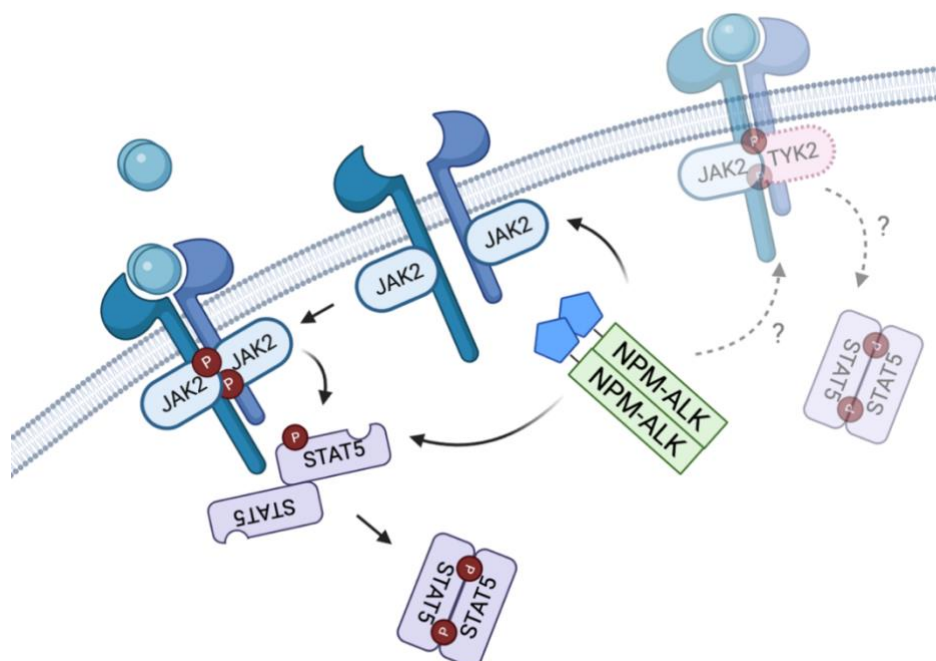


**Figure 40: NPM-ALK uncouples canonical JAK2-STAT5 signalling**

NPM-ALK regulates STAT5 activation by direct phosphorylation of STAT5 and indirectly via JAK2 phosphorylation.

#### 4.5.2 CDK6 kinase-independent functions seem to be important in NPM-ALK<sup>+</sup> lymphoma progression

*Stat5a* or *Stat5b* deficiencies failed to sensitise *NPM-ALK<sup>+</sup>* cell lines to the inhibition of kinase-dependent functions of CDK6 by Palbociclib treatment. Palbociclib inhibits the kinase-dependent functions of CDK6 and CDK4 while leaving the kinase-independent functions of CDK6 intact. We hypothesise that kinase-independent functions of CDK6 have an essential role in NPM-ALK-mediated disease progression.

Recent studies have shown that the sequence of pharmacological treatments influences the efficacy of Palbociclib. CDK4/6 inhibitors lead to an early cell cycle arrest, which might play a role in the cell susceptibility to other pharmacological perturbations (e.g., DNA-damaging or antimetabolic chemotherapies) (Salvador-Barbero et al., 2020). This aspect of a sequential treatment should be investigated in further studies.

We aimed to target the kinase-independent function of CDK6 by the use of CDK6 degraders – which ideally would mimic the *Cdk6*<sup>-/-</sup> situation. However, we (my own and also other unpublished data by B. Schmalzbauer or T. Brandstoetter) have observed that BSJ-03-123 fails to degrade CDK6 proteins completely, most likely due to the inability to target CDK6 in protein complexes. This probably explains why *Stat5a*<sup>-/-</sup> or *Stat5b*<sup>-/-</sup> *NPM-ALK*<sup>+</sup> cells showed no increased sensitivity when treated with the CDK6 degrader.

#### **4.5.3 Combinatorial treatments resulted in additive but not synergistic effects**

We speculated that the selective pressure during the *in vitro* outgrowth of the primary thymic lymphomas might have increased their mutational burden, thereby possibly having a significant role in the inhibitory response. To overcome this issue, we needed to simultaneously tackle CDK6 and STAT5A or STAT5B in an *NPM-ALK*<sup>+</sup> *wt* setting.

A combination of several treatment strategies is considered beneficial in cancer treatment: Resistance mechanisms can be avoided, and dosages/side effects can be reduced (Bayat Mokhtari et al., 2017). Thus, we proceeded with combinatorial treatments targeting STAT5 activation and CDK6 kinase-independent and/or -dependent functions in *NPM-ALK*<sup>+</sup> *wt cells*. The combinations of Ruxolitinib or Crizotinib with Palbociclib or the CDK6 degrader demonstrated additive, but not synergistic effects. We hypothesise that our combinatorial treatments were not successful due to various limitations of pharmacologic or cell-intrinsic origin (as described above).

In summary, we have shown that the ALK inhibitor Crizotinib is able to successfully inhibit *NPM-ALK*-dependent STAT5 activation. However, it does not target the intrinsic JAK2-STAT5 activation axis. Targeting JAK1/2 activation via Ruxolitinib should be able to inhibit the intrinsic cytokine-inducible JAK1/2-STAT5 signalling axis, as well as the *NPM-ALK*-mediated activation of STAT5 via JAK1/2 – but it does not account for direct *NPM-ALK*-mediated phosphorylation of STAT5. We postulate that a combinatorial treatment including ALK- and JAK1/2-inhibition – targeting cell-intrinsic and *NPM-ALK*-mediated STAT5 activation – on *NPM-ALK*<sup>+</sup> *Cdk6*<sup>-/-</sup> cells might reveal favourable (synergistic) effects. Nevertheless, JAK inhibitors like Ruxolitinib are imperfect treatment candidates due to off-target kinase- and toxic side effects at high concentrations.

Our combinatorial treatments revealed that higher synergy is obtained upon gross inhibition of the kinase-independent and kinase-dependent functions of CDK6 by BSJ-03-123 and STAT5

activation through Crizotinib treatment compared to Palbociclib and Ruxolitinib combinations. To conclude, our treatment attempts did not mimic the observed effects *in vivo*; however, we believe that novel improved CDK6 degraders and specific STAT5 inhibitors would provide us with more favourable results.

#### **4.6 STAT5A and STAT5B directly interact with CDK6, driving NPM-ALK-mediated transformation and disease maintenance**

We found a direct interaction between STAT5A and STAT5B with CDK6 in murine *NPM-ALK*<sup>+</sup> cell lines. When interrogating CDK6 and STAT5 interactions in hematopoietic progenitor cells without NPM-ALK, we failed to observe a comparable interaction. This indicates that the interaction is dependent on the NPM-ALK oncogene, nevertheless further experiments are necessary to confirm this finding and determine whether the interaction also extends to other oncogenic drivers.

This led us to speculate about these complexes driving gene expression patterns essential for NPM-ALK-mediated transformation and disease maintenance (e.g., proliferation and survival) – for simplicity referred to as gene pattern X (**Figure 41**). It is known that STAT5B is present in higher concentrations in haematopoietic cells compared to STAT5A (Maurer et al., 2019). We also found indications that *NPM-ALK*<sup>+</sup> *Stat5b*<sup>-/-</sup> cells contain a lower amount of STAT5A compared to STAT5B levels in *Stat5a*<sup>-/-</sup> cells. Thereby, the thymic lymphoma onset and the median survival of mice, as well as the proliferation rate of *NPM-ALK*<sup>+</sup> *Stat5a*<sup>-/-</sup> and *Stat5b*<sup>-/-</sup> cells, is positively correlated with total STAT5 levels. In the absence of CDK6, the cell upregulates the relative pY-STAT5 levels, thereby increasing the probability of STAT5 dimers binding to the gene pattern X promoter and driving transcription even in the absence of CDK6. Therefore, we hypothesise that the strength of gene pattern X transcription is positively correlated with the presence of CDK6 and higher levels of total or pY-STAT5. This mechanism would explain the combined necessity of *Cdk6* and *Stat5a* or *Stat5b* in NPM-ALK-mediated malignant transformation.

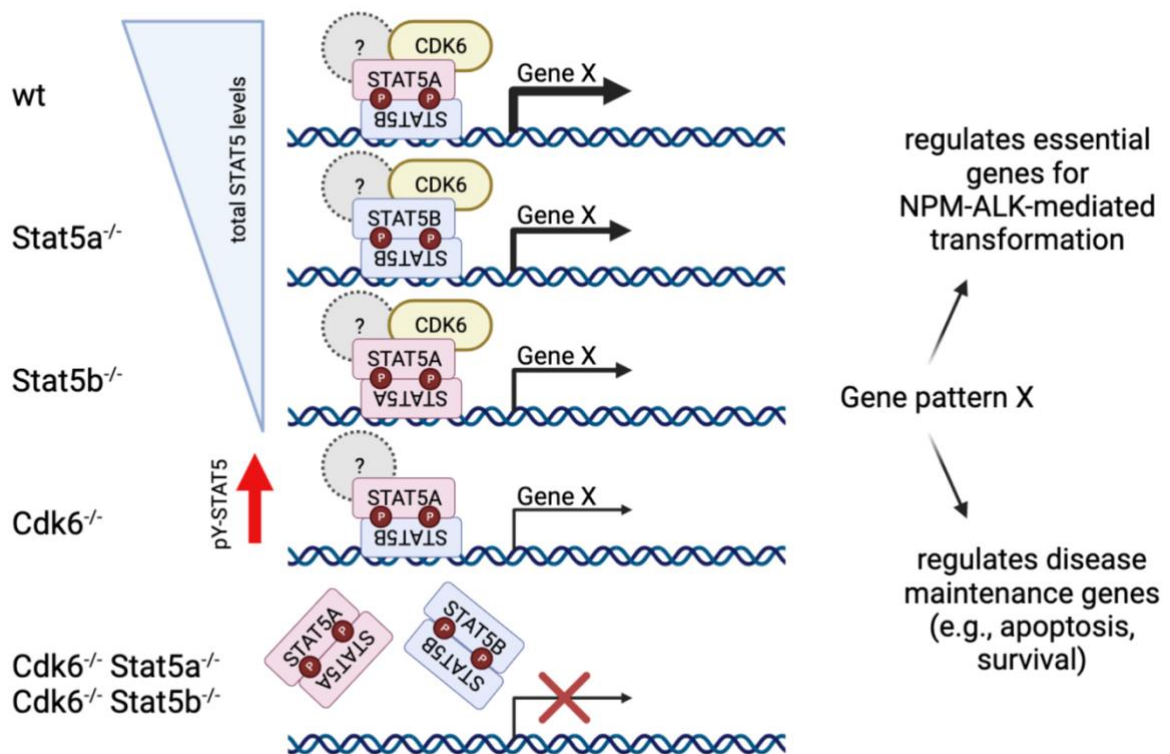


**Figure 41: Proposed regulation mechanism of NPM-ALK-mediated malignant transformation via CDK6 and STAT5 proteins**

In *NPM-ALK<sup>+</sup> wt* cells, STAT5A/B dimers form larger protein complexes with CDK6 (and possibly other proteins), thereby driving the expression of an unknown gene pattern (gene pattern X), which regulates transformation-essential and disease-maintenance genes. In *NPM-ALK<sup>+</sup> Stat5a<sup>-/-</sup>* cells, STAT5B forms homodimers and bind to CDK6 to drive the expression, while in *Stat5b<sup>-/-</sup>* cells, STAT5A homodimers are complexed with CDK6 to drive the gene pattern X expression. We hypothesise, that the absence of CDK6 destabilizes the regulatory complex, thereby preventing transcription of the gene pattern X. However, through our proposed compensatory mechanism – higher pY-STAT5 levels in the absence of CDK6 – a larger number of pY-STAT5 heterodimers increases the likelihood of STAT5 binding to the regulatory subunit (promotor) and driving the transcription. In the absence of CDK6 and STAT5A or STAT5B, we postulate that the pY-STAT5-mediated compensation is not possible due to the decreased overall STAT5 levels or the decreased binding ability of STAT5A or STAT5B homodimers in the absence of CDK6. In summary, we propose that the strength of gene pattern X regulation is correlated with the presence of CDK6 and the levels of total STAT5A/B or pY-STAT5.

#### 4.7 The interplay between STAT5A/B, CDK6 and NPM-ALK

We have demonstrated that in *NPM-ALK<sup>+</sup>* cells, CDK6 interacts with STAT5A and STAT5B. We have also shown that *NPM-ALK<sup>+</sup> Cdk6<sup>-/-</sup>* cells display increased levels of STAT5 phosphorylation, indicating that the presence of CDK6 in some way regulates STAT5 activation. Investigating whether CDK6 directly phosphorylates STAT5A/B at vital Serine

residues (e.g., Serine 726/731), would also give us an indication on the functional importance of the CDK6-STAT5 complex. In T cells, IL-2-activated STAT5 binds to the CDK6 super-enhancer, indicating that pY-STAT5 drives CDK6 expression and activation by promoting D-type cyclin expression (Li et al., 2017; Kanakura et al., 1999). Nevertheless, it remains unknown whether CDK6 is a direct STAT5A/B target gene.

NPM-ALK-mediated signalling has been shown to cause CDK6 activation by promoting the expression of various D-type Cyclins. We have also shown that NPM-ALK directly and indirectly phosphorylates STAT5A/B. As previously mentioned, literature states that STAT5A functions as a tumour suppressor by blocking NPM-ALK expression, while STAT5B functions as a downstream effector of NPM-ALK-mediated signalling (Zhang et al., 2007). However, our observations contradict the existing literature, indicating that further interrogation of the roles of STAT5A and STAT5B in the context of NPM-ALK are required.

## 5 Outlook

Due to time limitations, we were unable to obtain a more detailed characterisation of the thymic development and composition, as well as the submendelian ratio of *NPM-ALK<sup>+</sup> Cdk6<sup>-/-</sup> Stat5a<sup>-/-</sup>* or *Stat5b<sup>-/-</sup>* mice. To further interrogate the possible consequences of the concomitant *Cdk6* and *Stat5a* or *Stat5b* deficiency on the thymic composition and development we plan on performing Terminal deoxynucleotidyl transferase (TdT) and BCL-2 staining, as well as a quantification of the thymic medulla and cortex. Furthermore, to determine whether the absence of CDK6 and STAT5A or STAT5B is detrimental during embryogenesis or perinatally, we plan on investigating the *NPM-ALK<sup>+</sup> Cdk6<sup>-/-</sup> Stat5a<sup>-/-</sup>* or *Stat5b<sup>-/-</sup>* offspring/embryo ratios at birth or at E18.5, respectively. To gain further insight the potential cause of embryogenic lethality, we could also analyse haematocrit levels in *NPM-ALK<sup>+</sup> Cdk6<sup>-/-</sup> Stat5a<sup>-/-</sup>* or *Stat5b<sup>-/-</sup>* mice, which - when impaired - would indicate a defect in erythropoiesis. Taken together, we believe that also investigating the developmental and physiological roles of CDK6 and STAT5A or STAT5B might be of interest.

To further investigate the function of the CDK6-STAT5 complex, further characterisation of the interaction is needed. By performing functional mapping of CDK6 to the C- or N-terminus of STAT5A and STAT5B might provide indication regarding the purpose of the interaction. Mapping to the C-terminus might indicate a role in CDK6-mediated serine phosphorylation of STAT5.

A better understanding of the mechanism of CDK6/STAT5A/B-mediated NPM-ALK-driven transformation or disease progression is needed to suggest targeted treatments. To further test our hypothesis of potential common gene patterns downstream of CDK6 and STAT5A/B, essential in NPM-ALK mediated transformation and disease progression, we aim to identify transcriptional alterations in NPM-ALK<sup>+</sup> lymphoma-initiating cells.

To isolate the correct cell type for future RNA sequencing (RNA-Seq) experiments, we controlled for NPM-ALK transgene expression in different T cell development stages. NPM-ALK transgene expression is under the *Cd4* promoter, and hence, the expression should be induced in the DP stage. Recently, it has been shown that the DN population of NPM-ALK<sup>+</sup> thymocytes is required for inducing thymic lymphomagenesis (Kreutmair et al., 2020). In order to confirm the presence of NPM-ALK in DN cells, we analysed NPM-ALK expression in the DN and DP population of the NPM-ALK transgenic thymocytes. We found

the highest expression in the DN stage (**Figure 42a**) and plan an RNA-Seq of this cell type. As the *NPM-ALK<sup>+</sup> Stat5b<sup>-/-</sup> Cdk6<sup>-/-</sup>* and *Stat5a<sup>-/-</sup> Cdk6<sup>-/-</sup>* mice display the same phenotypic effect but only differ in severity, we decided to further focus on *NPM-ALK<sup>+</sup> Stat5b<sup>-/-</sup>* mice (**Figure 42b**).

The RNA-Seq analyses will be done on primary FACS-sorted DN thymocytes obtained from 8–10-week-old *NPM-ALK<sup>+</sup> wt*, *Cdk6<sup>-/-</sup>*, *Stat5b<sup>-/-</sup>* and *Cdk6<sup>-/-</sup> Stat5b<sup>-/-</sup>* mice (**Figure 42c**). We were able to collect all samples besides the *NPM-ALK<sup>+</sup> Stat5b<sup>-/-</sup>* samples (due to lack of available mice). Therefore, the results of the RNA-Seq were not yet available at the time of thesis submission. Nevertheless, the generated data will help us to uncover critical target genes and signalling pathways governed by CDK6 and STAT5B in *ALK<sup>+</sup>* thymic lymphoma development.

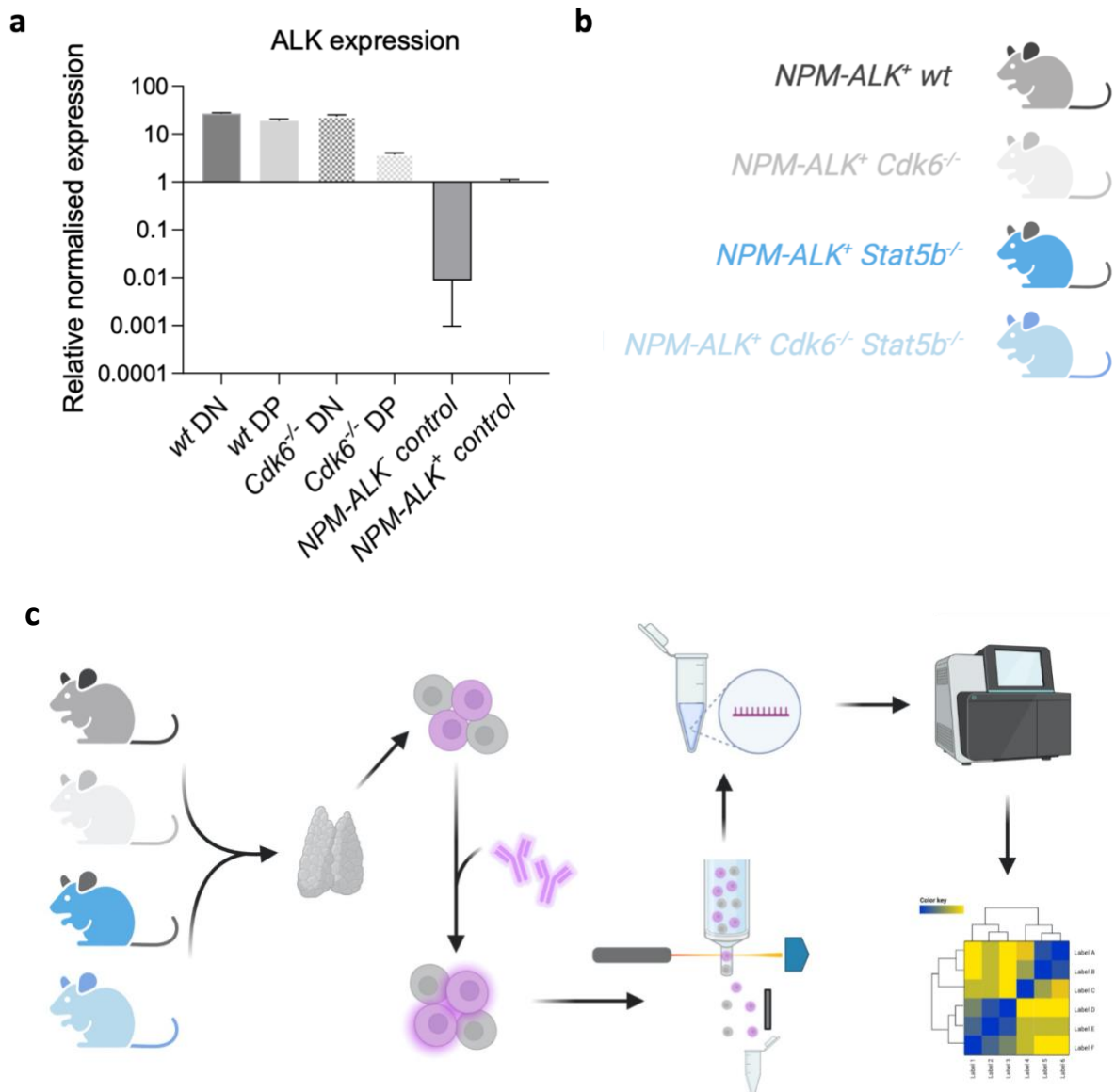


**Figure 42: The NPM-ALK transgene is expressed in DN and DP thymocytes**

**a)** qPCR showing NPM-ALK transgene expression of FACS-sorted DN and DP population of thymocytes derived from *NPM-ALK<sup>+</sup> wt* and *Cdk6<sup>-/-</sup>* mice, including negative (*NPM-ALK<sup>-</sup> Cdk6<sup>-/-</sup> Stat5b<sup>-/-</sup>*) and positive control (*NPM-ALK<sup>+</sup> wt cell line*). **b)** Murine models and **c)** the experimental setup of the mRNA sequencing experiment. In brief, thymic tissue is isolated from 8-week-old *NPM-ALK<sup>+</sup> wt*, *Cdk6<sup>-/-</sup>*, *Stat5b<sup>-/-</sup>* and *Cdk6<sup>-/-</sup> Stat5b<sup>-/-</sup>* mice and stained for TER-119, THY1.2, CD4 and CD8. mRNA is isolated from  $2-5 \times 10^5$  DN (TER-119<sup>-</sup>, THY1.2<sup>+</sup>, CD4<sup>-</sup>, CD8<sup>-</sup>) FACS-sorted thymocytes and sent for mRNA sequencing. The obtained reads are processed and analysed for differential gene expression.

One way to identify common direct targets of CDK6 and STAT5A/B in NPM-ALK<sup>+</sup> cells is to perform a chromatin immunoprecipitation sequencing (ChIP-Seq) of STAT5A and STAT5B, as well as CDK6. ChIP-Seq would allow us to obtain binding sites of each protein, map them to gene regulatory regions and by overlaying the obtained peaks, we would be able to identify common targets of both CDK6 and STAT5A/B proteins in NPM-ALK-driven thymic lymphomas. Furthermore, we would be able to overlay our differentially expressed genes in *NPM-ALK<sup>+</sup> Cdk6<sup>-/-</sup> Stat5b<sup>-/-</sup>* cells relative to *wt cells*, with the ChIP peak overlaps, thereby narrowing down the list of genes of interest. The identification of common critical downstream targets for therapeutic intervention will improve strategies to avoid the development of resistances and patient relapses.

To validate the hits, we can proceed with *in vitro* and *in vivo* target validation in NPM-ALK<sup>+</sup> mouse models, as well as the interrogation of targeted therapies in NPM-ALK<sup>+</sup> human cell lines and patient-derived cells. For example, a common RNA and ChIP-Seq hit/peak that is possibly connected to cytokine regulation might represent an interesting target for pharmacological inhibition. Subjecting mice to increased amounts of this cytokine might accelerate disease progression, indicating the existence of a positive autocrine reinforcement loop. The disruption of such a loop might delay disease onset and present a novel therapeutic opportunity for NPM-ALK<sup>+</sup> ALCL patients.

Based on our obtained data, we propose further interrogation of the following combination therapies and novel treatments:

(1) The identification of common downstream effectors of CDK6 and STAT5A/B could provide a novel specific target, whose inhibition will most likely not exhibit drastic effects in normal healthy cells. Treatment opportunities targeting this common downstream effector might also extend to other oncogenic drivers (e.g., BCR-ABL) that display a similar CDK6 and STAT5 dependency. To find potential responders, the significance of the identified “common effector”

can be confirmed in different oncogenic backgrounds by knockdown, knockout or pharmacological treatments.

(2) A more refined approach to target both STAT5A/B and CDK6 in NPM-ALK driven thymic lymphomas has to be developed. As previously mentioned, it has been shown that the order of treatment matters in combinatorial treatments with Palbociclib. Therefore, we believe a more thorough investigation of treatment dosage and timing (sequential or concomitant exposure) may reveal opportunities to sensitise NPM-ALK<sup>+</sup> cells to our targeted therapies.

(3) Novel STAT5 inhibitors can provide an excellent targeting tool without having excessive adverse effects on normal haematopoiesis (compared to JAK inhibitors).

(4) Targeting protein-protein interactions – via small molecule inhibitors – has emerged as a promising therapeutic approach for several types of cancer (Ivanov et al., 2013). Therefore, another opportunity to target NPM-ALK-mediated transformation is to disrupt the STAT5A/B-CDK6 complex by protein-protein interaction inhibitors. First, the actual presence of the hypothesised STAT5A/B/CDK6 complex – and the potential additional participating proteins – could be proven by performing mass spectrometry. Utilising computational modelling methods to predict interacting domains of CDK6 and STAT5A or STAT5B – based on high-resolution three-dimensional structures – would allow the development or repurposing of small molecule inhibitors aiming to disrupt the CDK6 and STAT5A or STAT5B complexes.

To conclude, the identification of common critical downstream targets for therapeutic intervention will improve therapeutic strategies to avoid the development of resistances and patient relapses.

## 6 Conclusion

Using a transgenic ALCL mouse model and primary murine cell lines, we demonstrated that the combined absence of CDK6 and STAT5A or STAT5B inhibits NPM-ALK-mediated malignant transformation and progression, thereby predisposing their combined inhibition for pharmaceutical interventions. In addition, we report that both STAT5A and STAT5B show oncogenic potential in NPM-ALK-driven lymphomagenesis, which is opposing to old literature (Nieborowska-Skorska et al., 2001), and that NPM-ALK can phosphorylate STAT5 without the implications of JAKs.

Due to various cell-intrinsic and pharmacologic limitations – such as a *Cdk6* deficiency-induced activation of STAT5 and the direct phosphorylation of STAT5A/B by NPM/ALK – we failed to replicate the effect of combined *Cdk6*- and *Stat5a*- or *Stat5b*- deficiencies with existing pharmacological inhibitors. However, we believe that novel, improved CDK6 degraders and specific STAT5 inhibitors or degraders would provide us with more favourable results.

Nevertheless, the combinatorial treatments indicated that CDK6 kinase-independent functions are potentially crucial in NPM-ALK<sup>+</sup> lymphoma progression. Indeed, we found STAT5A and STAT5B to directly interact with CDK6, indicative of a transcriptional complex essential for NPM-ALK-mediated transformation and disease maintenance. The planned RNA- and ChIP-sequencing in *NPM-ALK*<sup>+</sup> *wt*, *Cdk6*<sup>-/-</sup>, *Stat5b*<sup>-/-</sup> and *Cdk6*<sup>-/-</sup> *Stat5b*<sup>-/-</sup> murine thymi during early transformation should pinpoint to essential direct downstream effectors of CDK6 and STAT5.

In summary, the identification of a successful therapeutic combination targeting CDK6 and STAT5 activation or their common downstream effector could contribute to a beneficial and possibly curative outcome in not only refractory and relapsed ALK<sup>+</sup> ALCL patients but might also be extended to other oncogenic drivers that display a similar CDK6 and STAT5 dependency.

## 7 References

- Ambrogio, C., Martinengo, C., Voena, C., Tondat, F., Riera, L., di Celle, P. F., . . . Chiarle, R. (2009). NPM-ALK oncogenic tyrosine kinase controls T-cell identity by transcriptional regulation and epigenetic silencing in lymphoma cells. *Cancer Res*, *69*(22), 8611-8619. doi:10.1158/0008-5472.CAN-09-2655
- Ambrogio, C., Voena, C., Manazza, A. D., Piva, R., Riera, L., Barberis, L., . . . Chiarle, R. (2005). p130Cas mediates the transforming properties of the anaplastic lymphoma kinase. *Blood*, *106*(12), 3907-3916. doi:10.1182/blood-2005-03-1204
- Amin, H. M., Medeiros, L. J., Ma, Y., Feretzaki, M., Das, P., Leventaki, V., . . . Lai, R. (2003). Inhibition of JAK3 induces apoptosis and decreases anaplastic lymphoma kinase activity in anaplastic large cell lymphoma. *Oncogene*, *22*(35), 5399-5407. doi:10.1038/sj.onc.1206849
- Andraos, E., Dignac, J., & Meggetto, F. (2021). NPM-ALK: A Driver of Lymphoma Pathogenesis and a Therapeutic Target. *Cancers (Basel)*, *13*(1). doi:10.3390/cancers13010144
- Armstrong, F., Duplantier, M. M., Tremprat, P., Hieblot, C., Lamant, L., Espinos, E., . . . Touriol, C. (2004). Differential effects of X-ALK fusion proteins on proliferation, transformation, and invasion properties of NIH3T3 cells. *Oncogene*, *23*(36), 6071-6082. doi:10.1038/sj.onc.1207813
- Bai, J., Li, Y., & Zhang, G. (2017). Cell cycle regulation and anticancer drug discovery. *Cancer Biol Med*, *14*(4), 348-362. doi:10.20892/j.issn.2095-3941.2017.0033
- Bai, R. Y., Dieter, P., Peschel, C., Morris, S. W., & Duyster, J. (1998). Nucleophosmin-anaplastic lymphoma kinase of large-cell anaplastic lymphoma is a constitutively active tyrosine kinase that utilizes phospholipase C-gamma to mediate its mitogenicity. *Mol Cell Biol*, *18*(12), 6951-6961. doi:10.1128/mcb.18.12.6951
- Bai, R. Y., Ouyang, T., Miething, C., Morris, S. W., Peschel, C., & Duyster, J. (2000). Nucleophosmin-anaplastic lymphoma kinase associated with anaplastic large-cell lymphoma activates the phosphatidylinositol 3-kinase/Akt antiapoptotic signaling pathway. *Blood*, *96*(13), 4319-4327. Retrieved from <https://www.ncbi.nlm.nih.gov/pubmed/11110708>
- Bayat Mokhtari, R., Homayouni, T. S., Baluch, N., Morgatskaya, E., Kumar, S., Das, B., & Yeger, H. (2017). Combination therapy in combating cancer. *Oncotarget*, *8*(23), 38022-38043. doi:10.18632/oncotarget.16723
- Bellutti, F., Tigan, A. S., Nebenfuehr, S., Dolezal, M., Zojer, M., Grausenburger, R., . . . Sexl, V. (2018). CDK6 Antagonizes p53-Induced Responses during Tumorigenesis. *Cancer Discov*, *8*(7), 884-897. doi:10.1158/2159-8290.CD-17-0912
- Benharroch, D., Meguerian-Bedoyan, Z., Lamant, L., Amin, C., Brugieres, L., Terrier-Lacombe, M. J., . . . Delsol, G. (1998). ALK-positive lymphoma: a single disease with a broad spectrum of morphology. *Blood*, *91*(6), 2076-2084. Retrieved from <https://www.ncbi.nlm.nih.gov/pubmed/9490693>
- Berdasco, M., & Esteller, M. (2011). DNA methylation in stem cell renewal and multipotency. *Stem Cell Res Ther*, *2*(5), 42. doi:10.1186/scrt83
- Bernadó, P., Pérez, Y., Blobel, J., Fernández-Recio, J., Svergun, D. I., & Pons, M. (2009). Structural characterisation of unphosphorylated STAT5a oligomerization equilibrium in solution by small-angle X-ray scattering. *Protein science : a publication of the Protein Society*, *18*(4), 716-726. doi:10.1002/pro.83
- Bischof, D., Pulford, K., Mason, D. Y., & Morris, S. W. (1997). Role of the nucleophosmin (NPM) portion of the non-Hodgkin's lymphoma-associated NPM-anaplastic lymphoma kinase fusion protein in oncogenesis. *Mol Cell Biol*, *17*(4), 2312-2325. doi:10.1128/mcb.17.4.2312
- Blain, S. W., Montalvo, E., & Massague, J. (1997). Differential interaction of the Cyclin-dependent kinase (Cdk) inhibitor p27Kip1 with Cyclin A-Cdk2 and Cyclin D2-Cdk4. *J Biol Chem*, *272*(41), 25863-25872. doi:10.1074/jbc.272.41.25863
- Bliss, W. L. (1939). Early Man in western and Northwestern Canada. *Science*, *89*(2312), 365-366. doi:10.1126/science.89.2312.365-a
- Bonzheim, I., Geissinger, E., Roth, S., Zettl, A., Marx, A., Rosenwald, A., . . . Rudiger, T. (2004). Anaplastic large cell lymphomas lack the expression of T-cell receptor molecules or molecules of proximal T-cell receptor signaling. *Blood*, *104*(10), 3358-3360. doi:10.1182/blood-2004-03-1037
- Bottos, A., Gotthardt, D., Gill, J. W., Gattelli, A., Frei, A., Tzankov, A., . . . Hynes, N. E. (2016). Decreased NK-cell tumour immunosurveillance consequent to JAK inhibition enhances metastasis in breast cancer models. *Nat Commun*, *7*, 12258. doi:10.1038/ncomms12258
- Bousoik, E., & Montazeri Aliabadi, H. (2018). "Do We Know Jack" About JAK? A Closer Look at JAK-STAT Signaling Pathway. *Front Oncol*, *8*, 287. doi:10.3389/fonc.2018.00287
- Brachet-Botineau, M., Polomski, M., Neubauer, H. A., Juen, L., Hedou, D., Viaud-Massuard, M. C., . . . Gouilleux, F. (2020). Pharmacological Inhibition of Oncogenic STAT3 and STAT5 Signaling in Hematopoietic Cancers. *Cancers (Basel)*, *12*(1). doi:10.3390/cancers12010240
- Burchill, M. A., Goetz, C. A., Prlc, M., O'Neil, J. J., Harmon, I. R., Bensinger, S. J., . . . Farrar, M. A. (2003). Distinct effects of STAT5 activation on CD4+ and CD8+ T cell homeostasis: development of

- CD4+CD25+ regulatory T cells versus CD8+ memory T cells. *J Immunol*, 171(11), 5853-5864. doi:10.4049/jimmunol.171.11.5853
- Burke, J. R., Liban, T. J., Restrepo, T., Lee, H. W., & Rubin, S. M. (2014). Multiple mechanisms for E2F binding inhibition by phosphorylation of the retinoblastoma protein C-terminal domain. *J Mol Biol*, 426(1), 245-255. doi:10.1016/j.jmb.2013.09.031
- Buss, H., Handschick, K., Jurrmann, N., Pekkonen, P., Beuerlein, K., Muller, H., . . . Kracht, M. (2012). Cyclin-dependent kinase 6 phosphorylates NF-kappaB P65 at serine 536 and contributes to the regulation of inflammatory gene expression. *PLoS One*, 7(12), e51847. doi:10.1371/journal.pone.0051847
- Camidge, D. R., Bang, Y. J., Kwak, E. L., Iafrate, A. J., Varella-Garcia, M., Fox, S. B., . . . Shaw, A. T. (2012). Activity and safety of crizotinib in patients with ALK-positive non-small-cell lung cancer: updated results from a phase 1 study. *Lancet Oncol*, 13(10), 1011-1019. doi:10.1016/S1470-2045(12)70344-3
- Chiarle, R., Gong, J. Z., Guasparri, I., Pesci, A., Cai, J., Liu, J., . . . Inghirami, G. (2003). NPM-ALK transgenic mice spontaneously develop T-cell lymphomas and plasma cell tumors. *Blood*, 101(5), 1919-1927. doi:10.1182/blood-2002-05-1343
- Chiarle, R., Simmons, W. J., Cai, H., Dhall, G., Zamo, A., Raz, R., . . . Inghirami, G. (2005). Stat3 is required for ALK-mediated lymphomagenesis and provides a possible therapeutic target. *Nat Med*, 11(6), 623-629. doi:10.1038/nm1249
- Chiarle, R., Voena, C., Ambrogio, C., Piva, R., & Inghirami, G. (2008). The anaplastic lymphoma kinase in the pathogenesis of cancer. *Nat Rev Cancer*, 8(1), 11-23. doi:10.1038/nrc2291
- Chilosi, M., Doglioni, C., Yan, Z., Lestani, M., Menestrina, F., Sorio, C., . . . Inghirami, G. (1998). Differential expression of Cyclin-dependent kinase 6 in cortical thymocytes and T-cell lymphoblastic lymphoma/leukemia. *Am J Pathol*, 152(1), 209-217. Retrieved from <https://www.ncbi.nlm.nih.gov/pubmed/9422538>
- Choi, Y. J., & Anders, L. (2014). Signaling through Cyclin D-dependent kinases. *Oncogene*, 33(15), 1890-1903. doi:10.1038/onc.2013.137
- Classon, M., & Harlow, E. (2002). The retinoblastoma tumour suppressor in development and cancer. *Nat Rev Cancer*, 2(12), 910-917. doi:10.1038/nrc950
- Colomba, A., Courilleau, D., Ramel, D., Billadeau, D. D., Espinos, E., Delsol, G., . . . Gaits-Iacovoni, F. (2008). Activation of Rac1 and the exchange factor Vav3 are involved in NPM-ALK signaling in anaplastic large cell lymphomas. *Oncogene*, 27(19), 2728-2736. doi:10.1038/sj.onc.1210921
- Coluccia, A. M., Perego, S., Cleris, L., Gunby, R. H., Passoni, L., Marchesi, E., . . . Gambacorti-Passerini, C. (2004). Bcl-XL down-regulation suppresses the tumorigenic potential of NPM/ALK in vitro and in vivo. *Blood*, 103(7), 2787-2794. doi:10.1182/blood-2003-09-3144
- Congras, A., Hoareau-Aveilla, C., Caillet, N., Tosolini, M., Villarese, P., Cieslak, A., . . . Meggetto, F. (2020). ALK-transformed mature T lymphocytes restore early thymus progenitor features. *J Clin Invest*, 130(12), 6395-6408. doi:10.1172/JCI134990
- Cordon-Cardo, C. (1995). Mutations of cell cycle regulators. Biological and clinical implications for human neoplasia. *Am J Pathol*, 147(3), 545-560. Retrieved from <https://www.ncbi.nlm.nih.gov/pubmed/7677168>
- Crescenzo, R., Abate, F., Lasorsa, E., Tabbo, F., Gaudio, M., Chiesa, N., . . . the, A. x. C. G.-D. T. M. o. L. M. (2015). Convergent mutations and kinase fusions lead to oncogenic STAT3 activation in anaplastic large cell lymphoma. *Cancer Cell*, 27(4), 516-532. doi:10.1016/j.ccell.2015.03.006
- Cui, Y., Riedlinger, G., Miyoshi, K., Tang, W., Li, C., Deng, C. X., . . . Hennighausen, L. (2004). Inactivation of Stat5 in mouse mammary epithelium during pregnancy reveals distinct functions in cell proliferation, survival, and differentiation. *Mol Cell Biol*, 24(18), 8037-8047. doi:10.1128/mcb.24.18.8037-8047.2004
- Dao, K. T., Gotlib, J., Deininger, M. M. N., Oh, S. T., Cortes, J. E., Collins, R. H., Jr., . . . Tyner, J. W. (2020). Efficacy of Ruxolitinib in Patients With Chronic Neutrophilic Leukemia and Atypical Chronic Myeloid Leukemia. *J Clin Oncol*, 38(10), 1006-1018. doi:10.1200/jco.19.00895
- Davis, T. H., Morton, C. C., Miller-Cassman, R., Balk, S. P., & Kadin, M. E. (1992). Hodgkin's Disease, Lymphomatoid Papulosis, and Cutaneous T-Cell Lymphoma Derived from a Common T-Cell Clone. *New England Journal of Medicine*, 326(17), 1115-1122. doi:10.1056/NEJM199204233261704
- de Groot, R. P., Raaijmakers, J. A., Lammers, J. W., & Koenderman, L. (2000). STAT5-Dependent CyclinD1 and Bcl-xL expression in Bcr-Abl-transformed cells. *Mol Cell Biol Res Commun*, 3(5), 299-305. doi:10.1006/mcbr.2000.0231
- Debierre-Grockiego, F. (2004). Anti-apoptotic role of STAT5 in haematopoietic cells and in the pathogenesis of malignancies. *Apoptosis*, 9(6), 717-728. doi:10.1023/B:APPT.0000045785.65546.a2
- Duyster, J., Bai, R. Y., & Morris, S. W. (2001). Translocations involving anaplastic lymphoma kinase (ALK). *Oncogene*, 20(40), 5623-5637. doi:10.1038/sj.onc.1204594
- Dyson, N. (1998). The regulation of E2F by pRB-family proteins. *Genes Dev*, 12(15), 2245-2262. doi:10.1101/gad.12.15.2245
- Ehrentraut, S., Nagel, S., Scherr, M. E., Schneider, B., Quentmeier, H., Geffers, R., . . . MacLeod, R. A. F. (2013). t(8;9)(p22;p24)/PCM1-JAK2 Activates SOCS2 and SOCS3 via STAT5. *PLoS One*, 8(1), e53767. doi:10.1371/journal.pone.0053767

- Endo, T. A., Masuhara, M., Yokouchi, M., Suzuki, R., Sakamoto, H., Mitsui, K., . . . Yoshimura, A. (1997). A new protein containing an SH2 domain that inhibits JAK kinases. *Nature*, *387*, 921. doi:10.1038/43213
- Fellmann, C., Hoffmann, T., Sridhar, V., Hopfgartner, B., Muhar, M., Roth, M., . . . Zuber, J. (2013). An optimized microRNA backbone for effective single-copy RNAi. *Cell Rep*, *5*(6), 1704-1713. doi:10.1016/j.celrep.2013.11.020
- Fujimoto, J., Shiota, M., Iwahara, T., Seki, N., Satoh, H., Mori, S., & Yamamoto, T. (1996). Characterisation of the transforming activity of p80, a hyperphosphorylated protein in a Ki-1 lymphoma cell line with chromosomal translocation t(2;5). *Proc Natl Acad Sci U S A*, *93*(9), 4181-4186. doi:10.1073/pnas.93.9.4181
- Fukano, R., Mori, T., Sekimizu, M., Choi, I., Kada, A., Saito, A. M., . . . Nagai, H. (2020). Alectinib for relapsed or refractory anaplastic lymphoma kinase-positive anaplastic large cell lymphoma: An open-label phase II trial. *Cancer Sci*, *111*(12), 4540-4547. doi:10.1111/cas.14671
- Furumoto, Y., & Gadina, M. (2013). The arrival of JAK inhibitors: advancing the treatment of immune and hematologic disorders. *BioDrugs*, *27*(5), 431-438. doi:10.1007/s40259-013-0040-7
- Gadina, M., Johnson, C., Schwartz, D., Bonelli, M., Hasni, S., Kanno, Y., . . . O'Shea, J. J. (2018). Translational and clinical advances in JAK-STAT biology: The present and future of jakinibs. *J Leukoc Biol*, *104*(3), 499-514. doi:10.1002/JLB.5R10218-084R
- Gaulard, P., & de Leval, L. (2016). ALK-negative anaplastic large-cell lymphoma. *Blood*, *127*(2), 175-177. doi:10.1182/blood-2015-11-676916
- Goel, S., DeCristo, M. J., McAllister, S. S., & Zhao, J. J. (2018). CDK4/6 Inhibition in Cancer: Beyond Cell Cycle Arrest. *Trends Cell Biol*, *28*(11), 911-925. doi:10.1016/j.tcb.2018.07.002
- Gordon, G. M., & Du, W. (2011). Conserved RB functions in development and tumor suppression. *Protein Cell*, *2*(11), 864-878. doi:10.1007/s13238-011-1117-z
- Gu, T. L., Tothova, Z., Scheijen, B., Griffin, J. D., Gilliland, D. G., & Sternberg, D. W. (2004). NPM-ALK fusion kinase of anaplastic large-cell lymphoma regulates survival and proliferative signaling through modulation of FOXO3a. *Blood*, *103*(12), 4622-4629. doi:10.1182/blood-2003-03-0820
- Hammarén, H. M., Virtanen, A. T., Raivola, J., & Silvennoinen, O. (2018). The regulation of JAKs in cytokine signaling and its breakdown in disease. *Cytokine*. doi:<https://doi.org/10.1016/j.cyto.2018.03.041>
- Han, Y., Amin, H. M., Frantz, C., Franko, B., Lee, J., Lin, Q., & Lai, R. (2006). Restoration of shp1 expression by 5-AZA-2'-deoxycytidine is associated with downregulation of JAK3/STAT3 signaling in ALK-positive anaplastic large cell lymphoma. *Leukemia*, *20*(9), 1602-1609. doi:10.1038/sj.leu.2404323
- Handschiek, K., Beuerlein, K., Jurida, L., Bartkuhn, M., Muller, H., Soelch, J., . . . Kracht, M. (2014). Cyclin-dependent kinase 6 is a chromatin-bound cofactor for NF-kappaB-dependent gene expression. *Mol Cell*, *53*(2), 193-208. doi:10.1016/j.molcel.2013.12.002
- Harbour, J. W., Luo, R. X., Dei Santi, A., Postigo, A. A., & Dean, D. C. (1999). Cdk phosphorylation triggers sequential intramolecular interactions that progressively block Rb functions as cells move through G1. *Cell*, *98*(6), 859-869. doi:10.1016/s0092-8674(00)81519-6
- Harrington, R., Al Nokhatha, S. A., & Conway, R. (2020). JAK Inhibitors in Rheumatoid Arthritis: An Evidence-Based Review on the Emerging Clinical Data. *J Inflamm Res*, *13*, 519-531. doi:10.2147/jir.S219586
- Hassler, M. R., Klisaroska, A., Kollmann, K., Steiner, I., Bilban, M., Schiefer, A. I., . . . Egger, G. (2012). Antineoplastic activity of the DNA methyltransferase inhibitor 5-aza-2'-deoxycytidine in anaplastic large cell lymphoma. *Biochimie*, *94*(11), 2297-2307. doi:10.1016/j.biochi.2012.05.029
- Hassler, M. R., Pulverer, W., Lakshminarasimhan, R., Redl, E., Hacker, J., Garland, G. D., . . . Egger, G. (2016). Insights into the Pathogenesis of Anaplastic Large-Cell Lymphoma through Genome-wide DNA Methylation Profiling. *Cell Rep*, *17*(2), 596-608. doi:10.1016/j.celrep.2016.09.018
- Heltemes-Harris, L. M., & Farrar, M. A. (2012). The role of STAT5 in lymphocyte development and transformation. *Curr Opin Immunol*, *24*(2), 146-152. doi:10.1016/j.coi.2012.01.015
- Hoareau-Aveilla, C., & Meggetto, F. (2017). Crosstalk between microRNA and DNA Methylation Offers Potential Biomarkers and Targeted Therapies in ALK-Positive Lymphomas. *Cancers (Basel)*, *9*(8). doi:10.3390/cancers9080100
- Hoareau-Aveilla, C., Quelen, C., Congras, A., Caillet, N., Labourdette, D., Dozier, C., . . . Meggetto, F. (2019). miR-497 suppresses cycle progression through an axis involving CDK6 in ALK-positive cells. *Haematologica*, *104*(2), 347-359. doi:10.3324/haematol.2018.195131
- Hoelbl, A., Kovacic, B., Kerényi, M. A., Simma, O., Warsch, W., Cui, Y., . . . Sexl, V. (2006). Clarifying the role of Stat5 in lymphoid development and Abelson-induced transformation. *Blood*, *107*(12), 4898-4906. doi:10.1182/blood-2005-09-3596
- Honorat, J. F., Ragab, A., Lamant, L., Delsol, G., & Ragab-Thomas, J. (2006). SHP1 tyrosine phosphatase negatively regulates NPM-ALK tyrosine kinase signaling. *Blood*, *107*(10), 4130-4138. doi:10.1182/blood-2005-06-2421
- Hsu, F. Y., Johnston, P. B., Burke, K. A., & Zhao, Y. (2006). The expression of CD30 in anaplastic large cell lymphoma is regulated by nucleophosmin-anaplastic lymphoma kinase-mediated JunB level in a cell type-specific manner. *Cancer Res*, *66*(18), 9002-9008. doi:10.1158/0008-5472.CAN-05-4101

- Hu, M. G., Deshpande, A., Enos, M., Mao, D., Hinds, E. A., Hu, G. F., . . . Hinds, P. W. (2009). A requirement for Cyclin-dependent kinase 6 in thymocyte development and tumorigenesis. *Cancer Res*, *69*(3), 810-818. doi:10.1158/0008-5472.CAN-08-2473
- Hu, M. G., Deshpande, A., Schlichting, N., Hinds, E. A., Mao, C., Dose, M., . . . Hinds, P. W. (2011). CDK6 kinase activity is required for thymocyte development. *Blood*, *117*(23), 6120-6131. doi:10.1182/blood-2010-08-300517
- Huang, L., Zhang, F., Zeng, J., Guo, H., Liu, S., Wei, X., . . . Li, W. (2018). ALK expression plays different roles in anaplastic large-cell lymphomas and outcome of crizotinib use in relapsed/refractory ALK+ patients in a Chinese population. *Ann Hematol*, *97*(1), 149-159. doi:10.1007/s00277-017-3166-8
- Ianevski, A., Giri, A. K., & Aittokallio, T. (2020). SynergyFinder 2.0: visual analytics of multi-drug combination synergies. *Nucleic Acids Res*, *48*(W1), W488-w493. doi:10.1093/nar/gkaa216
- Ivanov, A. A., Khuri, F. R., & Fu, H. (2013). Targeting protein-protein interactions as an anticancer strategy. *Trends Pharmacol Sci*, *34*(7), 393-400. doi:10.1016/j.tips.2013.04.007
- Iwahara, T., Fujimoto, J., Wen, D., Cupples, R., Bucay, N., Arakawa, T., . . . Yamamoto, T. (1997). Molecular characterisation of ALK, a receptor tyrosine kinase expressed specifically in the nervous system. *Oncogene*, *14*(4), 439-449. doi:10.1038/sj.onc.1200849
- James, M. K., Ray, A., Leznova, D., & Blain, S. W. (2008). Differential modification of p27Kip1 controls its Cyclin D-cdk4 inhibitory activity. *Mol Cell Biol*, *28*(1), 498-510. doi:10.1128/MCB.02171-06
- Kanai, T., Seki, S., Jenks, J. A., Kohli, A., Kawli, T., Martin, D. P., . . . Nadeau, K. C. (2014). Identification of STAT5A and STAT5B target genes in human T cells. *PLoS One*, *9*(1), e86790. doi:10.1371/journal.pone.0086790
- Katzman, S. D., Hoyer, K. K., Dooms, H., Gratz, I. K., Rosenblum, M. D., Paw, J. S., . . . Abbas, A. K. (2011). Opposing functions of IL-2 and IL-7 in the regulation of immune responses. *Cytokine*, *56*(1), 116-121. doi:10.1016/j.cyto.2011.07.005
- Kelly, J., Spolski, R., Imada, K., Bollenbacher, J., Lee, S., & Leonard, W. J. (2003). A role for Stat5 in CD8+ T cell homeostasis. *J Immunol*, *170*(1), 210-217. doi:10.4049/jimmunol.170.1.210
- Kim, D., Koh, Y., & Yoon, S. S. (2020). Synergistic Effect of Alectinib and Everolimus on ALK-positive Anaplastic Large Cell Lymphoma Growth Inhibition. *Anticancer Res*, *40*(3), 1395-1403. doi:10.21873/anticancer.14081
- Kitagawa, Y., Wing, J. B., & Sakaguchi, S. (2015). Transcriptional and Epigenetic Control of Regulatory T Cell Development. *Prog Mol Biol Transl Sci*, *136*, 1-33. doi:10.1016/bs.pmbts.2015.07.011
- Klapper, W., Bohm, M., Siebert, R., & Lennert, K. (2008). Morphological variability of lymphohistiocytic variant of anaplastic large cell lymphoma (former lymphohistiocytic lymphoma according to the Kiel classification). *Virchows Arch*, *452*(6), 599-605. doi:10.1007/s00428-008-0616-7
- Kollmann, K., Heller, G., Schneckenleithner, C., Warsch, W., Scheicher, R., Ott, R. G., . . . Sexl, V. (2013). A kinase-independent function of CDK6 links the cell cycle to tumor angiogenesis. *Cancer Cell*, *24*(2), 167-181. doi:10.1016/j.ccr.2013.07.012
- Kollmann, K., & Sexl, V. (2013). CDK6 and p16INK4A in lymphoid malignancies. *Oncotarget*, *4*(11), 1858-1859. doi:10.18632/oncotarget.1541
- Kollmann, S., Grundschober, E., Maurer, B., Warsch, W., Grausenburger, R., Edlinger, L., . . . Sexl, V. (2019). Twins with different personalities: STAT5B-but not STAT5A-has a key role in BCR/ABL-induced leukemia. *Leukemia*, *33*(7), 1583-1597. doi:10.1038/s41375-018-0369-5
- Koppikar, P., Bhagwat, N., Kilpivaara, O., Manshour, T., Adli, M., Hricik, T., . . . Levine, R. L. (2012). Heterodimeric JAK-STAT activation as a mechanism of persistence to JAK2 inhibitor therapy. *Nature*, *489*(7414), 155-159. doi:10.1038/nature11303
- Kourentzi, K., Crum, M., Patil, U., Prebisch, A., Chavan, D., Vu, B., . . . Willson, R. C. (2020). Recombinant expression, characterisation, and quantification in human cancer cell lines of the Anaplastic Large-Cell Lymphoma-characteristic NPM-ALK fusion protein. *Sci Rep*, *10*(1), 5078. doi:10.1038/s41598-020-61936-w
- Kreutmair, S., Klingeberg, C., Poggio, T., Andrieux, G., Keller, A., Miething, C., . . . Illert, A. L. (2020). Existence of reprogrammed lymphoma stem cells in a murine ALCL-like model. *Leukemia*, *34*(12), 3242-3255. doi:10.1038/s41375-020-0789-x
- Kuefer, M. U., Look, A. T., Pulford, K., Behm, F. G., Pattengale, P. K., Mason, D. Y., & Morris, S. W. (1997). Retrovirus-mediated gene transfer of NPM-ALK causes lymphoid malignancy in mice. *Blood*, *90*(8), 2901-2910. Retrieved from <https://www.ncbi.nlm.nih.gov/pubmed/9376569>
- LaBaer, J., Garrett, M. D., Stevenson, L. F., Slingerland, J. M., Sandhu, C., Chou, H. S., . . . Harlow, E. (1997). New functional activities for the p21 family of CDK inhibitors. *Genes Dev*, *11*(7), 847-862. doi:10.1101/gad.11.7.847
- Laimer, D., Dolznig, H., Kollmann, K., Vesely, P. W., Schleder, M., Merkel, O., . . . Kenner, L. (2012). PDGFR blockade is a rational and effective therapy for NPM-ALK-driven lymphomas. *Nat Med*, *18*(11), 1699-1704. doi:10.1038/nm.2966

- Lamant, L., McCarthy, K., d'Amore, E., Klapper, W., Nakagawa, A., Fraga, M., . . . Le Deley, M. C. (2011). Prognostic impact of morphologic and phenotypic features of childhood ALK-positive anaplastic large-cell lymphoma: results of the ALCL99 study. *J Clin Oncol*, *29*(35), 4669-4676. doi:10.1200/JCO.2011.36.5411
- Leventaki, V., Drakos, E., Medeiros, L. J., Lim, M. S., Elenitoba-Johnson, K. S., Claret, F. X., & Rassidakis, G. Z. (2007). NPM-ALK oncogenic kinase promotes cell-cycle progression through activation of JNK/cJun signaling in anaplastic large-cell lymphoma. *Blood*, *110*(5), 1621-1630. doi:10.1182/blood-2006-11-059451
- Levy, D., & Marié, I. (2012). STATus Report on Tetramers. *Immunity*, *36*(4), 553-555. doi:10.1016/j.immuni.2012.04.003
- Levy, D. E., & Darnell Jr, J. E. (2002). STATs: transcriptional control and biological impact. *Nature Reviews Molecular Cell Biology*, *3*, 651. doi:10.1038/nrm909
- Li, P., Mitra, S., Spolski, R., Oh, J., Liao, W., Tang, Z., Mo, F., Li, X., West, E. E., Gromer, D., Lin, J. X., Liu, C., Ruan, Y., & Leonard, W. J. (2017). STAT5-mediated chromatin interactions in superenhancers activate IL-2 highly inducible genes: Functional dissection of the Il2ra gene locus. Proceedings of the National Academy of Sciences of the United States of America, *114*(46), 12111–12119. doi.org/10.1073/pnas.1714019114
- Lindstrom, M. S. (2011). NPM1/B23: A Multifunctional Chaperone in Ribosome Biogenesis and Chromatin Remodeling. *Biochem Res Int*, *2011*, 195209. doi:10.1155/2011/195209
- Liongue, C., Sertori, R., & Ward, A. C. (2016). Evolution of Cytokine Receptor Signaling. *The Journal of Immunology*, *197*(1), 11-18. doi:10.4049/jimmunol.1600372
- Liu, X., Robinson, G. W., Gouilleux, F., Groner, B., & Hennighausen, L. (1995). Cloning and expression of Stat5 and an additional homologue (Stat5b) involved in prolactin signal transduction in mouse mammary tissue. *Proc Natl Acad Sci U S A*, *92*(19), 8831-8835. doi:10.1073/pnas.92.19.8831
- Liu, X., Robinson, G. W., Wagner, K. U., Garrett, L., Wynshaw-Boris, A., & Hennighausen, L. (1997). Stat5a is mandatory for adult mammary gland development and lactogenesis. *Genes Dev*, *11*(2), 179-186. doi:10.1101/gad.11.2.179
- Luchtel, R. A., Zimmermann, M. T., Hu, G., Dasari, S., Jiang, M., Oishi, N., . . . Feldman, A. L. (2019). Recurrent MSC (E116K) mutations in ALK-negative anaplastic large cell lymphoma. *Blood*, *133*(26), 2776-2789. doi:10.1182/blood.2019000626
- Luo, C. T., & Li, M. O. (2013). Transcriptional control of regulatory T cell development and function. *Trends Immunol*, *34*(11), 531-539. doi:10.1016/j.it.2013.08.003
- Malcolm, T. I., Villarese, P., Fairbairn, C. J., Lamant, L., Trinquand, A., Hook, C. E., . . . Turner, S. D. (2016). Anaplastic large cell lymphoma arises in thymocytes and requires transient TCR expression for thymic egress. *Nat Commun*, *7*, 10087. doi:10.1038/ncomms10087
- Malumbres, M., & Barbacid, M. (2009). Cell cycle, CDKs and cancer: a changing paradigm. *Nat Rev Cancer*, *9*(3), 153-166. doi:10.1038/nrc2602
- Malumbres, M., Sotillo, R., Santamaria, D., Galan, J., Cerezo, A., Ortega, S., . . . Barbacid, M. (2004). Mammalian cells cycle without the D-type Cyclin-dependent kinases Cdk4 and Cdk6. *Cell*, *118*(4), 493-504. doi:10.1016/j.cell.2004.08.002
- Martinengo, C., Poggio, T., Menotti, M., Scalzo, M. S., Mastini, C., Ambrogio, C., . . . Chiarle, R. (2014). ALK-dependent control of hypoxia-inducible factors mediates tumor growth and metastasis. *Cancer Res*, *74*(21), 6094-6106. doi:10.1158/0008-5472.CAN-14-0268
- Matsumura, I., Kitamura, T., Wakao, H., Tanaka, H., Hashimoto, K., Albanese, C., Downward, J., Pestell, R. G., & Kanakura, Y. (1999). Transcriptional regulation of the cyclin D1 promoter by STAT5: its involvement in cytokine-dependent growth of hematopoietic cells. *The EMBO journal*, *18*(5), 1367–1377. doi.org/10.1093/emboj/18.5.1367
- Marzec, M., Kasprzycka, M., Liu, X., Raghunath, P. N., Wlodarski, P., & Wasik, M. A. (2007). Oncogenic tyrosine kinase NPM/ALK induces activation of the MEK/ERK signaling pathway independently of c-Raf. *Oncogene*, *26*(6), 813-821. doi:10.1038/sj.onc.1209843
- Matsushime, H., Quelle, D. E., Shurtleff, S. A., Shibuya, M., Sherr, C. J., & Kato, J. Y. (1994). D-type Cyclin-dependent kinase activity in mammalian cells. *Mol Cell Biol*, *14*(3), 2066-2076. doi:10.1128/mcb.14.3.2066
- Maurer, B., Brandstoecker, T., Kollmann, S., Sexl, V., & Prchal-Murphy, M. (2020). Inducible deletion of CDK4 and CDK6 - deciphering CDK4/6 inhibitor effects in the hematopoietic system. *Haematologica*. doi:10.3324/haematol.2020.256313
- Maurer, B., Kollmann, S., Pickem, J., Hoelbl-Kovacic, A., & Sexl, V. (2019). STAT5A and STAT5B-Twins with Different Personalities in Hematopoiesis and Leukemia. *Cancers (Basel)*, *11*(11). doi:10.3390/cancers11111726

- Maurer, B., Nivarthi, H., Wingelhofer, B., Pham, H. T. T., Schlederer, M., Suske, T., . . . Moriggl, R. (2020). High activation of STAT5A drives peripheral T-cell lymphoma and leukemia. *Haematologica*, *105*(2), 435-447. doi:10.3324/haematol.2019.216986
- Medeiros, L. J., & Elenitoba-Johnson, K. S. (2007). Anaplastic Large Cell Lymphoma. *Am J Clin Pathol*, *127*(5), 707-722. doi:10.1309/r2q9ccvutlrycf3h
- Mestas, J., & Hughes, C. C. (2004). Of mice and not men: differences between mouse and human immunology. *J Immunol*, *172*(5), 2731-2738. doi:10.4049/jimmunol.172.5.2731
- Morgan, D. O. (1997). Cyclin-dependent kinases: engines, clocks, and microprocessors. *Annu Rev Cell Dev Biol*, *13*, 261-291. doi:10.1146/annurev.cellbio.13.1.261
- Moriggl, R., Sexl, V., Kenner, L., Duntsch, C., Stangl, K., Gingras, S., . . . Beug, H. (2005). Stat5 tetramer formation is associated with leukemogenesis. *Cancer Cell*, *7*(1), 87-99. doi:10.1016/j.ccr.2004.12.010
- Morris, R., Kershaw, N. J., & Babon, J. J. (2018). The molecular details of cytokine signalling via the JAK-STAT pathway. *Protein Science*, *0*(ja). doi:10.1002/pro.3519
- Morris, S. W., Kirstein, M. N., Valentine, M. B., Dittmer, K. G., Shapiro, D. N., Saltman, D. L., & Look, A. T. (1994). Fusion of a kinase gene, ALK, to a nucleolar protein gene, NPM, in non-Hodgkin's lymphoma. *Science*, *263*(5151), 1281-1284. doi:10.1126/science.8122112
- Morris, S. W., Naeve, C., Mathew, P., James, P. L., Kirstein, M. N., Cui, X., & Witte, D. P. (1997). ALK, the chromosome 2 gene locus altered by the t(2;5) in non-Hodgkin's lymphoma, encodes a novel neural receptor tyrosine kinase that is highly related to leukocyte tyrosine kinase (LTK). *Oncogene*, *14*(18), 2175-2188. doi:10.1038/sj.onc.1201062
- Moti, N., Malcolom, T., Hamoudi, R., Mian, S., Garland, G., Hook, C. E., . . . Turner, S. D. (2015). Anaplastic large cell lymphoma-propagating cells are detectable by side population analysis and possess an expression profile reflective of a primitive origin. *Oncogene*, *34*(14), 1843-1852. doi:10.1038/onc.2014.112
- Murphy, K. M., & Weaver, C. (2016). *Janeway's Immunobiology*: Garland Science, Taylor & Francis Group, LLC.
- Myllymäki, H., & Rämetsä, M. (2014). JAK-STAT Pathway in Drosophila Immunity. *Scandinavian Journal of Immunology*, *79*(6), 377-385. doi:doi:10.1111/sji.12170
- Nebenfuehr, S., Kollmann, K., & Sexl, V. (2020). The role of CDK6 in cancer. *Int J Cancer*, *147*(11), 2988-2995. doi:10.1002/ijc.33054
- Neculai, D., Neculai, A. M., Verrier, S., Straub, K., Klumpp, K., Pfitzner, E., & Becker, S. (2005). Structure of the Unphosphorylated STAT5a Dimer. *Journal of Biological Chemistry*, *280*(49), 40782-40787. doi:10.1074/jbc.M507682200
- Nieborowska-Skorska, M., Slupianek, A., Xue, L., Zhang, Q., Raghunath, P. N., Hoser, G., . . . Skorski, T. (2001). Role of signal transducer and activator of transcription 5 in nucleophosmin/ anaplastic lymphoma kinase-mediated malignant transformation of lymphoid cells. *Cancer Res*, *61*(17), 6517-6523. Retrieved from <https://www.ncbi.nlm.nih.gov/pubmed/11522649>
- Nivarthi, H., Prchal-Murphy, M., Swoboda, A., Hager, M., Schlederer, M., Kenner, L., . . . Ermakova, O. (2015). Stat5 gene dosage in T cells modulates CD8+ T-cell homeostasis and attenuates contact hypersensitivity response in mice. *Allergy*, *70*(1), 67-79. doi:10.1111/all.12535
- Norbury, C., & Nurse, P. (1992). Animal cell cycles and their control. *Annu Rev Biochem*, *61*, 441-470. doi:10.1146/annurev.bi.61.070192.002301
- Onishi, M., Nosaka, T., Misawa, K., Mui, A. L., Gorman, D., McMahon, M., . . . Kitamura, T. (1998). Identification and characterisation of a constitutively active STAT5 mutant that promotes cell proliferation. *Mol Cell Biol*, *18*(7), 3871-3879. doi:10.1128/mcb.18.7.3871
- Orlova, A., Wagner, C., de Araujo, E. D., Bajusz, D., Neubauer, H. A., Herling, M., . . . Moriggl, R. (2019). Direct Targeting Options for STAT3 and STAT5 in Cancer. *Cancers (Basel)*, *11*(12). doi:10.3390/cancers11121930
- Owen, D. L., & Farrar, M. A. (2017). STAT5 and CD4 (+) T Cell Immunity. *F1000Res*, *6*, 32. doi:10.12688/f1000research.9838.1
- Palacios, R., & Steinmetz, M. (1985). Il-3-dependent mouse clones that express B-220 surface antigen, contain Ig genes in germ-line configuration, and generate B lymphocytes in vivo. *Cell*, *41*(3), 727-734. doi:10.1016/s0092-8674(85)80053-2
- Parekh, C., & Crooks, G. M. (2013). Critical differences in hematopoiesis and lymphoid development between humans and mice. *J Clin Immunol*, *33*(4), 711-715. doi:10.1007/s10875-012-9844-3
- Parham, C., Chirica, M., Timans, J., Vaisberg, E., Travis, M., Cheung, J., . . . Moore, K. W. (2002). A receptor for the heterodimeric cytokine IL-23 is composed of IL-12Rbeta1 and a novel cytokine receptor subunit, IL-23R. *J Immunol*, *168*(11), 5699-5708. doi:10.4049/jimmunol.168.11.5699
- Parrilla Castellar, E. R., Jaffe, E. S., Said, J. W., Swerdlow, S. H., Ketterling, R. P., Knudson, R. A., . . . Feldman, A. L. (2014). ALK-negative anaplastic large cell lymphoma is a genetically heterogeneous disease with widely disparate clinical outcomes. *Blood*, *124*(9), 1473-1480. doi:10.1182/blood-2014-04-571091
- Pfizer (Producer). (2021). Pfizer's Xalkori (crizotinib) approved by FDA for ALK-positive anaplastic large cell lymphoma in children and young adults. .

- Pham, H. T. T., Maurer, B., Prchal-Murphy, M., Grausenburger, R., Grundschober, E., Javaheri, T., . . . Moriggl, R. (2018). STAT5BN642H is a driver mutation for T cell neoplasia. *J Clin Invest*, *128*(1), 387-401. doi:10.1172/jci94509
- Pinto, J. A., Raez, L. E., & Domingo, G. (2020). Clinical consequences of resistance to ALK inhibitors in non-small cell lung cancer. *Expert Rev Respir Med*, *14*(4), 385-390. doi:10.1080/17476348.2020.1721285
- Piva, R., Pellegrino, E., Mattioli, M., Agnelli, L., Lombardi, L., Boccalatte, F., . . . Inghirami, G. (2006). Functional validation of the anaplastic lymphoma kinase signature identifies CEBPB and BCL2A1 as critical target genes. *J Clin Invest*, *116*(12), 3171-3182. doi:10.1172/JCI29401
- Porpaczy, E., Tripolt, S., Hoelbl-Kovacic, A., Gisslinger, B., Bago-Horvath, Z., Casanova-Hevia, E., . . . Sexl, V. (2018). Aggressive B-cell lymphomas in patients with myelofibrosis receiving JAK1/2 inhibitor therapy. *Blood*, *132*(7), 694-706. doi:10.1182/blood-2017-10-810739
- Prokoph, N., Larose, H., Lim, M. S., Burke, G. A. A., & Turner, S. D. (2018). Treatment Options for Paediatric Anaplastic Large Cell Lymphoma (ALCL): Current Standard and beyond. *Cancers (Basel)*, *10*(4). doi:10.3390/cancers10040099
- Prokoph, N., Probst, N. A., Lee, L. C., Monahan, J. M., Matthews, J. D., Liang, H. C., . . . Turner, S. D. (2020). IL10RA modulates crizotinib sensitivity in NPM1-ALK+ anaplastic large cell lymphoma. *Blood*, *136*(14), 1657-1669. doi:10.1182/blood.2019003793
- Prutsch, N., Gurnhofer, E., Suske, T., Liang, H. C., Schleder, M., Roos, S., . . . Merkel, O. (2019). Dependency on the TYK2/STAT1/MCL1 axis in anaplastic large cell lymphoma. *Leukemia*, *33*(3), 696-709. doi:10.1038/s41375-018-0239-1
- Pulford, K., Morris, S. W., & Turturro, F. (2004). Anaplastic lymphoma kinase proteins in growth control and cancer. *J Cell Physiol*, *199*(3), 330-358. doi:10.1002/jcp.10472
- Querfeld, C., Khan, I., Mahon, B., Nelson, B. P., Rosen, S. T., & Evens, A. M. (2010). Primary cutaneous and systemic anaplastic large cell lymphoma: clinicopathologic aspects and therapeutic options. *Oncology (Williston Park)*, *24*(7), 574-587. Retrieved from <https://www.ncbi.nlm.nih.gov/pubmed/20669794>
- Rana, S., Bendjennat, M., Kour, S., King, H. M., Kizhake, S., Zahid, M., & Natarajan, A. (2019). Selective degradation of CDK6 by a palbociclib based PROTAC. *Bioorg Med Chem Lett*, *29*(11), 1375-1379. doi:10.1016/j.bmcl.2019.03.035
- Rani, A., & Murphy, J. J. (2015). STAT5 in Cancer and Immunity. *Journal of Interferon & Cytokine Research*, *36*(4), 226-237. doi:10.1089/jir.2015.0054
- Redl, E., Sheibani-Tezerji, R., Cardona, C. J., Hamminger, P., Timelthaler, G., Hassler, M. R., . . . Egger, G. (2021). Requirement of DNMT1 to orchestrate epigenomic reprogramming for NPM-ALK-driven lymphomagenesis. *Life Sci Alliance*, *4*(2). doi:10.26508/lsa.202000794
- Rubin, S. M., Gall, A. L., Zheng, N., & Pavletich, N. P. (2005). Structure of the Rb C-terminal domain bound to E2F1-DP1: a mechanism for phosphorylation-induced E2F release. *Cell*, *123*(6), 1093-1106. doi:10.1016/j.cell.2005.09.044
- Ruchatz, H., Coluccia, A. M., Stano, P., Marchesi, E., & Gambacorti-Passerini, C. (2003). Constitutive activation of Jak2 contributes to proliferation and resistance to apoptosis in NPM/ALK-transformed cells. *Exp Hematol*, *31*(4), 309-315. doi:10.1016/s0301-472x(03)00007-9
- Russo, A. A., Tong, L., Lee, J. O., Jeffrey, P. D., & Pavletich, N. P. (1998). Structural basis for inhibition of the Cyclin-dependent kinase Cdk6 by the tumour suppressor p16INK4a. *Nature*, *395*(6699), 237-243. doi:10.1038/26155
- Salvador-Barbero, B., Álvarez-Fernández, M., Zapatero-Solana, E., El Bakkali, A., Menéndez, M. D. C., López-Casas, P. P., . . . Malumbres, M. (2020). CDK4/6 Inhibitors Impair Recovery from Cytotoxic Chemotherapy in Pancreatic Adenocarcinoma. *Cancer Cell*, *37*(3), 340-353.e346. doi:10.1016/j.ccell.2020.01.007
- Sattler, M., Mohi, M. G., Pride, Y. B., Quinnan, L. R., Malouf, N. A., Podar, K., . . . Neel, B. G. (2002). Critical role for Gab2 in transformation by BCR/ABL. *Cancer Cell*, *1*(5), 479-492. doi:10.1016/s1535-6108(02)00074-0
- Savage, K. J., Harris, N. L., Vose, J. M., Ullrich, F., Jaffe, E. S., Connors, J. M., . . . International Peripheral, T. C. L. P. (2008). ALK- anaplastic large-cell lymphoma is clinically and immunophenotypically different from both ALK+ ALCL and peripheral T-cell lymphoma, not otherwise specified: report from the International Peripheral T-Cell Lymphoma Project. *Blood*, *111*(12), 5496-5504. doi:10.1182/blood-2008-01-134270
- Scarfo, I., Pellegrino, E., Mereu, E., Kwee, I., Agnelli, L., Bergaggio, E., . . . European, T. C. L. S. G. (2016). Identification of a new subclass of ALK-negative ALCL expressing aberrant levels of ERBB4 transcripts. *Blood*, *127*(2), 221-232. doi:10.1182/blood-2014-12-614503
- Scheicher, R., Hoelbl-Kovacic, A., Bellutti, F., Tigan, A. S., Prchal-Murphy, M., Heller, G., . . . Sexl, V. (2015). CDK6 as a key regulator of hematopoietic and leukemic stem cell activation. *Blood*, *125*(1), 90-101. doi:10.1182/blood-2014-06-584417
- Schwartz, D. M., Kanno, Y., Villarino, A., Ward, M., Gadina, M., & O'Shea, J. J. (2017). JAK inhibition as a therapeutic strategy for immune and inflammatory diseases. *Nat Rev Drug Discov*, *16*(12), 843-862. doi:10.1038/nrd.2017.201

- Sharma, G. G., Mota, I., Mologni, L., Patrucco, E., Gambacorti-Passerini, C., & Chiarle, R. (2018). Tumor Resistance against ALK Targeted Therapy-Where It Comes From and Where It Goes. *Cancers (Basel)*, *10*(3). doi:10.3390/cancers10030062
- Sherr, C. J., Beach, D., & Shapiro, G. I. (2016). Targeting CDK4 and CDK6: From Discovery to Therapy. *Cancer Discov*, *6*(4), 353-367. doi:10.1158/2159-8290.CD-15-0894
- Sherr, C. J., & Roberts, J. M. (1999). CDK inhibitors: positive and negative regulators of G1-phase progression. *Genes Dev*, *13*(12), 1501-1512. doi:10.1101/gad.13.12.1501
- Sherr, C. J., & Roberts, J. M. (2004). Living with or without Cyclins and Cyclin-dependent kinases. *Genes Dev*, *18*(22), 2699-2711. doi:10.1101/gad.1256504
- Shiota, M., Fujimoto, J., Semba, T., Satoh, H., Yamamoto, T., & Mori, S. (1994). Hyperphosphorylation of a novel 80 kDa protein-tyrosine kinase similar to Ltk in a human Ki-1 lymphoma cell line, AMS3. *Oncogene*, *9*(6), 1567-1574. Retrieved from <https://www.ncbi.nlm.nih.gov/pubmed/8183550>
- Shuai, K. (2000). Modulation of STAT signaling by STAT-interacting proteins. *Oncogene*, *19*(21), 2638-2644. doi:10.1038/sj.onc.1203522
- Slupianek, A., & Skorski, T. (2004). NPM/ALK downregulates p27Kip1 in a PI-3K-dependent manner. *Exp Hematol*, *32*(12), 1265-1271. doi:10.1016/j.exphem.2004.11.002
- Sobhani, N., D'Angelo, A., Pittacolo, M., Roviello, G., Miccoli, A., Corona, S. P., . . . Otto, T. (2019). Updates on the CDK4/6 Inhibitory Strategy and Combinations in Breast Cancer. *Cells*, *8*(4). doi:10.3390/cells8040321
- Staber, P. B., Vesely, P., Haq, N., Ott, R. G., Funato, K., Bambach, I., . . . Hoefler, G. (2007). The oncoprotein NPM-ALK of anaplastic large-cell lymphoma induces JUNB transcription via ERK1/2 and JunB translation via mTOR signaling. *Blood*, *110*(9), 3374-3383. doi:10.1182/blood-2007-02-071258
- Stein, H., Foss, H. D., Durkop, H., Marafioti, T., Delsol, G., Pulford, K., . . . Falini, B. (2000). CD30(+) anaplastic large cell lymphoma: a review of its histopathologic, genetic, and clinical features. *Blood*, *96*(12), 3681-3695. Retrieved from <https://www.ncbi.nlm.nih.gov/pubmed/11090048>
- Stein, H., Mason, D. Y., Gerdes, J., O'Connor, N., Wainscoat, J., Pallesen, G., . . . et al. (1985). The expression of the Hodgkin's disease associated antigen Ki-1 in reactive and neoplastic lymphoid tissue: evidence that Reed-Sternberg cells and histiocytic malignancies are derived from activated lymphoid cells. *Blood*, *66*(4), 848-858. Retrieved from <https://www.ncbi.nlm.nih.gov/pubmed/3876124>
- Sung, H., Ferlay, J., Siegel, R. L., Laversanne, M., Soerjomataram, I., Jemal, A., & Bray, F. (2021). Global cancer statistics 2020: GLOBOCAN estimates of incidence and mortality worldwide for 36 cancers in 185 countries. *CA Cancer J Clin*. doi:10.3322/caac.21660
- Talluri, S., & Dick, F. A. (2012). Regulation of transcription and chromatin structure by pRB: here, there and everywhere. *Cell Cycle*, *11*(17), 3189-3198. doi:10.4161/cc.21263
- Tartari, C. J., Gunby, R. H., Coluccia, A. M., Sottocornola, R., Cimbri, B., Scapozza, L., . . . Gambacorti-Passerini, C. (2008). Characterisation of some molecular mechanisms governing autoactivation of the catalytic domain of the anaplastic lymphoma kinase. *J Biol Chem*, *283*(7), 3743-3750. doi:10.1074/jbc.M706067200
- ten Berge, R. L., Oudejans, J. J., Ossenkoppelle, G. J., & Meijer, C. J. (2003). ALK-negative systemic anaplastic large cell lymphoma: differential diagnostic and prognostic aspects--a review. *J Pathol*, *200*(1), 4-15. doi:10.1002/path.1331
- Tigan, A. S., Bellutti, F., Kollmann, K., Tebb, G., & Sexl, V. (2016). CDK6-a review of the past and a glimpse into the future: from cell-cycle control to transcriptional regulation. *Oncogene*, *35*(24), 3083-3091. doi:10.1038/onc.2015.407
- Tolomeo, M., Meli, M., & Grimaudo, S. (2019). STAT5 and STAT5 Inhibitors in Hematological Malignancies. *Anticancer Agents Med Chem*, *19*(17), 2036-2046. doi:10.2174/1871520619666190906160848
- UBC. (2021, 27.04.2021). Cell Cycle and Cancer. *Cancer Genetics Ebook*. Retrieved from <http://www.cubocube.com/dashboard.php?a=1642&b=1691&c=1>
- Udy, G. B., Towers, R. P., Snell, R. G., Wilkins, R. J., Park, S. H., Ram, P. A., . . . Davey, H. W. (1997). Requirement of STAT5b for sexual dimorphism of body growth rates and liver gene expression. *Proc Natl Acad Sci U S A*, *94*(14), 7239-7244. doi:10.1073/pnas.94.14.7239
- Uras, I. Z., Maurer, B., Nivarthi, H., Jodl, P., Kollmann, K., Prchal-Murphy, M., . . . Sexl, V. (2019). CDK6 coordinates JAK2 (V617F) mutant MPN via NF-kappaB and apoptotic networks. *Blood*, *133*(15), 1677-1690. doi:10.1182/blood-2018-08-872648
- Vacchio, M. S., & Bosselut, R. (2016). What Happens in the Thymus Does Not Stay in the Thymus: How T Cells Recycle the CD4+CD8+ Lineage Commitment Transcriptional Circuitry To Control Their Function. *Journal of immunology (Baltimore, Md. : 1950)*, *196*(12), 4848-4856. doi:10.4049/jimmunol.1600415
- Vainchenker, W., & Constantinescu, S. N. (2013). JAK-STAT signaling in hematological malignancies. *Oncogene*, *32*(21), 2601-2613. doi:10.1038/onc.2012.347
- Vasmatazis, G., Johnson, S. H., Knudson, R. A., Ketterling, R. P., Braggio, E., Fonseca, R., . . . Feldman, A. L. (2012). Genome-wide analysis reveals recurrent structural abnormalities of TP63 and other p53-related genes in peripheral T-cell lymphomas. *Blood*, *120*(11), 2280-2289. doi:10.1182/blood-2012-03-419937

- Villarino, A., Laurence, A., Robinson, G. W., Bonelli, M., Dema, B., Afzali, B., . . . O'Shea, J. J. (2016). Signal transducer and activator of transcription 5 (STAT5) paralog dose governs T cell effector and regulatory functions. *Elife*, *5*. doi:10.7554/eLife.08384
- Villarino, A. V., Kanno, Y., & O'Shea, J. J. (2017). Mechanisms and consequences of Jak-STAT signaling in the immune system. *Nature Immunology*, *18*, 374. doi:10.1038/ni.3691
- Virtanen, A., Haikarainen, T., Raivola, J., & Silvennoinen, O. (2019). Selective JAKinibs: Prospects in Inflammatory and Autoimmune Diseases. *BioDrugs*, *33*(1), 15-32. doi:10.1007/s40259-019-00333-w
- Voena, C., Conte, C., Ambrogio, C., Boeri Erba, E., Boccalatte, F., Mohammed, S., . . . Chiarle, R. (2007). The tyrosine phosphatase Shp2 interacts with NPM-ALK and regulates anaplastic lymphoma cell growth and migration. *Cancer Res*, *67*(9), 4278-4286. doi:10.1158/0008-5472.CAN-06-4350
- Vose, J., Armitage, J., Weisenburger, D., & International, T. C. L. P. (2008). International peripheral T-cell and natural killer/T-cell lymphoma study: pathology findings and clinical outcomes. *J Clin Oncol*, *26*(25), 4124-4130. doi:10.1200/JCO.2008.16.4558
- Waters, M. J., & Brooks, A. J. (2015). JAK2 activation by growth hormone and other cytokines. *The Biochemical journal*, *466*(1), 1-11. doi:10.1042/BJ20141293
- Wellmann, A., Doseeva, V., Butscher, W., Raffeld, M., Fukushima, P., Stetler-Stevenson, M., & Gardner, K. (1997). The activated anaplastic lymphoma kinase increases cellular proliferation and oncogene up-regulation in rat 1a fibroblasts. *Faseb j*, *11*(12), 965-972. doi:10.1096/fasebj.11.12.9337149
- Wingelhofer, B., Maurer, B., Heyes, E. C., Cumaraswamy, A. A., Berger-Becvar, A., de Araujo, E. D., . . . Moriggl, R. (2018). Pharmacologic inhibition of STAT5 in acute myeloid leukemia. *Leukemia*, *32*(5), 1135-1146. doi:10.1038/s41375-017-0005-9
- Wormald, S., & Hilton, D. J. (2004). Inhibitors of Cytokine Signal Transduction. *Journal of Biological Chemistry*, *279*(2), 821-824. doi:10.1074/jbc.R300030200
- Wright, C. W., Rumble, J. M., & Duckett, C. S. (2007). CD30 activates both the canonical and alternative NF-kappaB pathways in anaplastic large cell lymphoma cells. *J Biol Chem*, *282*(14), 10252-10262. doi:10.1074/jbc.M608817200
- Yamada, O., & Kawachi, K. (2013). The role of the JAK-STAT pathway and related signal cascades in telomerase activation during the development of hematologic malignancies. *Jakstat*, *2*(4), e25256. doi:10.4161/jkst.25256
- Yamaji, D., Na, R., Feuermann, Y., Pechhold, S., Chen, W., Robinson, G. W., & Hennighausen, L. (2009). Development of mammary luminal progenitor cells is controlled by the transcription factor STAT5A. *Genes Dev*, *23*(20), 2382-2387. doi:10.1101/gad.1840109
- Yang, C., Li, Z., Bhatt, T., Dickler, M., Giri, D., Scaltriti, M., . . . Chandralapaty, S. (2017). Acquired CDK6 amplification promotes breast cancer resistance to CDK4/6 inhibitors and loss of ER signaling and dependence. *Oncogene*, *36*(16), 2255-2264. doi:10.1038/onc.2016.379
- Yao, Z., Cui, Y., Watford, W. T., Bream, J. H., Yamaoka, K., Hissong, B. D., . . . O'Shea, J. J. (2006). Stat5a/b are essential for normal lymphoid development and differentiation. *Proc Natl Acad Sci U S A*, *103*(4), 1000-1005. doi:10.1073/pnas.0507350103
- Zamo, A., Chiarle, R., Piva, R., Howes, J., Fan, Y., Chilosi, M., . . . Inghirami, G. (2002). Anaplastic lymphoma kinase (ALK) activates Stat3 and protects hematopoietic cells from cell death. *Oncogene*, *21*(7), 1038-1047. doi:10.1038/sj.onc.1205152
- Zhang, Q., Raghunath, P. N., Xue, L., Majewski, M., Carpentieri, D. F., Odum, N., . . . Wasik, M. A. (2002). Multilevel dysregulation of STAT3 activation in anaplastic lymphoma kinase-positive T/null-cell lymphoma. *J Immunol*, *168*(1), 466-474. doi:10.4049/jimmunol.168.1.466
- Zhang, Q., Wang, H. Y., Liu, X., & Wasik, M. A. (2007). STAT5A is epigenetically silenced by the tyrosine kinase NPM1-ALK and acts as a tumor suppressor by reciprocally inhibiting NPM1-ALK expression. *Nat Med*, *13*(11), 1341-1348. doi:10.1038/nm1659
- Zhang, Q., Wei, F., Wang, H. Y., Liu, X., Roy, D., Xiong, Q. B., . . . Wasik, M. A. (2013). The potent oncogene NPM-ALK mediates malignant transformation of normal human CD4(+) T lymphocytes. *Am J Pathol*, *183*(6), 1971-1980. doi:10.1016/j.ajpath.2013.08.030
- Zhong, M., Henriksen, M. A., Takeuchi, K., Schaefer, O., Liu, B., ten Hoeve, J., . . . Darnell, J. E., Jr. (2005). Implications of an antiparallel dimeric structure of nonphosphorylated STAT1 for the activation-inactivation cycle. *Proceedings of the National Academy of Sciences of the United States of America*, *102*(11), 3966-3971. doi:10.1073/pnas.0501063102
- Zhou, T., Georgeon, S., Moser, R., Moore, D. J., Cafilisch, A., & Hantschel, O. (2014). Specificity and mechanism-of-action of the JAK2 tyrosine kinase inhibitors ruxitinib and SAR302503 (TG101348). *Leukemia*, *28*(2), 404-407. doi:10.1038/leu.2013.205